FAILURE PREDICTION OF COMPLEX LOAD CASES IN SHEET METAL FORMING

EMPHASIS ON NON-LINEAR STRAIN PATHS, STRETCH-BENDING AND EDGE EFFECTS

Alexander Barlo

Blekinge Institute of Technology
Licentiate Dissertation Series No. 2023:03

Department of Mechanical Engineering

Failure Prediction of Complex Load Cases in Sheet Metal Forming

Emphasis on Non-Linear Strain Paths, Stretch-Bending and Edge Effects

Alexander Barlo

Blekinge Institute of Technology Licentiate Dissertation Series
No 2023:03

Failure Prediction of Complex Load Cases in Sheet Metal Forming

Emphasis on Non-Linear Strain Paths, Stretch-Bending and Edge Effects

Alexander Barlo

Licentiate Dissertation in Mechanical Engineering

Department of Mechanical Engineering
Blekinge Institute of Technology
SWEDEN

Department of Mechanical Engineering
Publisher: Blekinge Institute of Technology
SE-371 79 Karlskrona, Sweden
Printed by Media-Tryck, Lund, Sweden, 2023
ISBN: 978-91-7295-451-9
ISSN: 1650-2140
urn: urn:nbn:se:bth-24300

The definition of insanity is doing the same thing over and over and expecting different results.

- Albert Einstein

ACKNOWLEDGEMENT

The research presented in this Thesis is carried out at the Department of Mechnical Engineering at Blekinge Institute of Technology, Karlskrona, Sweden. The research carried out is a part of the PREDICT project (grant number 2020-02986) funded through the Sustainable Production sub-program within Vehicle Strategic Research and Innovation (FFI) program by the Swedish Innovation Agency (VINNOVA).

I would like to express my sincere gratitude towards my supervisor Dr. Mats Sigvant for sharing his knowledge and his constant words of encouragement and motivation. I would also like to express my gratitude towards my supervisors Dr. Md. Shafiqul Islam and Dr. Johan Pilthammar for their valuable inputs and constructive criticism during the research. A special 'thank you' is directed towards my supervisor Prof. Tobias Larsson for his ability to make me take a step back and look at the larger picture of my research. I would also like to extend a wholeheartedly 'thank you' to all the industrial collaborators I have had the pleasure of collaborating with during the research, whom have provided interesting and challenging discussions and cases. I would also like to direct my gratitude towards my colleagues at the Department of Mechanical Engineering at Blekinge Institute of Technology for the engaging discussions about research along with fun times outside of the office.

Lastly, I would like to thank my family and friends for their everlasting support of the journey I am on. Without their support, this would not be possible.

Alexander Barlo
Karlskrona, February 2023

ABSTRACT

With the increased focus on reducing carbon emissions in today's society, several industries have to overcome new challenges, where especially the automotive industry is under a lot of scrutiny to deliver improved and more environmentally friendly products. To meet the demands from customers and optimize vehicles aerodynamically, new cars often contain complex body geometries, together with advanced materials that are introduced to reduce the total vehicle weight.
With the introduction of the complex body components and advanced materials, one area in the automotive industry that has to overcome these challenges is manufacturing engineering, and in particular the departments working with the sheet metal forming process. In this process complex body component geometries can lead to non-linear strain paths and stretch bending load cases, and newly introduced advanced materials can be prone to exhibit behaviour of edge cracks not observed in conventional sheet metals.

This thesis takes it onset in the challenges seen in industry today with predicting failure of the three complex load cases: Non-Linear Strain Paths, Stretch-Bending, and Edge Cracks. Through Finite Element simulation attempts are made to accurately predict failure caused by aforementioned load cases in industrial components or experimental setups in an effort to develop post-processing methods that are applicable to all cases.

Keywords: Sheet Metal Forming, Failure Prediction, Non-Linear Strain Paths, Stretch Bending, Edge Cracks, Finite Element Simulation

SAMMANFATTNING

Med det ökade fokuset på att minska koldioxidutsläppen i dagens samhälle behöver flera branscher övervinna nya utmaningar, där framförallt fordonsindustrin är under stor press för att leverera förbättrade och mer miljövänliga produkter. För att möta kraven från kunder och optimera fordon aerodynamiskt innehåller nya bilar ofta komplexa karossgeometrier, tillsammans med avancerade material som introduceras för att minska den totala fordonsvikten och öka dess prestanda.
Med introduktionen av de komplexa karosskomponenterna och avancerade materialen är tillverkningsteknik ett område inom bilindustrin som måste övervinna dessa utmaningar, och i synnerhet de som arbetar med plåtformningsprocessen. I denna process kan komplexa kroppskomponentgeometrier leda till icke-linjära töjningsvägar och sträckböjningsbelastningar, och nyligen introducerade avancerade material kan vara benägna att uppvisa beteende av kantsprickor som inte observeras i konventionell plåt.

Den här avhandlingen tar sin början i de utmaningar som finns inom industrin idag kring att förutsäga fel i de tre komplexa belastningsfallen: icke-linjära töjningsvägar, sträckböjning och kantsprickor. Genom Finita Element-simulering görs försök att exakt förutsäga fel orsakade av ovannämnda belastningsfall i industriella komponenter eller experimentella uppställningar i ett försök att utveckla efterbearbetningsmetoder som är tillämpliga i alla fall.

RESUMÉ

Med det øgede fokus på at reducere kulstofsemmisionerne i dagens samfund, er der flere industrier, der står over for nye udfordringer. Især bilindustrien er under stor bevågenhed for at levere forbedrede og mere miljøvenlige produkter. For at imødekomme kundernes krav og optimere køretøjerne aerodynamisk, indeholder nye biler ofte komplekse karosserigeometrier, sammen med avancerede materialer, der anvendes for at reducere bilens totalvægt. En gruppe der beskæftiger sig med disse komplekse karosserikomponenter og avancerede materialer er produktionsingeniørerne med kompetenceområde indenfor pladeformgivning. Med den stigende komponentkompleksitet introduceres også komplekse lasttilfælde så som ikke-lineære tøjningsveje og kombineret stræk og bøjning. Ligeledes med introduktionen af avancerede materialer, er der en øget risiko for kantsprækker, som ikke nødvendigvis ses i konventionelle plademetaller.

Denne afhandling tager derfor udgangspunkt, i de udfordrigner der findes i industrien i dag med at forudse fejl i produktionen forårsaget af de tre komplekse lasttilfælde: ikke-lineære tøjningsveje, kombineret stræk og bøjning, samt kantsprækker. Gennem Finite Element simulering forsøges det, med høj nøjagtighed, at forudsige hvor fejl vil opstå grundet de tre førnævnte lasttilfælde i indsturielle komponenter eller forsøgsopstillinger. Alt dette med henblik på at udvikle databehandlingsmetoder, der er generelt anvendelige.

LIST OF APPENDED PAPERS

Paper A

A Barlo, M Sigvant, and B Endelt (2019). ”On the Failure Prediction of Dual-Phase Steel and Aluminium Alloys Exposed to Combined Tension and Bending”. In: *IOP Conference Series: Materials Science and Engineering* 651, p. 012030 DOI: 10.1088/1757-899X/651/1/012030

Paper B

A Barlo, N Manopulo, M Sigvant, B Endelt, and K Trana (2019). ”Investigation of a Bending Corrected Forming Limit Surface for Failure Prediction in Sheet Metals”. In: *Conference Proceedings, Forming Technology Forum 2019, September 19-20, Munich, Germany*.

Paper C

A Barlo, M Sigvant, N Manopulo, M S Islam, and J Pilthammar (2022). ”Failure Prediction of Automotive Components Utilizing a Path Independent Forming Limit Criterion”. In: *Key Engineering Materials* 926, pp. 906-916. DOI: 10.4028/p-u6g3p6

Paper D

A Barlo, M Sigvant, L Pérez, M S Islam, and J Pilthammar (2022). ”A Study of the Boundary Conditions in the ISO-16630 Hole Expansion Test”. In: *IOP Conference Series: Materials Science and Engineering* 1238.1, p. 012031. DOI: 10.1088/1757-899X/1238/1/012031

CONTENTS

1 INTRODUCTION 1
- 1.1 Background . . . 1
- 1.2 Research Questions . . . 3
- 1.3 Hypotheses . . . 3

2 RESEARCH METHODOLOGY 5
- 2.1 Areas of Relevance and Contribution . . . 5
- 2.2 Qualification as Research Area . . . 7
- 2.3 Research Quality and Validity . . . 7
- 2.4 Mapping of Papers to the DRM Framework . . . 7

3 RELATED WORK 9
- 3.1 Review of Related Work . . . 9
  - 3.1.1 Non-Linear Strain Paths . . . 9
  - 3.1.2 Stretch-Bending . . . 10
  - 3.1.3 Edge Effects . . . 10
  - 3.1.4 Upstream Impact of Increased Model Accuracy . . . 11
- 3.2 Reference Model . . . 12
- 3.3 Impact Model . . . 14

4 SHEET METAL FORMING SIMULATIONS 15
- 4.1 The Application of Sheet Metal Forming Simulations . . . 15
- 4.2 The Importance of Applied Constitutive Model . . . 17
- 4.3 The Importance of Tribology Models . . . 21
- 4.4 The Importance of Accurate Tool and Press Line Parameters 24

5 EXPERIMENTAL WORK 25
- 5.1 Digital Image Correlation . . . 25
- 5.2 Stretch-Bending . . . 26
- 5.3 Hole Expansion Test . . . 28
  - 5.3.1 Modified Experimental Setup . . . 30
  - 5.3.2 Modified Post-Processing . . . 30
- 5.4 Pre-Straining of Sheets . . . 33

5.5 Relation of Experiments to Thesis 36

6 FAILURE PREDICTION IN SHEET METAL FORMING 39
6.1 Definition of Failure in a Sheet Metal Forming Context 39
6.2 Components experiencing Non-Linear Strain Paths 42
6.3 Components experiencing Stretch-Bending 46
6.4 Components experiencing Edge Effects 48

7 SUMMARY OF APPENDED PAPERS 51
7.1 Paper A 51
7.2 Paper B 52
7.3 Paper C 52
7.4 Paper D 53

8 RESULTS 55
8.1 Non-Linear Strain Paths 55
8.2 Stretch-Bending 56
8.3 Edge Effects 58

9 CONCLUSIONS 61
9.1 Sub-question s.RQ. 1 61
9.2 Sub-question s.RQ. 2 62
9.3 Sub-question s.RQ. 3 62
9.4 Overall Statement 63

10 FUTURE WORK 65
10.1 Evaluation Space Transformation 65
10.2 Bending Correction 66
10.3 Hole Expansion Test 66
10.4 Overall Outlook on Sheet Metal Forming Research 66

REFERENCES 69

PAPER A

PAPER B

PAPER C

PAPER D

Chapter 1
INTRODUCTION

1.1 Background

Sheet metal forming is a manufacturing process that has been used for decades to transform thin sheets of metal into finished components or products. The manufacturing process has a wide range of application from simple components such as kitchen appliances like sinks and pots, to more complex components such as structural and body components in cars. The sheet metal forming process can on a high level be broken down into three main steps: (i) material selection, (ii) blanking process, and (iii) the forming operation. In the first step, a suitable material is selected during the design process of the component, and once a decision to manufacture a certain design is made, the material is ordered. In the sheet metal industry, the sheet material is most often received on large coils with several hundred meters of material. Therefore, in order to be able to manufacture components from the received material, the second step, named the blanking process is needed. In the blanking process, the coil is cut into smaller pieces, called blanks. Over the years, there has been a shift where companies have begun to design tailored blanks i.e. the blanks are not cut out as rectangles. This is done to reduce the amount of scarp material cut from the formed component, thereby utilizing more of the material. Once the blanks have been cut into the designed shapes, they enter the third step of the manufacturing process - the forming itself. The forming operation most often occurs in a press line, meaning that several forming and trimming (removal of unwanted material) operations are performed before the blank has been transformed into the designed product. An overview of the three overall steps in the sheet metal forming manufacturing process can be found in Figure 1.1.

In the past five to six decades the concept of Computer Aided Engineering (CAE) has rapidly been making its entry in a wide variety of engineering disciplines, with sheet metal forming being no exception. The application of numerical simulations in the form of Finite Element models has become a crucial step in the manufacturing feasibility study of newly designed components. In recent years however, there has been an increased focus on sustainability in almost every branch of the

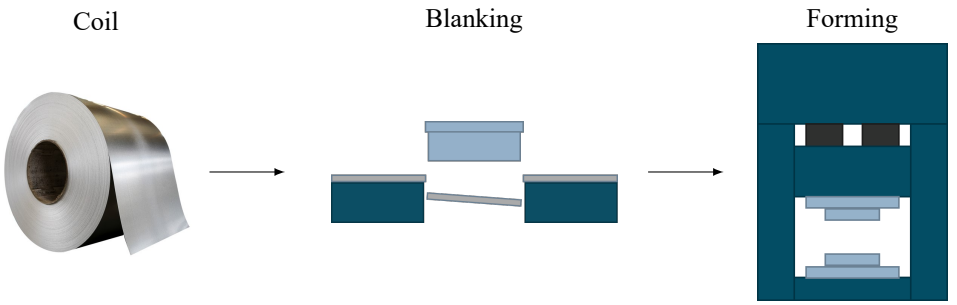

Figure 1.1: Fundamental process flow of the sheet metal forming manufacturing process.

manufacturing industry, aligning with the United Nations Global Goal 12 concerning responsible consumption and production (United Nations 2023). Taking the automotive industry as an example, this shift in focus has resulted in a demand for vehicle weight reduction and complex geometrical shapes of the components benefiting the aerodynamic features of the car in order to reduce the fuel consumption as well as being competitive on aesthetics. This paired with a strong wish to swiftly introduce more sustainable and 'green' materials into production from both industry and customers pushes the capabilities of the existing Finite Element tools to the limit. One area where this is observed in the application of numerical tools in the sheet metal forming community is on the topic of failure prediction. As component geometry and material behaviour becomes increasingly complex, the current methods for predicting failure during the manufacturing process through the application of digital tools becomes increasingly difficult. The current industry standard for assessing the remaining formability of a component was developed in the mid 1960's, and while it has been performing well since then, its shortcomings more and more often becomes a problem for CAE engineers. These shortcomings especially comes to light when attempting to predict failure of complex load cases such as non-linear strain paths, combined stretching and bending, as well as edge effects caused by blanking or trimming. These complex load cases will serve as a starting point for this thesis.

1.2 Research Questions

In order to be able to extend the use of digital tools such as Finite Element models in manufacturing feasibility studies of components and/or products, the model accuracy must be increased. This thesis will take its offset in the following research question:

How can failure, caused by complex load cases, in the sheet metal forming process accurately be predicted?

As the term *complex load cases* covers a variety of load situations, the research question can be split into three sub-questions:

s.RQ. 1: How can failure caused by non-linear strain paths be accurately predicted in manufacturing feasibility studies?

s.RQ. 2: How can failure caused by combined bending and tension be accurately predicted in manufacturing feasibility studies?

s.RQ. 3: How can failure caused by edge effects accurately predicted in manufacturing feasibility studies?

1.3 Hypotheses

As the main research question is too broad to be covered by a single hypothesis, three hypotheses will be presented - one related to each of the sub-questions presented above. The hypotheses will be presented so that hypothesis 1 will related to sub-question 1 and so forth:

H. 1: A transformation of the formability evaluation from the standard $(\varepsilon_2, \varepsilon_1)$-space to a space independent of the load history will increase the prediction accuracy

H. 2: A bending correction of the standard Forming Limit Diagram will increase the failure prediction accuracy of components experiencing stretch-bending.

H. 3: Inverse modelling of the ISO 16630 Hole Expansion Test to obtain a limit strain value will increase the failure prediction accuracy of components experiencing edge effects.

Chapter 2
RESEARCH METHODOLOGY

The following chapter outlines the research methodology used by the author. The research methodology employed during the thesis work is based on the Design Research Methodology (DRM) described by Blessing and Chakrabarti 2009.

2.1 Areas of Relevance and Contribution

The Areas of Relevance and Contribution (ARC) diagram is a visualization of the disciplines and domains of knowledge that a researcher expects to either contribute to or be relevant for the research to be conducted. The diagram is build around a central key focus area - in this thesis, that key area is "*Increased Accuracy in Sheet Metal Forming (SMF) Failure Models*" - and building on that key focus area, the researcher maps out which connected areas a scientific contribution is expected, and what knowledge is essential to do so. For the research presented in this thesis, an ARC diagram has been created and is presented in Figure 2.1.
In the presented ARC diagram, three branches are connected to the key focus area; Failure Phenomena, Experimental Work, and Virtual Prototyping. In order to achieve an increased failure model accuracy for the complex load cases that is the centre of the research questions, an extended knowledge on the different failure phenomena is essential. Observing Figure 2.1 the reader will notice that the failure phenomena is not marked as essential knowledge, but instead as a contribution. This is because the main target of the presented research is to contribute with knowledge on these failure phenomena, but in order to do so, existing knowledge is essential. The second branch is Experimental Work, where the research is expected to bring a contribution to test methods and data analysis either through improvement of existing methods or development of new approaches. As experimental work is a physical entity, there are some essentials that are needed in order to perform the tests, namely test equipment such as Digital Image Correlation (DIC), and press and tooling. Besides the test equipment, the sheet metal that should be tested is naturally also essential. The last branch concerns Virtual Prototyping, which in this context is synonymous with Finite Element models. As the research targets

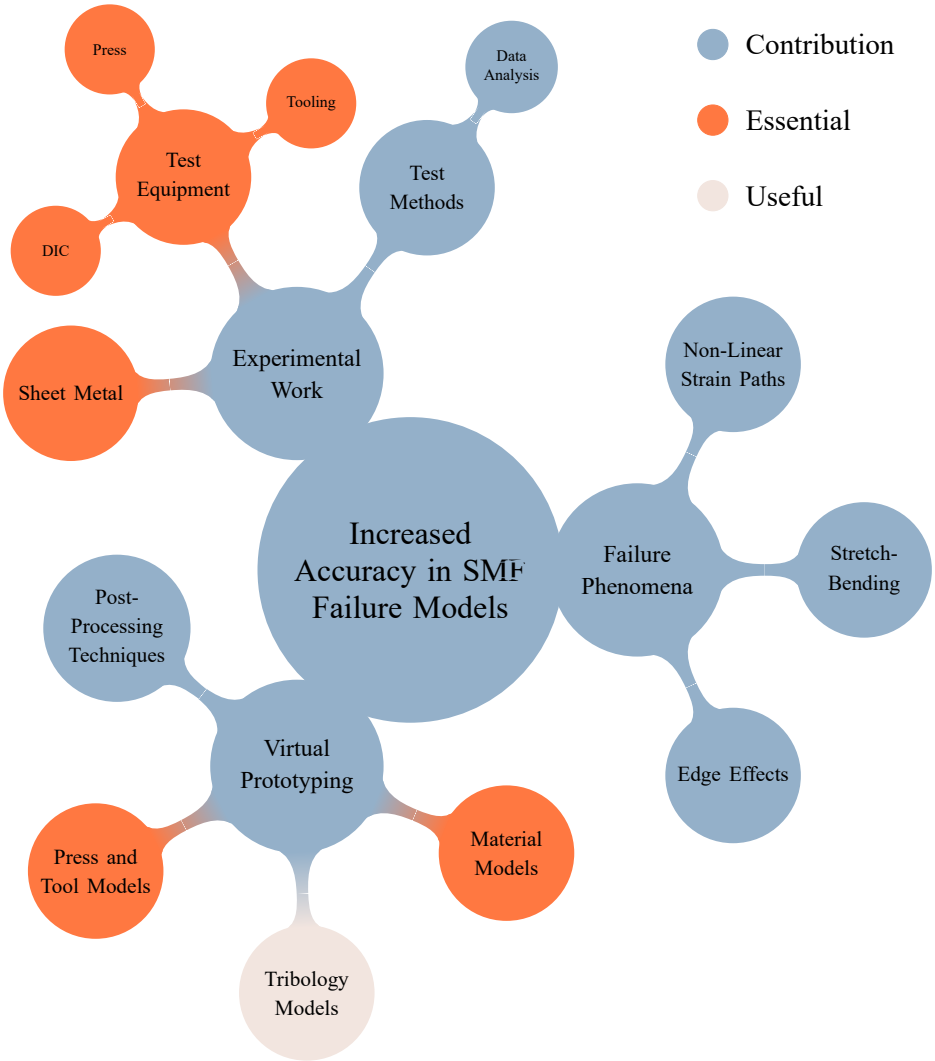

Figure 2.1: Areas of Relevance and Contribution (ARC) diagram. Areas where contribution is made are highlighted with blue, essential related areas are highlighted with orange, and useful related areas are highlighted with tan.

failure prediction, there is a clear expectation that the presented research will bring a contribution to the virtual prototypes, and post-processing techniques in particular. In order to do so, knowledge on the press line and tool geometries along with an accurate description of material behaviour during deformation are essential. Besides the essential knowledge on press line, tool and material models, advanced tribology models could also become useful if reaching a point where the standard Coulomb friction model is no longer sufficient to describe the friction conditions between the tool and blank.

2.2 Qualification as Research Area

All research conducted is subject to scrutinizing from their respective communities. Before conducting any research, any researcher must ensure that the chosen topic qualifies as a research topic. To make this assessment, Blessing and Chakrabarti 2009 have proposed three requirements that needs to be fulfilled - the research must be *academically worthwhile*, *practically worthwhile*, and *realistic*. The research presented in this thesis fulfills all three requirements. During a review of related work (presented in Chapter 3) it was found that numerous other research is already being conducted on the topic of failure prediction of complex load cases by other academic institutes and industrial actors, thereby making the research *practically worthwhile*. In terms of the research being academically worthwhile and realistic, the problem(s) posted in this research area are highly relevant and challenging to a degree where industry leaders have yet to agree on a solution. Therefore the research is highly expected to contribute to both knowledge and understanding.

2.3 Research Quality and Validity

To ensure the quality and validity of the research presented in this thesis all of the included papers have been peer-reviewed and published in the conference proceedings of highly recognized conferences within the sheet metal forming community. All simulations presented in the thesis have been performed based on best practice from industry leaders, and all experiments have been conducted in close collaboration with Research Institutes of Sweden (RISE). Data analysis and collection as well as publication of papers have been done in collaboration with external partners. Additional information on each paper is available in Chapter 7.

2.4 Mapping of Papers to the DRM Framework

The Design Research Methodology is divided into four different phases, the Research Clarification (RC) phase, the Descriptive Study I (DS-I), the Prescriptive

	RC	DS-I	PS	DS-II
s.RQ. 1	Review-Based	Comprehensive		
s.RQ. 2	Review-Based	Comprehensive	Initial	
s.RQ. 3	Review-Based	Comprehensive		

Table 2.1: Different types of research projects in the DRM framework used for this Thesis.

	RC	DS-I	PS	DS-II
Paper A		x		
Paper B			x	
Paper C		x		
Paper D		x		

Table 2.2: Mapping of the included papers to the phases of the research projects. The colors represented in the table corresponds to the color coding of the research projects in Table 2.1.

Study (PS), and the Descriptive Study II (DS-II). Each phase can have a degree of depth to it, which is *Review-Based*, *Comprehensive*, or *Initial*, which have been defined by Blessing and Chakrabarti 2009. The *Review-Based* depth relies on a literature survey of the state-of-the-art, and is primarily used in the RC phase of the project. The *Comprehensive* depth builds on a combination of literature surveys and data generated by the researcher. Final the *Initial* depth is used to build on top of findings and present initial models, and draw conclusions.
Since the three sub-research questions presented in the Thesis is not directly related, it was decided to treat them as three separate research projects, each with their own type of research project according to the DRM framework. The three types chosen can be found in Table 2.1, and a mapping of the included papers to the phases of the projects can be found in Table 2.2.

Chapter 3

RELATED WORK

3.1 Review of Related Work

As presented in Chapter 1, the research questions center around three complex load cases in sheet metal forming; non-linear strain paths, stretch-bending and edge cracks. These three complex load cases are highly relevant to the sheet metal forming industry, where Manopulo and Carleer 2019 recently coined the term *Advanced Formability Analysis (AFA) framework* to address the three aforementioned load cases. Advances within model accuracy on these three topics will not only benefit the stakeholders in the sheet metal forming industry, but society in general, as advanced failure models will ease the effort to introduce new complex, lightweight, and sustainable materials into e.g. the automotive and aerospace industries (Andrade et al. 2016; Manopulo and Carleer 2019). The following subsections will present an overview of some of the work that has currently been done on the topic of the three load cases.

3.1.1 Non-Linear Strain Paths

Since the pioneering work by Graf and Hosford 1993, uncovering that strain path non-linearity has an impact on the standard Forming Limit Diagram (FLD), several authors have been working on developing a reliable failure model that could predict failure due to non-linear strain paths. One of the early attempts was proposed by Stoughton 2000 where a fundamental change in how failure should be assessed was proposed. Historically, since the original FLD was proposed by Keeler and Backofen 1964, the major and minor strains have been used to assess the remaining formability of a metal sheet, however, with the proposal of Stoughton 2000 the remaining formability should be assessed in terms of the major and minor stresses. Another method that has been proposed, and has gained traction in some parts of the sheet metal forming community, is the Generalized Incremental Stress State Damage Model (GISSMO) orginally proposed by Neukamm, Feucht, and Haufe 2008 where the standard Forming Limit Curve (FLC) is transfromed from the principal

strain space (ε_2,ε_1) to a 2D alternative evaluation space defined by the equivalent plastic strain $\bar{\varepsilon}^p$ and the stress triaxiality η, and later extended to a 3D evaluation space with the addition of the Lode angle θ by Basaran et al. 2010. A promising method for predicting failure due to non-linear strain paths has been proposed by Volk and Suh 2013. The Generalized Forming Limit Concept (GFLC) is a phenomenological meta-model based on a large number of experiments with a bi-linear deformation history. Based on the meta-model, the forming operation in question can be compared to one of the pre-run experiments.

3.1.2 Stretch-Bending

The failure mode of stretch-bending has been discussed in the sheet metal forming community for a while, where an early example of the influence stretch-bending influence was presented by Sriram et al. 2003. Since then both Atzema et al. 2010 and Ertürk, Sester, and Selig 2018 have been investigating how this phenomenon could be accounted for in failure prediction, before Barlo 2019 and Barlo et al. 2019 proposed the Bending Corrected Forming Limit Surface (BC-FLS)

3.1.3 Edge Effects

The approach to failure prediction caused by edge effects differs significantly from that of non-linear strain paths and stretch-bending. Failure due to non-linear strain paths and stretch-bending is caused by the deformation modes and -history of a component, i.e. these occur during the actual forming operation. For edge effects on the other hand, the failure observed here is highly influenced by the blank preparation process, i.e. before the actual forming operation. For this section, two types of edge types are considered; a straight cut edge and a circular hole. In terms of lab scale tests to identify the edge formability of a material Table 3.1 outlines some of the most common approaches used.

Circular Hole	**Straight Cut Edge**
Hole Expansion Test	Double-Bending Test
KWI Test	Diabolo Test
Open Hole Tensile Test	

Table 3.1: Outline of different lab-scale test designed to evaluate the edge formability of a material.

The majority of research on edge effects in circular holes centers around the ISO standardized Hole Expansion Test (ISO 16630, *Metallic materials – Sheet and strip – Hole expanding test* 2018), where a conical punch with a tip angle of 60° is driven through a punched hole with a diameter of 10 [mm]. In the ISO standard, the hole

preparation method is specified so that the hole should be punched with a cutting clearance of $12 \pm 1\%$ if the sheet thickness $t \geq 2.0$ or $12 \pm 2\%$ if the sheet thickness $t < 2.0$. According to Wang, Greve, and Wierzbicki 2015 the hole punching process impacts the edge formability of the material, as micro-cracks on the wall of the hole in the thickness direction can be created during this process. The work of Yoon et al. 2016 investigated the impact of these micro-cracks by subjecting a punched hole to a subsequent milling process to remove the micro-cracks and neutralize the accumulated shear damage. The investigation was carried out for three steels; CR TWIP, a CR strainless (CR SUS304), and a CR low carbon (CR LC), utilizing the approach for the Hole Expansion Test presented in the ISO standard. The reported finds can be see in Table 3.2 .

	Punching	**Milling**
CR TWIP	42 %	68 %
CR SUS304	26 %	73 %
CR LC	57 %	112 %

Table 3.2: Hole Expansion Ratio values reported by Yoon et al. 2016 displaying the impact of micro-cracks and accumulated shear damage from the hole punching process.

As can be seen from the reported results by Yoon et al. 2016 the neutralization of the accumulated shear damage has a large impact on the Hole Expansion Ratio of the test. A similar trend was presented by Liewald and Gall 2013 for the straight cut edge, where the major strain at failure was seen varying with two different cutting clearances for a new and worn tool. In this study, it was presented, that a large cutting clearance (15 %) was much more sensitive to the tool condition than a tight cutting clearance (5 %).

3.1.4 Upstream Impact of Increased Model Accuracy

When investigating the impact of increased model accuracy, one should not only look at the impact on the manufacturing feasibility studies, but also turn the attention to the larger upstream impacts. As already mentioned in the introduction of this section, both Manopulo and Carleer 2019 and Andrade et al. 2016 have explained how the introduction of higher failure model accuracy will result in a reduced effort to introduce more advanced materials into production, where the two most predominant drivers for doing so is lightweight structures, and more sustainable products. According to Manopulo and Carleer 2019 and Manopulo and Carleer 2020 the increase in failure model accuracy will not only ease the introduction of new materials, but also aid in reducing the development time for a given component or product. The reduction in development time, can further be split into two benefits. Firstly, according to Bylund 2004, a reduction in development

time will results in a reduction in 'time-to-market' i.e. the length of time from the decision to launch a new/updated product until it is released to the market. Secondly, experience tells us, that a reduction in development time equals a reduction in development costs. Common for these two benefits are, that they both have a positive impact of the same thing - the profit.
Besides reducing development time and the effort to introduce more advanced materials, the increase of failure model accuracy is also expected to have an impact on two other areas; the amount of scrap material in production, and the time spent on error resolution of non-conforming (NC) parts. Starting with the reduction in scrap, it is assumed, that once failure model accuracy is increased, and a certain level of confidence in these is obtained, that CAE engineers will feel more confident in utilizing a higher percentage of the material formability potential, whereas today a relatively large safety margin is in place to account for the shortcomings of the current failure models. By utilizing more of the formability potential, less surplus material is needed, less material is cut away during the manufacturing process, and a increased design freedom is obtained. Next, experience says, that an increase in failure model accuracy will reduce the time spent on resolving issues related to non-conforming parts in production. With increased model accuracy (and trust), it will be easier to perform root-cause analyses to understand how a problem could occur, which was not there in the beginning e.g. due to shifting conditions in the press-line setup, tool wear, etc.

3.2 Reference Model

The following section presents the initial reference model for the research presented in this Thesis according to the DRM framework by Blessing and Chakrabarti 2009. The reference model is used to link information gathered from the review of the related work together to obtain the bigger picture of which goal one is working towards. Based on the review presented in the previous section, a reference model has been created for this research, which is presented in Figure 3.1.

Ref #	Reference
1	Manopulo and Carleer 2019
2	Bylund 2004
3	Manopulo and Carleer 2020
4	Andrade et al. 2016
5	Banabic 2010
6	Barlo et al. 2019

Table 3.3: References used for the initial reference model.

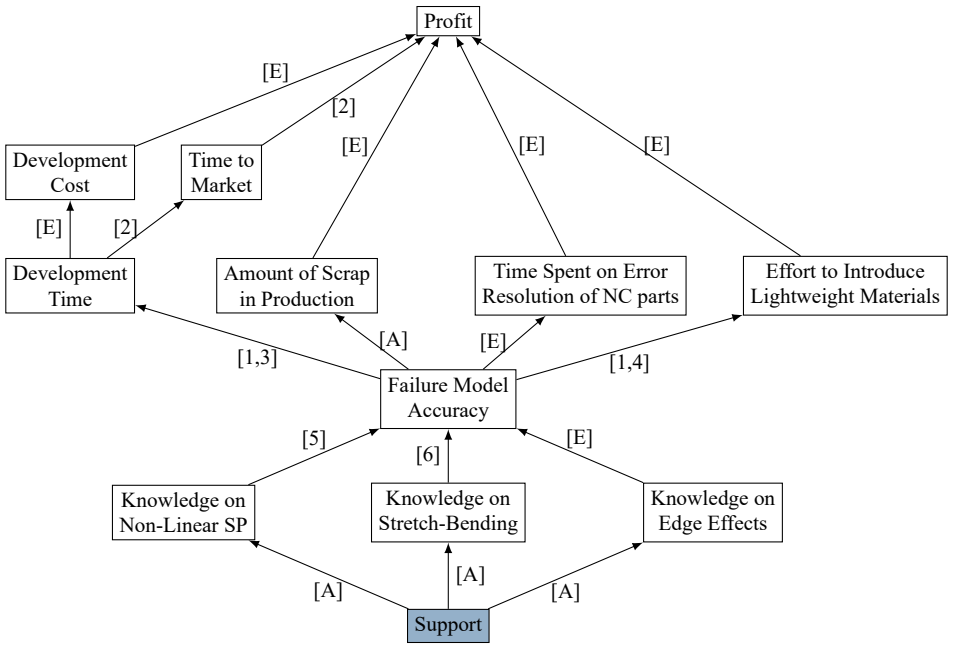

Figure 3.1: Initial reference model. The links between the boxes are denoted either [A] for assumption, [E] for experience, or e.g. [1] for information retrieved from a reference. The references used can be found in Table 3.3.

3.3 Impact Model

Based on the reference model presented in Figure 3.1, an impact model can be created outlining what impact the conducted research will have. Based on the research questions and the ARC diagram presented in Section 2.1, the following impact is expected:

- Understanding of strain path changes
- Understanding of the influence of bending and the importance of surface versus membrane straining.
- Understanding of the mechanics of edge effects and their impact on failure strain.
- Advanced Failure Analysis framework and implementation in commercial FE-code.

Figure 3.2 presents the impact model, where the expected impacted areas are highlighted with green, and those not expected to be directly impacted by the research are highlighted with red.

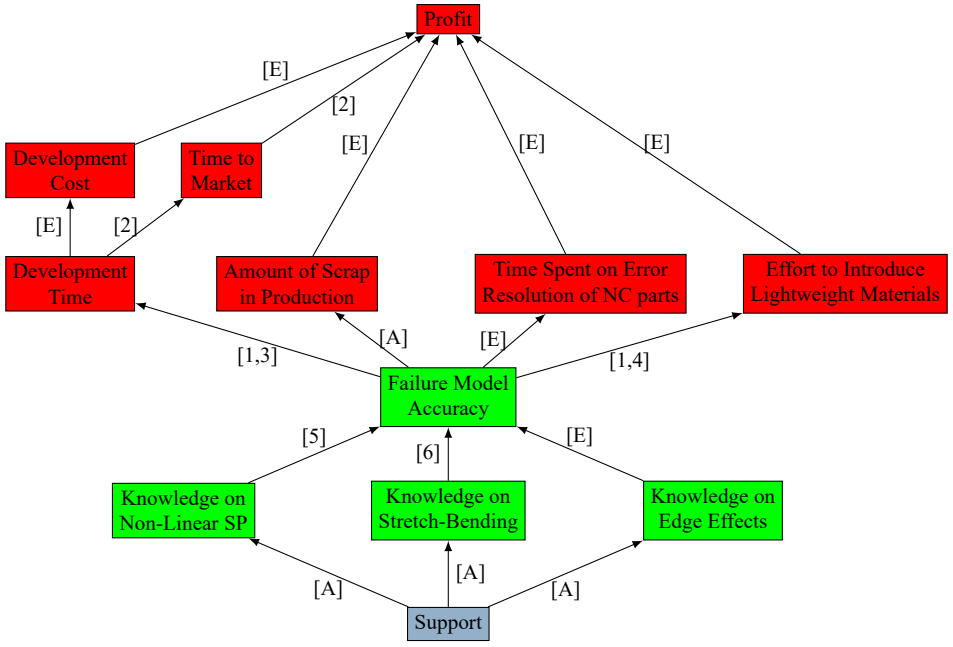

Figure 3.2: Impact model.

Chapter 4

SHEET METAL FORMING SIMULATIONS

4.1 The Application of Sheet Metal Forming Simulations

With the purpose of ensuring the manufacturing feasibility of designed sheet metal components, simulations have been used for decades, with the first models presented in the 1960's (Ablat and Qattawi 2017). Since then various methods have been used, including (but not limited to) the Finite Difference Method (FDM), the Finite Element Method (FEM) and the meshfree (meshless) method. Since the 1970's the Finite Element Method has been the industry standard, which it still is to this date. According to Cook et al. 2002 the Finite Element Method can be defined as "*a method for numerical solution of field problems*" where in the mathematical world, field problems are described by differential equations or by an integral expression. When discussing the Finite Element Method within sheet metal forming, one have to consider the non-linear interrelations between parameters such as tribology, large deformations, and constitutive relations. Therefore, for the application of the Finite Element Method, the Newton-Raphson method with a radial return scheme is used to solve the differential equations, where the main target of the Newton-Raphson scheme is to reach a state where the residual force ψ is as close to zero as possible. The residual force ψ is defined as:

$$\psi = \boldsymbol{f}_{int} - \boldsymbol{f} \tag{4.1}$$

where the internal ($\boldsymbol{f}_{int}$) and external ($\boldsymbol{f}$) forces are defined as:

$$\boldsymbol{f}_{int} = \int_V \boldsymbol{B}^T \boldsymbol{\sigma} \, \mathrm{d}V \qquad ; \qquad \boldsymbol{f} = \int_S \boldsymbol{N}^T \boldsymbol{t} \, \mathrm{d}S + \int_V \boldsymbol{N}^T \boldsymbol{b} \, \mathrm{d}V \tag{4.2}$$

For sheet metal forming, the target is to have a lasting deformation of the sheet, why an elasto-plastic approach to the Finite Element Method must be taken, where the transition between elastic and plastic deformation is seen when the following condition is no longer fulfilled:

$$\bar{\sigma} - \sigma_{y0} < 0 \tag{4.3}$$

where $\bar{\sigma}$ is the equivalent stress governed by the choice of constitutive model, and σ_{y0} is the initial yield stress of the material. Working with sheet metal, the thickness of the blanks are significantly smaller than the measurements in the other directions, which allows for an assumption of plane stress ($\sigma_{13} = \sigma_{23} = \sigma_{33} = 0$). The plane stress assumption further allows for the application of shell elements in the Finite Element models, significantly reducing computational time compared to using the three-dimensional solid elements.
Running Finite Element Models with the purpose of validating a design in sheet metal forming, the objective is to investigate three main outputs; necking and fracture, surface defects, and springback. The first output, necking and fracture, indicates if the designed component can be manufactured without it losing it's structural integrity. The output covers both the terms necking and fracture, but could in fact be labelled failure since, depending on the loading history, the failure label changes between the two definitions. A more clear definition of the term "failure" used in this thesis will be presented in Chapter 6. The second output is surface defects, and lies close to the first output, however, here the surface of the component is investigated to see if any peculiarities are present. One thing is to investigate the structural integrity of the component, but another objective is to ensure that the surface is fit for use, where e.g. in the automotive components visible on the outside of the car, there is a high demand for no defects. Lastly, the third objective is on springback, which is a phenomenon caused by the elastic properties and stress level of the material stamped. The amount of springback must be investigated (and compensated) to ensure that the stamped panel is within geometrical specifications to allow for down-stream assembly, e.g. in the automotive industry for the Body-in-White (BiW).
In order to be able to asses these outputs, the Finite Element Model takes a variety of input, where these can be split into three main groups; Material Parameters, Tribology, and Tool and Press Line Parameters. The first group, material parameters, covers the mathematical description of how the material behaves during deformation, also named the constitutive model. The second group, tribology, covers the information around lubrication, and how the friction between sheet and tool develops during the forming process. Lastly, the third group, Tool and Press Line parameters, covers the tool geometries, and the press line setup, such as forming and trimming stages, as well as the operation velocity and the blank holder forces. An overview of the input and output groups are presented in Figure 4.1. The following sections in this chapter will present the importance and impact of the input parameters to the model, whereas the assessment of output parameters handled in this thesis will be limited to the objective necking and fracture, and will be presented in Chapter 6.

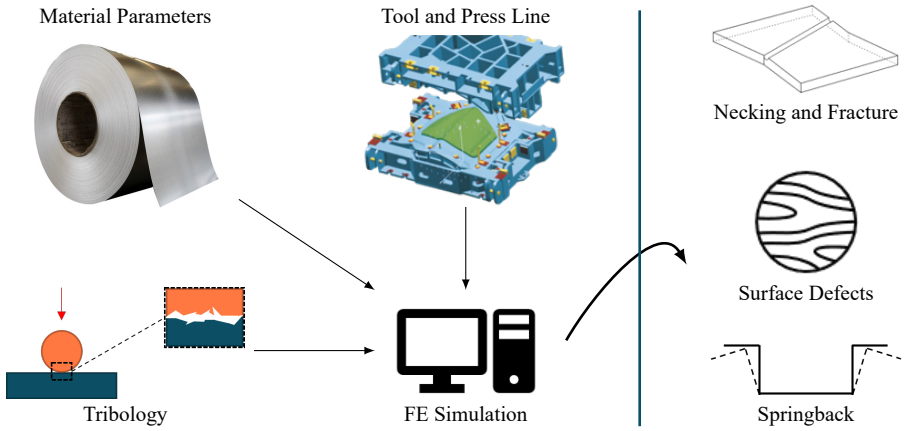

Figure 4.1: Critical input and valuable outputs from a Finite Element simulation in a sheet metal forming context. The model is adopted from the work by Sigvant, Pilthammar, et al. 2018.

4.2 The Importance of Applied Constitutive Model

One of the most influential aspects of any Finite Element model in a sheet metal forming context, is the constitutive model (also known as material model) applied. The constitutive model governs the relationship between stresses and strains once a component transitions from elastic deformation to plastic deformation. As most current and popular failure evaluation methods relies on the evaluation of strains (major, minor, or plastic), the choice of constitutive model is of great importance. According to Banabic 2010 the yield criteria for constitutive models can be divided into three groups; *yield criteria for isotropic materials*, *yield criteria for anisotropic materials*, and *advanced anisotropic yield criteria*, where isotropy refers the materials mechanical properties with respect to the rolling direction. Without running any Finite Element simulations, the impact of the chosen constitutive model can be seen on the yield surface of a given material. To exemplify this, a VDA239 CR4 mild steel alloy has been chosen, where the hardening curve can be seen in Figure 4.2, and a comparison of the yield surface of three different constitutive models can be seen in Figure 4.3.

For the comparison presented in Figure 4.3, a constitutive model from each of the three groups have been chosen, where the isotropic yield criteria is represented by the von Mises constitutive model, the anisotropic yield criteria is represented by the Hill'48 constitutive model, and the advanced anisotropic yield criteria is represented by the BBC2005 constitutive model. Observing the comparison in Figure 4.3, the Hill'48 and BBC2005 constitutive models display highly similar behaviour for this particular material, however, slight deviations are observed, which can have

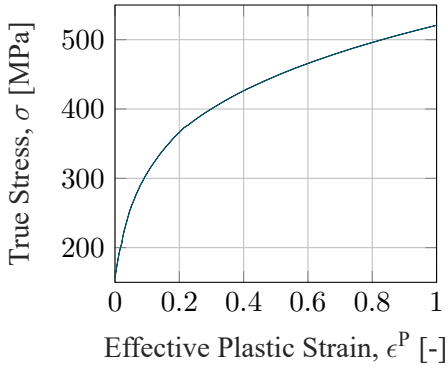

Figure 4.2: Hardening Curve of the VDA239 CR4 material.

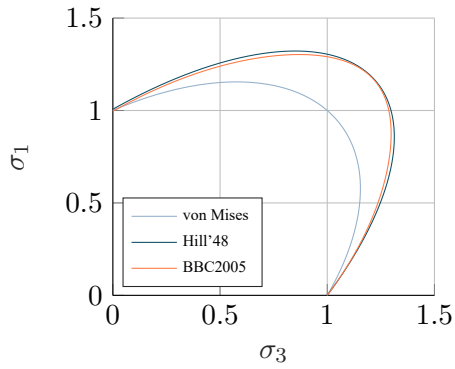

Figure 4.3: Comparison of the von Mises, Hill'48, and BBC2005 constitutive models for the VDA239 CR4 material.

a significant impact on the strain predictions for the simulation. To exemplify the impact, a comparison of simulated and experimental strain profiles of an Limiting Dome Height (LDH) test was presented by Sigvant and Pilthammar 2019 for the same VDA239 CR4 mild steel grade. Figure 4.4 presents this comparison where it can be seen, that even though the yield surfaces are highly similar, the minor deviations have a large impact on the strain predictions.

However, running simulations with material models from the advanced anisotropic yield criteria group does require extensive material testing to obtain a valid and accurate material model. Table 4.1 outlines the number of material parameters that needs to be calibrated in order to set up a valid material model. The easiest constitutive models to set up is the isotropic models (exemplified by von Mises) as only the yield stress in one direction is needed. As isotropic material behaviour is assumed, the same value can be used in all directions (0°, 45°, 90°). For the anisotropic yield criteria (exemplified by Hill'48) a few more parameters are needed to calibrate the material model, as the mechanical properties in the different directions are needed. Table 4.1 presents a case, where the yield stress is determined in one direction, and the Lankford coefficients (r_i) are used to obtain the yield stresses in the different directions. Lastly, for the advanced anisotropic yield criteria (exemplified by BBC2005) a full set of material parameters are needed for the calibration of the constitutive model. Besides characterizing the yield stresses and the Lankford coefficients in the three directions with respect to the rolling direction, a yield stress and Lankford coefficient are also determined for the biaxial point (σ_b and r_b). A more interesting aspect of the BBC2005 constitutive model is the material parameter M. Observing the expression for the equivalent stress $\bar{\sigma}$ presented in Eq. 4.4, the material parameter M replaces the integer exponent so that $M = 2k$. Ac-

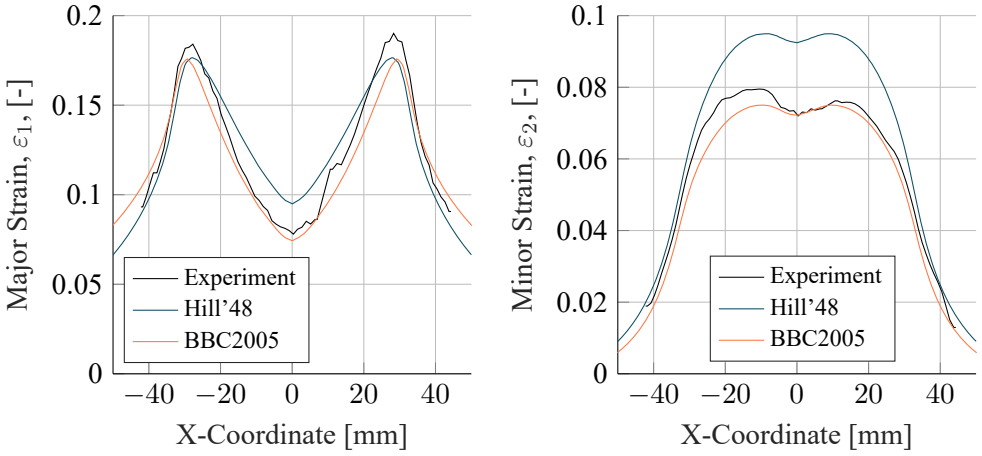

Figure 4.4: Strain profiles over a cross-section of a LDH-test of the VDA239 CR4 mild steel. Experimental results compared to simulations using Hill'48 and BBC2005 constitutive models (Sigvant and Pilthammar 2019).

Constitutive Model	σ_0	σ_{45}	σ_{90}	σ_b	r_0	r_{45}	r_{90}	r_b	M
von Mises	x								
Hill'48	x				x	x	x		
BBC2005	x	x	x	x	x	x	x	x	x

Table 4.1: Material parameters needed for calibration of different constitutive models. The table is adapted from Banabic 2010.

cording to Banabic and Sester 2012 the parameter k takes on a fixed integer value depending on the crystallographic structure of the material, so that for Body Centered Cubic (BCC) materials $k = 3$ and for Face Centered Cubic (FCC) materials, $k = 4$, meaning that the constitutive model would take $M = 6$ and $M = 8$ for BCC and FCC materials respectively.

$$\bar{\sigma} = \left[a(\Lambda + \Gamma)^{2k} + a(\Lambda - \Gamma)^{2k} + b(\Lambda + \Psi)^{2k} + b(\Lambda - \Psi)^{2k}\right]^{\frac{1}{2k}} \tag{4.4}$$

Applying the BBC2005 constitutive model with the proposed values for M will increase the model accuracy compared to the Hill'48 and especially the von Mises constitutive models. However, more accurate values for the M-parameter can be obtained through inverse modelling. Once again, using the VDA239 CR4 mild steel alloy as an example, the mild steel is a BCC structured material, and therefore by default taking on the value $M = 6.0$. Performing the inverse modelling with the intend to further calibrate the M-parameter, a value of $M = 4.5$ can be found. A comparison of the influence of the M-parameter on the yield surface can be found in Figure 4.5. In the comparison, the deviations most significant between the two yield surfaces are located in and around the area that effects the plane strain region.

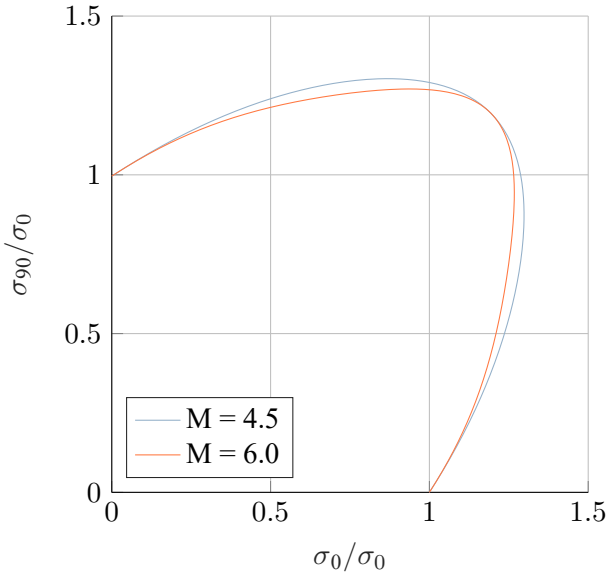

Figure 4.5: Comparison of the BBC2005 yield surface with changes to the material exponent M

To understand the actual impact of the change in the M-parameter on the strain predictions, an industrial example is used. Figure 4.6 presents an automotive component - a wheel house from a first generation Volvo XC60 manufactured from the

VDA239 CR4 mild steel alloy. As can be observed, the component displays a split, however, this particular issue is not of interest in this particular case (this has been addressed in Paper C, and will be address later on as well).

Figure 4.6: First generation Volvo XC60 wheel house manufactured from the VDA239 CR4 mild steel alloy.

To investigate the impact, two simulations are run in the commercial Finite Element code AutoForm® R10 where the only difference between the two models is the M-parameter. Figure 4.7 (a)-(d) presents the outcome of the simulation, where figures (a) and (c) displays the advanced formability option on the component, and figures (b) and (d) presents the strain field in the Forming Limit Diagram.
As can be seen, both models provide a false negative in predicting the split in the physical component presented in Figure 4.6, however in this context, more interesting is the strain field in the remaining areas of the component. Using the calibrated M-value of 4.5, a reasonable fit with reality is obtained, with no failure indication on the component. However, observing the results obtained from the simulation with the standard value of M, a false positive failure is indicated, in an area that does not display signs of failure in the physical component.

4.3 The Importance of Tribology Models

Another important, aspect of setting up a valid Finite Element model is the tribology, i.e. the description of the frictional behaviour between tool and sheet. One of the commonly used friction models used in sheet metal forming simulations is the Coulomb friction model, where a constant friction coefficient μ_c is used. Throughout the years, several authors such as Hol et al. 2012 have discussed and proven the inefficiencies of the Coulomb friction model due to its inability to account for contact pressure between the sheet and tool, the straining of the sheet, and the relative

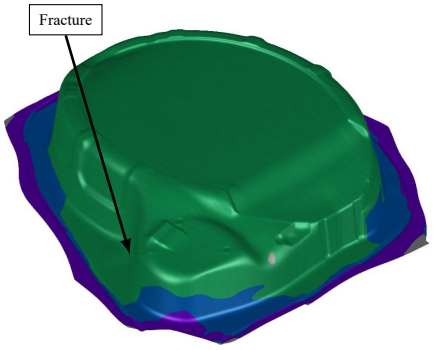

(a) Advanced Failure (M = 4.5)

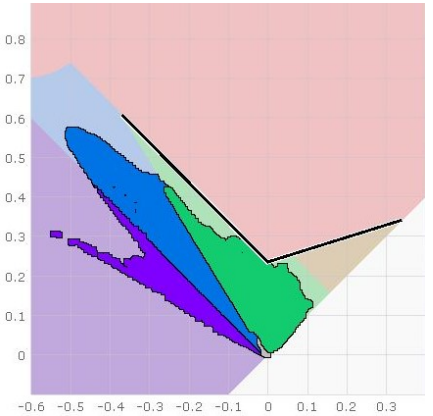

(b) Strain field (M = 4.5)

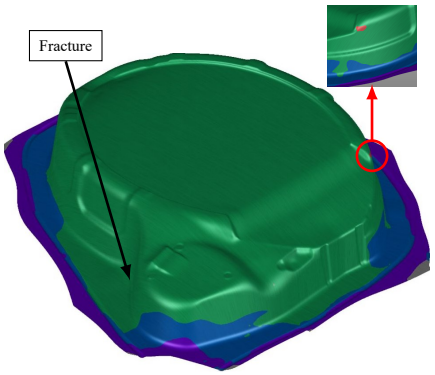

(c) Advanced failure (M = 6.0)

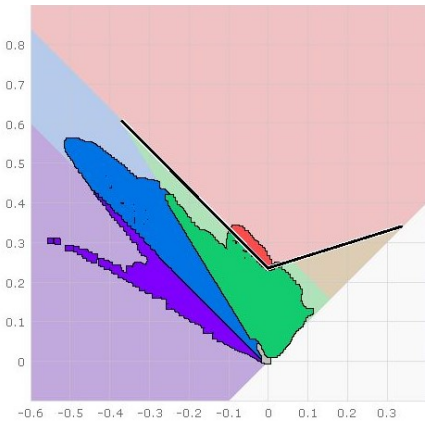

(d) Strain field (M = 6.0)

Figure 4.7: Comparison of strain predictions using the BBC2005 constitutive model with the material parameter M = 4.5 and M = 6.0.

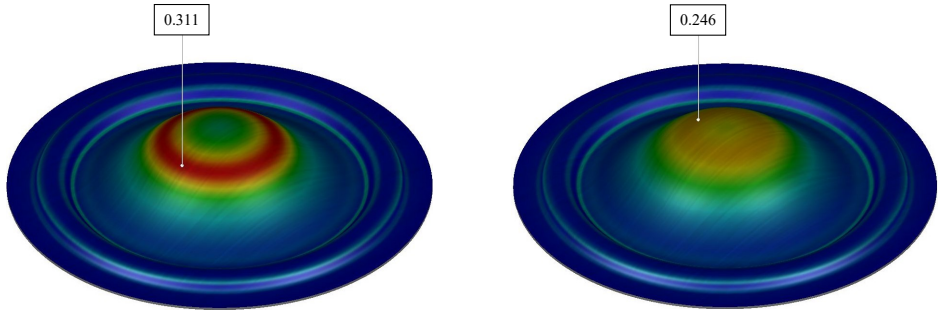

Figure 4.8: Illustration of the impact of tribology model on the maximum major strain in a Limiting Dome Height (LDH) test. Figure (a) presents the Finite Element model run with a Coulomb friction model with $\mu_c = 0.15$ and figure (b) presents the same model, but run with a TriboForm model for Dual Phase AHSS (GI Coated) lubricated with draw oil on tool steel, and a lubrication amount of 1 [g/m^2].

velocity of the sheet. To account for the aforementioned parameters' impact on the friction, the TriboForm software can be utilized as a plug-in to AutoForm R10. To exemplify the impact of a static (Coulomb) versus a dynamic (TriboForm) friction model, two simulations has been run of a Limiting Dome Height (LDH) test of a DP800 dual-phase high strength steel (AHSS) alloy. All numerical parameters are identical except for the modelling of the friction conditions. For the static friction model, a constant coefficient of friction $\mu_c = 0.15$ (AutoForm R10 default value) was used. For the dynamic friction model, a standard library model for a dual phase AHSS (GI coated) alloy was used with the lubrication specified as draw oil, and tool type 'tool steel'. Further parameters can be modified to change the model, such as lubrication amount, sheet roughness, and tooling roughness - however for this exemplification, the standard values were kept (1.0 [g/m^2], 1.0 [μm], and 0.6 [μm]). For comparison, the magnitude and location of the maximum major strain in the Finite Element model is chosen. Figure 4.8 presents the major strain fringe plots (equal scales, 0-0.32) of the two run models with 4.8(a) presenting the results for the static friction model, and 4.8(b) presenting the results for the dynamic friction model.

From Figure 4.8 it becomes clear that the change in friction model has a significant impact on the major strain distribution of the LDH test. The first, and most notable difference is the magnitude of maximum major strain value, which is reduced from 0.311 to 0.246 by switching from a static to a dynamic friction model. Another important difference to notice is the location of the maximum major strain, which has shifted from the static to the dynamic friction model. Lastly, the strain distribution should also be noted, where in the Finite Element model run with the static friction

model, a strain concentration is seen in a ring, whereas a more evenly distribution of strain in the area of punch contact is seen for the Finite Element model with the dynamic friction model.

4.4 The Importance of Accurate Tool and Press Line Parameters

The last main group of input is the tool and press line parameters. It is only logical, that when building a Finite Element model to investigate if a component is manufacturable, the model must replicate the conditions of which the part is to be manufactured under. Here, especially important is the tooling that will be used is modelled accurately. Today, the tooling is designed in CAD software, ensuring that a digital 3D model is available, thereby easing the setup of the Finite Element model. In the Finite Element models used today, an assumption of rigidity is used for the tooling - i.e. the tools are not subject to deformations during the forming process. However, in the work presented by Pilthammar 2017, it was presented how the tooling and press do experience elastic deformations during the stamping process, potentially causing an issue when moving the manufacturing of the component from the virtual to the real world.
Besides the modelling of the tools, it is also important to model the process (press line) parameters correctly, where parameters such as the ram speed (velocity of the forming operation) and the draw depth are the most dominant.

Chapter 5
EXPERIMENTAL WORK

The following chapter will outline the experimental work performed in relation to this Thesis. Each of the following sections will present experimental procedures and targets for a variety of experimental setups, however the majority of the results will be presented later on in Chapter 8. Lastly, an overview of the relation between the experiments and the sub-research questions (s.RQ) will be presented.

5.1 Digital Image Correlation

When running experiments, one must naturally be able to evaluate the experiment afterwards. In most cases in sheet metal forming, the principal strains of a test piece is of interest, why the principal strain field history during deformation is desirable to capture. For this purpose Digital Image Correlation (DIC) is often used. Digital Image Correlation is by the International Digital Image Correlation Society (iDICs) defined as "*an optically-based technique used to measure the evolving full-field 2D or 3D coordinates on the surface of a test piece throughout a mechanical test.*" (*A Good Practice Guide for Digital Image Correlation* 2018). Based on these measured evolution of coordinates, quantities-of-interest can be determined, e.g. displacements, strains, velocities, etc. The DIC technique relies on the tracking of points on the test piece, where the common approach to apply these points is a stochastic speckle pattern. An illustration of a speckle pattern can be found in Figure 5.1.
The process of applying the speckle pattern is initially to apply a white coat of paint to the region of interest (RoI) of the specimen, and subsequently apply the stochas-

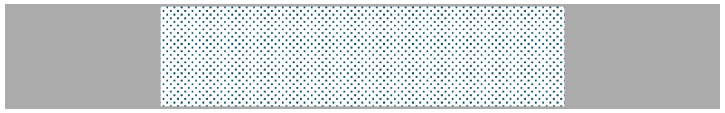

Figure 5.1: Speckle pattern, exemplified on a tensile test, used for recording the evolution of the full-field coordinates in the DIC technique.

tic speckle pattern with black paint. The motivation for initially applying the white coat of paint is to create a sharp contrast between the black speckles and the background that make it easier for the correlation algorithm to detect the movement. Several factors can influence the quality of the speckle pattern, however, Corres 2022 found that one of the crucial steps to ensure a usable speckle pattern is to de-grease the test specimen prior to applying the white coat of paint. If not done properly, the white coat of paint will not stick to the specimen during deformation, and the coat will crack off during deformation, as illustrated in Figure 5.2.

Figure 5.2: Cracked paint due to insufficient de-greasing of test specimen (Corres 2022).

For the experimental work presented in this thesis, an ARAMIS DIC system is used. The ARAMIS system is, within the sheet metal forming community, the most used system, and for the presented work, ARAMIS is used when out-of-plane deformations are present in the experiment. The two cameras used for the ARAMIS system is mounted on top of the die in a mechanical press, thereby shielding it from reflections from the test piece. The ARAMIS camera and lighting setup can be seen in Figure 5.3(a) and example of a strain field captured by ARAMIS can be seen in Figure 5.3(b).

5.2 Stretch-Bending

The execution of the stretch-bending experiments is related to the work presented in Papers A and B, where it is investigated how the current available failure prediction approaches capture the stretch-bending phenomenon. The stretch-bending tests are carried out with three different punch nose radii of 3, 6, and 10 [mm] on an AA6016 aluminium alloy, and a cross-section view of the experimental setup can be seen in Figure 5.4.
In the experimental setup, the punch is offset 6 [mm] to one side from the center,

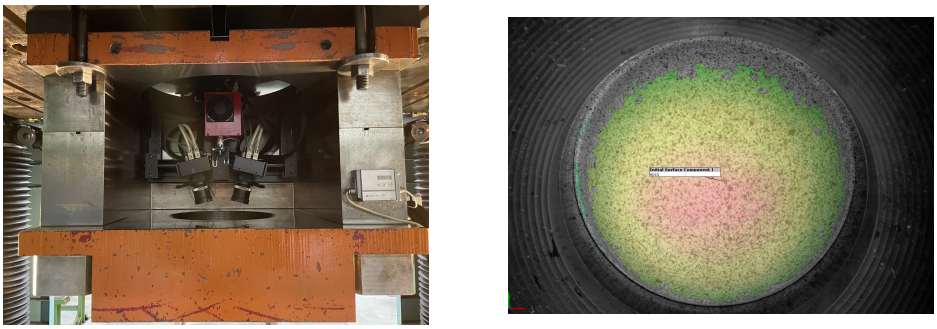

(a) (b)

Figure 5.3: Presentation of (a) the ARAMIS 3D DIC system, and (b) a strain field captured with the ARAMIS DIC system.

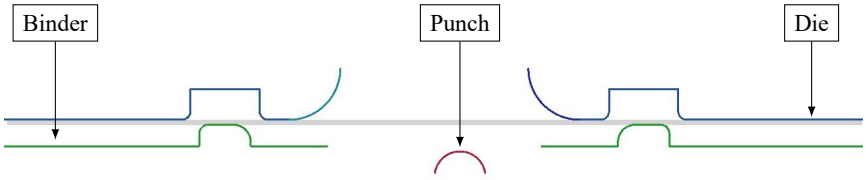

Figure 5.4: Cross-section view of the stretch-bending experimental setup.

to eliminate the stochastic behaviour of the location of the resulting fracture, so that it always occur in the same position. For the same reason, the punch used is double-curved with a major radius of 3, 6, or 10 [mm] and a minor radius of 100 [mm].

In order to identify the failure mode of the stretch-bending test (more on failure modes in Chapter 6), a single experiment was performed and terminated approximately 0.5 [mm] before the reported fracture depth. Figure 5.5 presents a microscopic examination of the cross-section of this specimen. As can be seen, to the right of the punch tip, the material is thinner than in the rest of the material, indicating that the material in the experimental setup fails in a necking mode, and is not subject to direct fracture. As the failure mode is determined to be the onset of necking, failure strain values of the stretch-bending experiments, must be determined at the onset of necking. To determine the onset of necking, the approach proposed by Sigvant, Mattiasson, and Larsson 2008 was used. Identifying the maximum major strain values ($\varepsilon_{1,\,\max}$), and the corresponding minor strain values (ε_2), the values in Table 5.1 are obtained at the onset of localized necking. To be able to visualize the impact of the bending contribution, the maximum major strain values are plotted

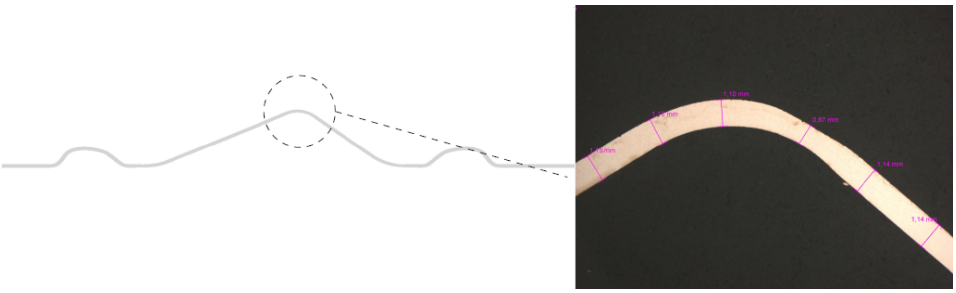

Figure 5.5: Indication of necking in the stretch-bending experimental test presented in Paper A.

as a function of the parameter α, which is defined as:

$$\alpha = \frac{t}{R} \tag{5.1}$$

where t is the sheet thickness (for the given AA6016 alloy, $t = 1.16$ [mm]) and R is the tool nose radius. To further strengthen the argument that the stretch-bending load case has an impact on the formability of the material, the obtained failure strain values are compared to the result obtained with a standard Nakajima test, where $R = 50$ [mm]. To be able to make an accurate comparison, the minor strain values obtained for the stretch-bending test are observed. Here it can be seen that all three radii produces points that are located in the plane strain region of the standard Forming Limit Diagram. Therefore, for comparison, the plane strain point of the Forming Limit Curve of the AA6016 aluminium alloy is used. The impact of the tool radius on the formability of the material can be seen in Figure 5.6.

	R3	**R6**	**R10**
$\varepsilon_{1,\,\max}$	0.282	0.260	0.200
ε_2	0.022	0.011	0.001

Table 5.1: Strain pair for point with maximum strain at the onset of localized necking.

5.3 Hole Expansion Test

The execution of the Hole Expansion Test (HET) is related to the work presented in Paper D, where the boundary conditions of the hole expansion test are investigated. The hole expansion test is standardized in ISO 16630 *Metallic materials – Sheet and strip – Hole expanding test* 2018 and targets to determine the Hole Expansion

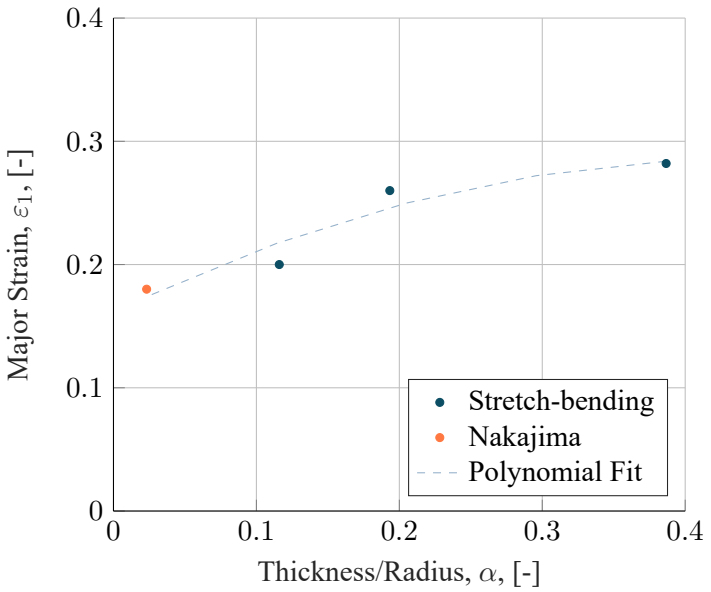

Figure 5.6: Impact of the tool radius on the failure strain value of the stretch-bending experimental setup. The tool radius is represented by the parameter α.

Ratio (HER, λ). The overall process of the hole expansion test consists of two parts:

- **Part I:** Specimen preparation.
- **Part II:** Forming operation.

For Part I the ISO standard specifies that a hole should be punched into a flat sheet using a punch with a diameter of 10 [mm], and the cutting clearance c should adhere to the following conditions:

$$c = \begin{cases} 12 \pm 2\% & \text{if} \quad 2.0 > t \\ 12 \pm 1\% & \text{if} \quad 2.0 \leq t \end{cases} \tag{5.2}$$

Furthermore, the center of the hole should be located at least 45 [mm] from the edge of the specimen, and if multiple holes are punched in the same specimen, at a minimum distance of 90 [mm] between the two hole centers should be ensured. For Part II the ISO standard specifies how the experiment should be carried out i.e. a clamping force of 50 [kN] or greater and that the specimen should be tested in a burr-up configuration. The standard also specifies how the test should be terminated. This is specified as when the operator notice a *through-thickness crack*, the test should be terminated, meaning the test is highly operator reliant. For the determination of the hole expansion ratio λ, the initial hole diameter D_o is compared to

the expanded hole diameter after rupture D_h as presented in Eq. 5.3, where the new diameter should be the average hole diameter of two on each other perpendicular measurements using a sliding caliper.

$$\lambda = \frac{D_h - D_o}{D_o} \times 100 \tag{5.3}$$

Several authors, including Schneider et al. 2015 and Larour et al. 2014, have criticized the ISO 16630 standard for the high scatter in the results, and often blaming it on the heavily operator reliant post-processing. Therefore, for the experimental setup used in this Thesis, two significant modifications are made to the standardized setup; (I) the die and binder from a Nakajima test was used to ensure no draw-in would occur during the test, and (II) images from a DIC recording of the test was used for post-processing.

5.3.1 Modified Experimental Setup

As earlier mentioned, the primary issue with the standardized hole expansion test, is the scatter of the results when repeating the test. In an effort to reduced this scatter, draw beads were introduced into the setup by re-purposing the Nakajima test setup and changing the punch from the hemispherical to a conical punch with a tip-angle of 60°. Re-purposing the Nakajima tool adds the benefit of having an ARAMIS DIC measurement system incorporated into the die. A cross-section of the modified test setup can be seen on Figure 5.7. As the Nakajima die and binder were adopted, the blank geometry will be modeled based on the full-width Nakajima specimen (Ø200) and a hole will be punched in the center. The blank geometry can be seen in Figure 5.8 (a).
With the introduction of the draw beads, a slighe pre-forming operation will occur when the beads are formed, which will results in a slight enlargement of the initial hole diameter. Figure 5.8 (a)-(d) presents a conceptual ((a) and (b)) and real life ((c) and (d)) illustration of the bead forming. A test was run without the punch to investigate the impact of the pre-forming, and it was found that the new initial hole diameter was $D_h = 10.047$ [mm] corresponding to $\lambda_{pre} = 0.34\%$.

5.3.2 Modified Post-Processing

As previously mentioned, by utilizing components from the Nakajima experimental setup, this also allows for the application of DIC, however, not in a conventional way. According to Larour et al. 2014 3D DIC cannot be applied to materials where $\lambda > 70\,\%$ as the cameras fails to focus once a punch displacement of 50 [mm] has been reached. Therefore, a re-purposing of the DIC system is done to only utilized the images captured from the experiment. Doing so, will allow for a more accurate determination of when a through-thickness crack has appeared, and the operator

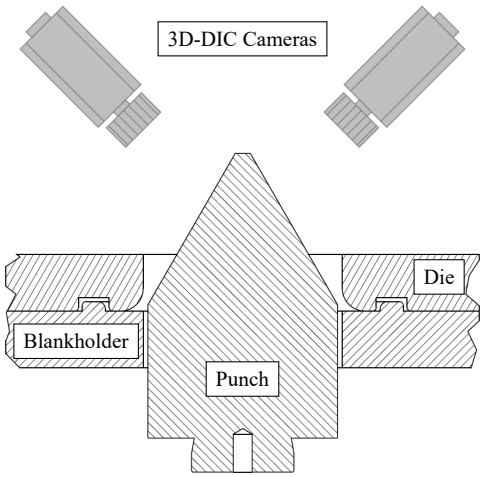

Figure 5.7: Cross-section view of the new experimental setup introducing draw beads and DIC system to the Hole Expansion Test presented in Paper D.

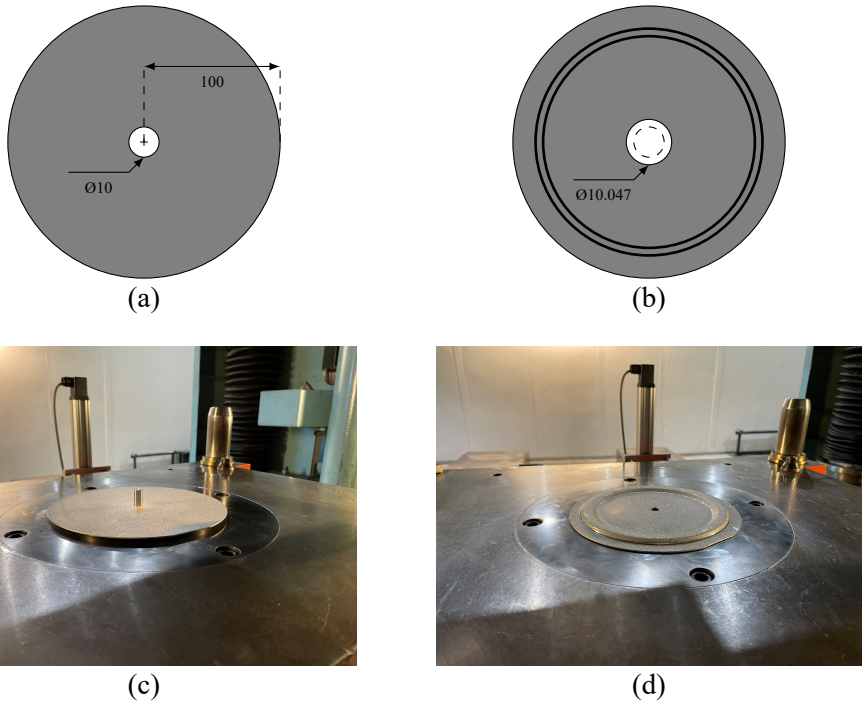

Figure 5.8: Modified blank geometry with (a) and (c) presenting the punched blank, and (b) and (d) presenting the blank after the pre-forming of the draw beads.

can run the test to maximum punch depth. To exemplify this, Figure 5.9 presents two stages captured by the DIC where (a) exhibits crack initiation (surface failure) and (b) exhibits a through-thickness crack. The difference between the draw depth in (a) and (b) is approximately 0.17 [mm], which allows for little to no time for the operator to react, if the same crack propagation rate is kept.

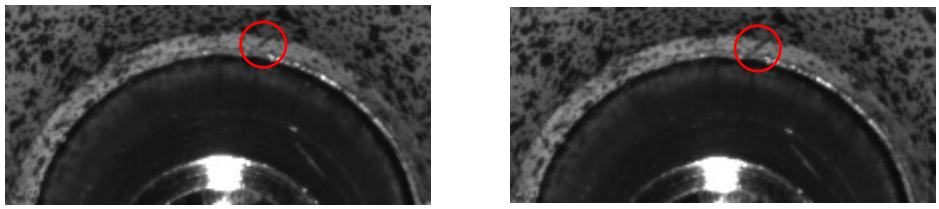

(a) (b)

Figure 5.9: Close up of test specimen collar with (a) exhibiting crack initiation and (b) exhibiting a through-thickness crack. The difference in draw depth between (a) and (b) is approximately 0.17 [mm].

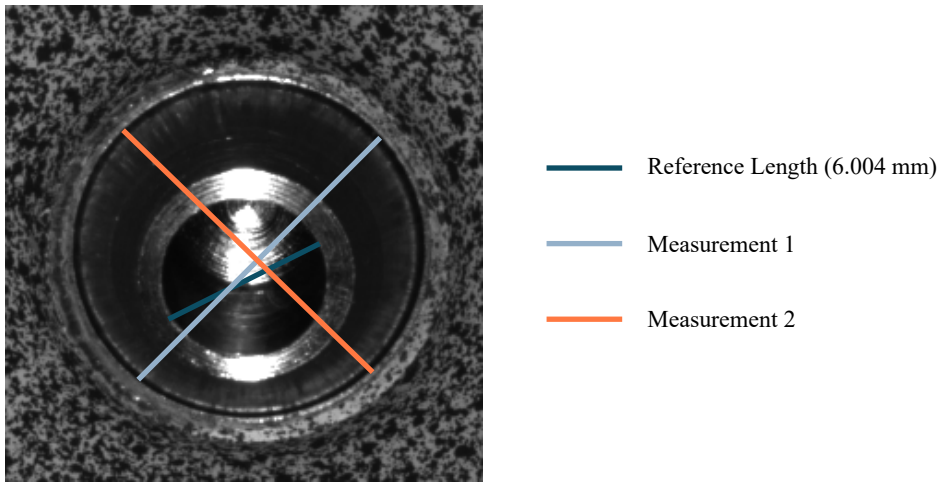

Figure 5.10: Illustration of measurement technique at appearance of through-thickness crack. The measurement is performed for both images captured by the DIC for the stage.

By having determined the time of through-thickness crack one uncertainty has been reduced, however, the second uncertainty of the manual measurement of the operator can also be addressed by utilizing the images from DIC. Figure 5.10 presents the concept of the digitally based evaluation of the failure stage of the experiment. As specified by the ISO standard, two on each other perpendicular measurements

are taken (Measurement 1 and 2) using a pixel mapping method, where the number of pixels is compared to a known reference length. However, having two images from the 3D DIC system, this process is repeated two times, and in total four diameter measurements are obtained. Therefore, the average hole expansion ratio $\bar{\lambda}$ can be determined as presented in 5.4.

$$\bar{\lambda} = \left(\frac{\left(\frac{D_{h1}+D_{h2}+D_{h3}+D_{h4}}{4} \right) - D_o}{D_0} \right) \times 100 \tag{5.4}$$

5.4 Pre-Straining of Sheets

For the evaluation of existing and newly proposed failure prediction approaches targeting non-linear strain paths, a large number of experiments are needed. Therefore, a new experimental setup has been developed with the intent of performing a pre-straining operation. A new punch was developed based on a Marciniack-type approach with material removed in the centre of the punch to avoid contact between sheet and tool in the centre of the blank. The argument for wanting to avoid the contact in this area (even though it increases the manufacturing cost) is to avoid the impact of friction in the area that is to be evaluated, thereby producing a pure material test. Initially, the tool was developed as a 3D CAD geometry, which serves two purposes - as a foundation for the manufacturing of the punch, and the 3D geometry can be imported into the Finite Element software for initial investigation. Both the 3D CAD geometry and the manufacture punch can be found in Figure 5.11.

The initial numerical study of the newly designed punch was conducted by Olofsson and Al-Fadhli 2022 of a DP800 AHSS grade. The study targeted the design of blank geometries to be able to obtain a pre-straining level of 30% of the forming limit curve in the uniaxial, plane strain, and biaxial directions, which produced the three blank geometries presented in Figure 5.12.

For the evaluation of the formed blanks, two circles of Ø100 and Ø200 [mm] with their centre place in blank coordinate (0,0). The reasoning for these two circles are that the larger circle aligns with the diameter of a Nakajima full-width specimen, and the smaller circle aligns with the diameter of a Nakajima punch. Since the presented punch only produces linear straining, a second forming operation is needed to produce a bi-linear (non-linear) strain path. For this purpose, the Nakajima test was chosen, as it is a well known experiment, and experience have been built up over the years regarding testing and post-processing. The described flow is presented in Figure 5.13.

The three blank geometries presented by Olofsson and Al-Fadhli 2022 was evaluated according to the aforementioned criteria, and the results can be seen in Figure

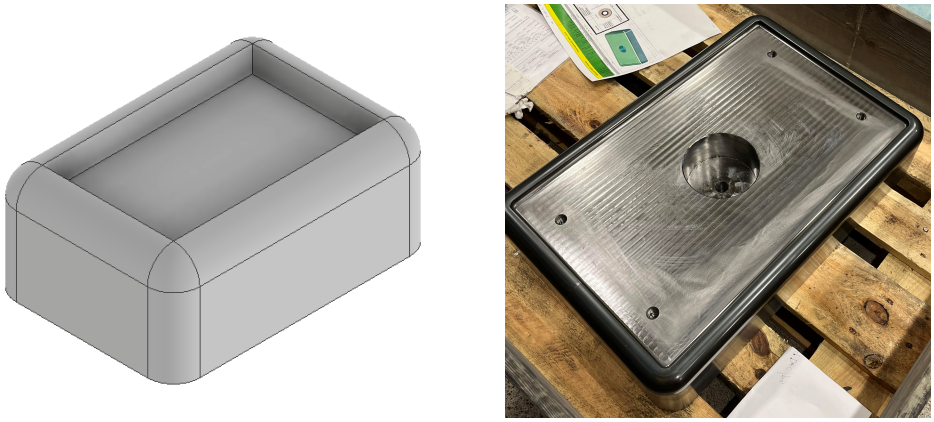

(a) (b)

Figure 5.11: Pre-straining punch with (a) presenting a 3D CAD geometry imported into AutoForm R10, and (b) presenting the manufactured punch.

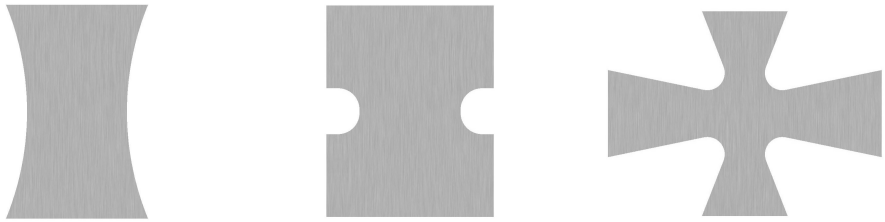

(a) (b) (c)

Figure 5.12: Blank geometries developed by Olofsson and Al-Fadhli 2022 for the pre-straining operation with (a) producing the uniaxial direction, (b) the plane strain direction, and (c) the biaxial direction.

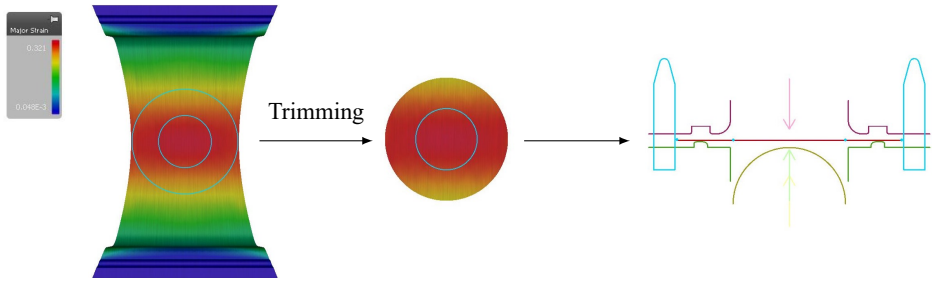

Figure 5.13: Post-straining operation flow. Exemplified here is a uniaxial pre-straining blank with a subsequent trimming operation into a full-width Nakajima blank, resulting in a uniaxial pre-straining, and a biaxial post-straining.

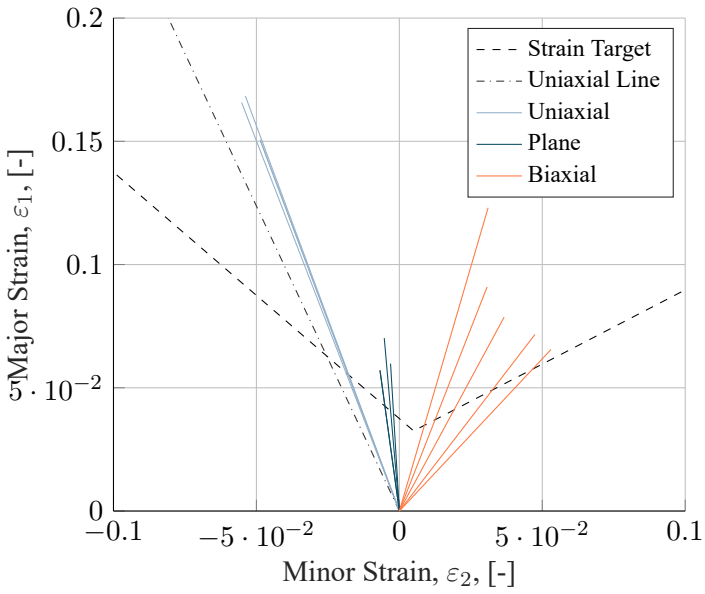

Figure 5.14: Pre-straining levels reported by Olofsson and Al-Fadhli 2022.

5.14. While the results at a first glance seems to be promising, there are some issues that needs to be addressed for the uniaxial and biaxial pre-straining. Starting with the uniaxial pre-straining, the evaluated points are well above the strain target, however, they do deviate from the theoretical uniaxial strain path for this grade. The theoretical uniaxial strain path is determined using Eq. 5.5 and $r_0 = 0.678$.

$$\varepsilon_1 = -\frac{(1 + r_0) \cdot \varepsilon_2}{r_0} \tag{5.5}$$

For the biaxial strain paths, two issues are worth noticing. Initially, the biaxial strain paths presented in Figure 5.14 are on the border to not be classified as biaxial. The definition of the target (equi-biaxial) is that the strain ratio $\varepsilon_2/\varepsilon_1 = 1$, however, the strain ratios reported for the presented strain paths ranges between $0.24 - 0.81$. This spread in strain ratio also presents the second issue to be addressed for the biaxial pre-straining. In order to cut out a Nakajima test from the pre-strained blank, the strain distribution within the Ø100 [mm] should be fairly uniform, to no have areas of the blank that are closer to failure than other. This is not the case with the presented data, where the major strain values range between approximately $0.065 - 0.12$.

In order to test out and validate potential methods for predicting failure in non-linear strain paths developed, a similar investigation is started on the VDA239 CR4 mild steel used for the first generation XC60 wheel house. Initially, the uniaxial direction was chosen, and the blank geometry proposed for the DP800 HSS grade

was used. Pre-straining levels of 25 and 55% were targeted, and an initial attempt of the of producing the bi-linear strain path was also performed, with the uniaxial pre-straining and a biaxial post-straining. For the evaluation of this investigation, the strain paths of three control points of the formed Nakajima blank was chosen, where one control points is located on the top of the dome, and the other two are located on the side of the dome in approximately 90 degrees to each other to monitor the impact of the material anisotropy. The strain paths and the location of the control points can be found in Figure 5.15.

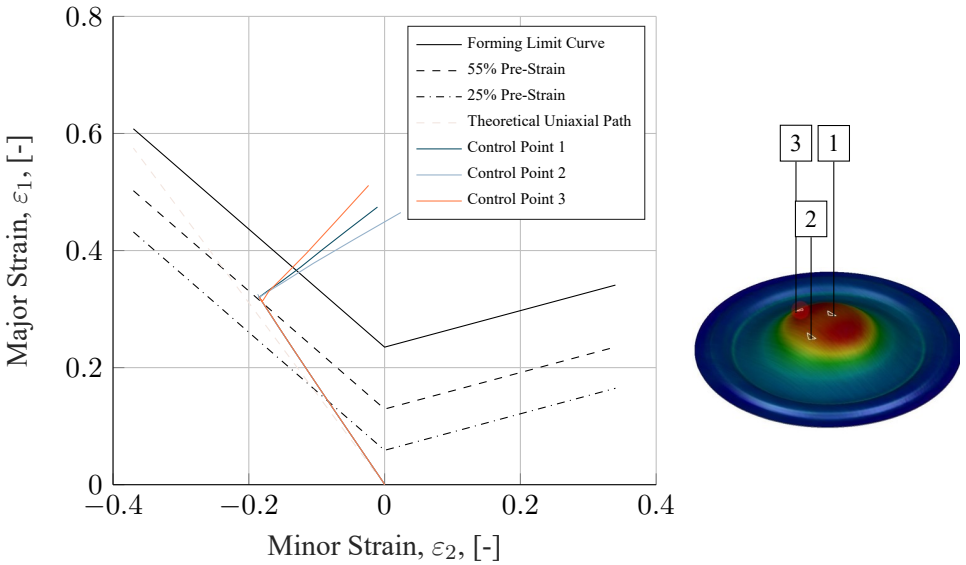

Figure 5.15: Biaxial straining of the VDA239 CR4 mild steel. The forming process follows the process presented in Figure 5.13 with a uniaxial pre-straining and a biaxial post-straining.

The presented results show that the bi-linear strain paths are obtainable with the setup in the numerical investigation. It should however be noted, that as for the DP800, the uniaxial pre-straining does not follow the theoretical uniaxial strain path completely. Therefore, further numerical investigations into blank shapes are needed before moving on with the experimental setup.

5.5 Relation of Experiments to Thesis

The presented experimental work all relates to the sub-research questions (s.RQ) presented in Chapter 1. Each of the three experiments presented relates to a single s.RQ and the link between experiments and question can be found in Table 5.2.

Test	s.RQ. 1	s.RQ. 2	s.RQ. 3
Stretch-Bending		x	
Hole Expansion			x
Pre-Straining	x		

Table 5.2: Relation between performed experimental tests and the sub-research questions of the Thesis.

Chapter 6

FAILURE PREDICTION IN SHEET METAL FORMING

The following chapter builds on top of the presented information in Chapter 4, and contextualizes it in regards to the data-flow presented in Figure 4.1 with an emphasis on the prediction of failure and fracture. The chapter will initially present a definition of the term ”failure” in a sheet metal context, followed by a presentation of the mechanics experienced by the three complex load cases that concerns the work in this thesis.

6.1 Definition of Failure in a Sheet Metal Forming Context

When discussing the term ’failure’ in a mechanical engineering context, the phenomenon of fracture is often brought forward, where one distinguishes between ductile and brittle failure. However, when discussing failure, two separate modes of failure must be considered - necking (illustrated in Figure 6.1 (a)) and fracture (illustrated in Figure 6.1 (b)). Necking is a failure mode where a high amount of straining localizes in a small region of the material, ultimately causing the component to loose its structural integrity.

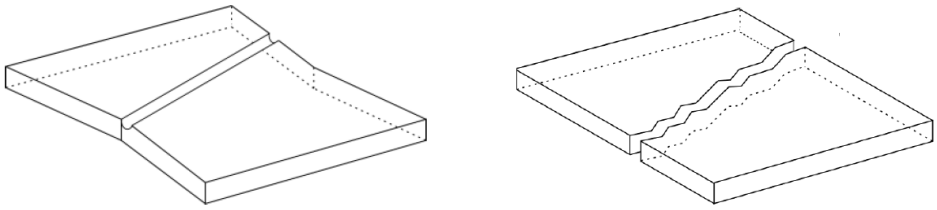

(a) (b)

Figure 6.1: Illustration of (a) the combined diffuse and localized necking phenomena and (b) the fracture phenomenon.

The above definition of necking is by far the most popular, however, several authors, including Sowerby and Duncan 1971 and Needleman and Tvergaard 1977, have argued for the presence of an intermediate stage between plastic deformation and localized necking, named diffuse necking. The diffuse necking phenomenon is known from tensile test where a reduction in the specimen width is seen before the strain localization causing the localized necking phenomenon is initiated. However, when discussing bi- or multi-axial loading of a specimen, the diffuse necking phenomenon is assumed not to occur, due to the loading in the width direction that otherwise would decrease. Therefore, when talking about bi- or multi-axial load situations (which are the by far most common in industrial sheet metal forming) Mattiasson, Jergéus, and DuBois 2014 presented three different scenarios for how a specimen behaves between onset of plastic deformation and fracture. These three scenarios can be seen in Figure 6.2

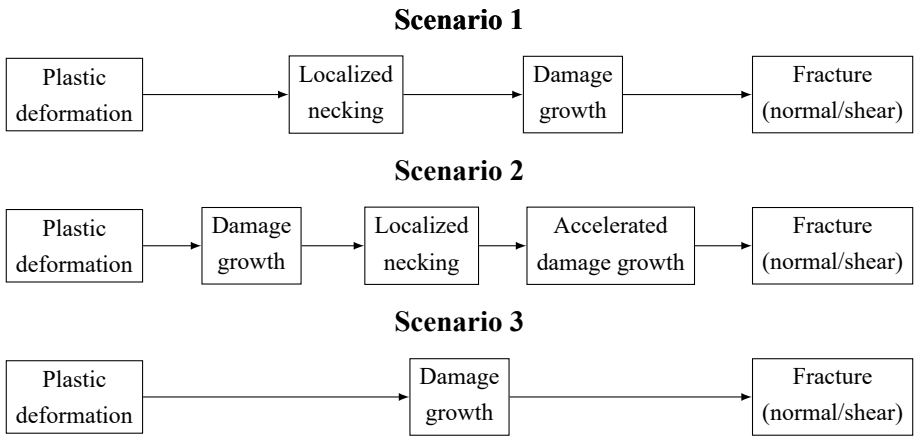

Figure 6.2: Different load scenarios leading to fracture according to Mattiasson, Jergéus, and DuBois 2014.

For the remainder of this Thesis, when the concept of necking is mentioned, this will refer to Scenario 1 presented in Figure 6.2, where it is assumed that a no damage growth happens between the onset of plastic deformation and localized necking, and the first mode of necking encountered is the localized necking. The reason for defining necking as failure should be found in the previous presented definition of localized necking, mainly that it causes the component to *loose its structural integrity*. From an industrial point of view, the loss of structural integrity would result in a non-conforming part that would not meet the quality standards for e.g. a car body component. Therefore, the default definition of failure should always be necking, however, in some cases, components do not display the phenomenon of necking, and goes directly to fracture, i.e. Scenario 3 in Figure 6.2. Even in cases where a suspicion of direct fracture is present, one should check for necking, as the

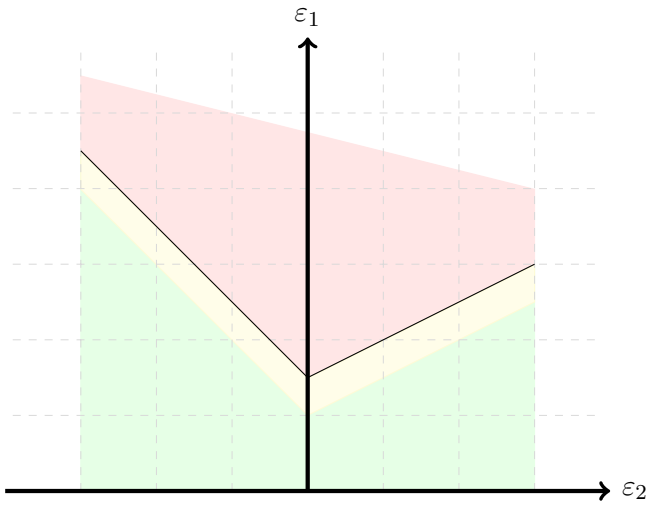

Figure 6.3: The Forming Limit Diagram (FLD). The green zone indicates at safe part, the yellow zone indicates risk of failure, and the red zone indicates failure.

deformation level between necking and fracture in cases can be very small.

When assessing whether an experimental specimen or industrial component have failed, the most common tool to use is the Forming Limit Diagram (FLD). The FLD was originally proposed by Keeler and Backofen 1964, and is based on an evaluation space defined by the major (ε_1) and minor (ε_2) strains, where the forming limit is given as the Forming Limit Curve (FLC). An example of a FLD can be seen in Figure 6.3. The fact that the evaluation space is based on the major and minor strains makes it a powerful and easily accessible tool for engineers, as during experimental tests, these can be recorded with Digital Image Correlation (DIC) (or other alternatives), yielding an indication of the remaining formability of the material, independent of any constitutive model. Since the introduction of the FLD in the 1960's, engineers have become to rely on this approach, and it has been standardized in the ISO standard 12004: *Metallic materials – Sheet and strip – Determination of forming-limit curves* 2008. It is however well known in the sheet metal forming community that the FLD has it's shortcomings. First, and most important, is that the FLC is determined using the Nakajima test generating linear strain paths, which does not allow it to factor in the impact of pre-straining on the formability of a material (more on this in Section 6.2). Secondly, utilizing the Nakajima test, the FLC is determined based on an experimental setup with a punch radius of 50 [mm], failing to account for the impact of bending over small radii (more on this in Section 6.3). Finally, as the Nakajima setup utilizes draw beads on an intact sheet, any cut edges are placed outside the deformation area (for the full size blank), why no effects of edge conditions are recorded. Furthermore, the

Nakajima blanks fails not close to the edges, why the edge strains are not recorded (more on this in Section 6.4).
Having presented the definition of the concept of "failure" in a sheet metal forming context, and provided a brief introduction of the FLD and its shortcomings, the next three sections will focus on the mechanics behind the three complex load cases handled in this Thesis.

6.2 Components experiencing Non-Linear Strain Paths

As mentioned in the previous section, the FLD does not account for non-linear strain paths. Non-linear strain paths occur when a change in the loading direction is present in the forming operation, or as a result of multiple forming operations as often seen in industry. An example of non-linear strain paths caused by multiple forming operations can be seen in Figure 6.4, presenting the first generation Volvo XC60 wheel house. The Forming Limit Diagram presented in Figure 6.4 (c) shows four arbitrarily chosen elements in areas experiencing high plastic strain along with the strain path in the critical element where the fracture presented in Figure 6.4 (a) is expected to have its origin. The strain paths presented displays a varying degree of non-linearity from Element 2 shown almost no non-linearity, to the critical element displaying a 90° turn in the strain path.
As previously presented in Section 3.1.1, several attempts have been made to accurately predict failure in components experiencing non-linear strain paths. One of the most promising methods is the Generalized Forming Limit Concept (GFLC) proposed by Volk and Suh 2013, and implemented in AutoForm R10 as the *Advanced Forming Limit Diagram*. This approach was used in an attempt to predict the fracture in the wheel house, and the results of the Advanced Forming Limit Diagram analysis was presented in Figure 4.7 (b). Here it was presented, that the failure model marks the component safe in a necking context, even though a full blown fracture is present in the manufactured component (Figure 4.6). It should however be noted that the Advanced Forming Limit Diagram approach implemented in AutoForm R10 does improve the failure prediction compared to the standard Forming Limit Diagram. Observing the Max Failure value (i.e. how close the part is to failing) the standard Forming Limit Diagram yields a result of 0.822 and the Advanced Forming Limit Diagram yields 0.854, indicating the the Advanced Forming Limit Diagram does account for strain path non-linearity, however it fails to accurately predict the failure in this case, due to the abrupt change in strain path direction with respect to the rolling direction in the critical element. An attempt to capture this exact phenomenon with strain path direction changes, on the same industrial component, was made by Norz et al. 2022 where the current GFLC approach was extended into the 3D-GFLC with the use of loading angle α, to indicate the change in the strain path. Their approach showed promising results by being able to predict

(a)

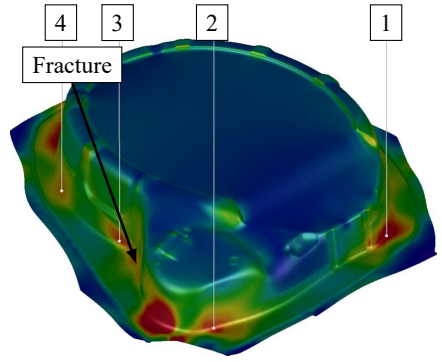

(b)

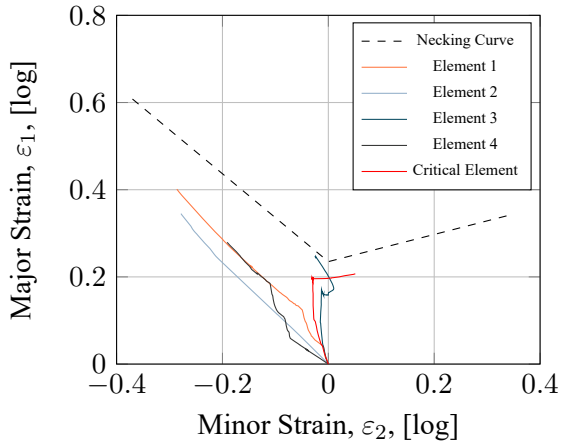

(c)

Figure 6.4: First generation Volvo XC60 wheel house. Figure (a) shows the error noticed in production, figure (b) presents a contour plot of the plastic strain from simulation, and figure (c) presents the strain paths from the four control elements and the critical element.

failure in the critical element, however, some areas of the component also showed a false positive failure.
Therefore, in an attempt to capture this phenomenon of strain path changes with respect to the rolling direction, a different approach will be tested out, based on a different transformation of the standard evaluation space (ε_2, ε_1) to a space defined by the equivalent plastic strain $\bar{\varepsilon}^p$ and the relationship between the increment in minor and major strain in the last stage of the simulation, denoted α, which is defined as in Eq. 6.1

$$\alpha = \frac{\dot{\varepsilon}_2}{\dot{\varepsilon}_1} \tag{6.1}$$

This approach was originally proposed by Zeng et al. 2009 as an alternative to the stress-based Forming Limit Diagram proposed by Stoughton 2000, due to the parameter α being closely related to the strass ratio σ_2/σ_1 for the associated flow rule. Introducing the equivalent plastic strain as an evaluation parameter complicates the process, as the evaluation of the simulation is now even more dependent on the constitutive model of choice. In the work by Zeng et al. 2009, a Hill'48 constitutive model was used, but as presented in Section 4.2 this is not a good fit for the strain predictions of the XC60 wheel house component. In an attempt to simplify the approach, an investigation of the impact of the constitutive model on the transformation of the Forming Limit Curve is performed. The same three constitutive models as presented in Section 4.2 is used, and an assumption of linear (and proportional) deformation from zero to limit strain is made, i.e. $d\varepsilon_i = \varepsilon_i$ during the determination of the Forming Limit Curve. Three points from the experimental FLC curve are used for the transformation, and are presented in Table 6.1. However, both Zeng et al. 2009 and Mattiasson, Jergéus, and DuBois 2014 have reported a 'curved' limit curve in the new evaluation space, why in total 49 data points are used in the curve, obtained through linear interpolation.

FLC Point [-]	**Major Strain, ε_1, [-]**	**Minor Strain, ε_2, [-]**
Uniaxial Tension	0.608	-0.370
Plane Strain	0.235	0.000
Equi-biaxial Tension	0.341	0.340

Table 6.1: Experimental FLC points for the VDA239 CR4 mild steel.

For the determination of the equivalent plastic strain limit values, these can be determined analytically for the von Mises constitutive model using Eq. 6.2 and Hill'48 using Eq. 6.3, where the parameters F, H, and G are determined using Eq. 6.4.

$$\bar{\varepsilon}^p = \sqrt{\frac{4}{2} \cdot (\varepsilon_1^2 + \varepsilon_2^2 + \varepsilon_1 \cdot \varepsilon_2)} \tag{6.2}$$

$$\bar{\varepsilon}^p = \sqrt{\frac{1}{F \cdot H + F \cdot G + G \cdot H} \cdot \left[(F+H) \cdot \varepsilon_1^2 + 2 \cdot H \cdot \varepsilon_1 \cdot \varepsilon_2 + (G+H) \cdot \varepsilon_2^2 \right]} \tag{6.3}$$

$$\begin{aligned} F &= \frac{1}{2} \cdot \left(\frac{1}{R_{22}^2} + \frac{1}{R_{33}^2} - 1 \right) \\ G &= \frac{1}{2} \cdot \left(-\frac{1}{R_{22}^2} + \frac{1}{R_{33}^2} + 1 \right) \\ H &= \frac{1}{2} \cdot \left(\frac{1}{R_{22}^2} - \frac{1}{R_{33}^2} + 1 \right) \\ R_{22} &= \sqrt{\frac{r_{90} \cdot (r_{00}+1)}{r_{00} \cdot (r_{90}+1)}} \\ R_{33} &= \sqrt{\frac{r_{90} \cdot (r_{00}+1)}{r_{00}+r_{90}}} \end{aligned} \tag{6.4}$$

For the transformation using the BBC 2005 constitutive model, a numerical approach must however be adapted. In order to do so, the approach presented by Bandpay 2015 was used. The transformed curves can be seen in Figure 6.5.

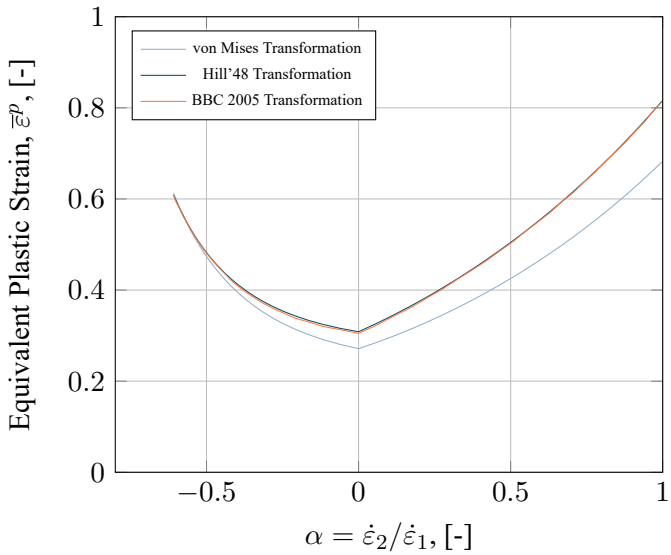

Figure 6.5: Forming Limit Curve transformed from the traditional principal strain space into the new evaluation space based on three different yield criteria.

As can be seen from the transformed curves, the Hill'48 and BBC 2005 constitutive models provide a highly similar limit curve, however, since the differences found between the two curves are in the plane strain region (which is the domain in which the critical element operates), it is concluded that the transformation of the limit curve cannot be decoupled from the choice of constitutive model. This finding is well in line with the shape of the yield surfaces presented in Figure 4.3.

6.3 Components experiencing Stretch-Bending

Just as for the non-linear strian paths, the standard Forming Limit Diagram has been known not to perform optimally for the stretch-bending load cases. One of the reasons for this is that commercial Finite Element softwares like AutoForm R10 evaluates the formability using the strains from the membrane layer of the shell element. Figure 6.6 present the major strain distribution and local maximum from (a) the membrane layer, and (b) the top layer at roughly 3 [mm] before maximum punch depth of the experiments, obtained through simulation in AutoForm R10.

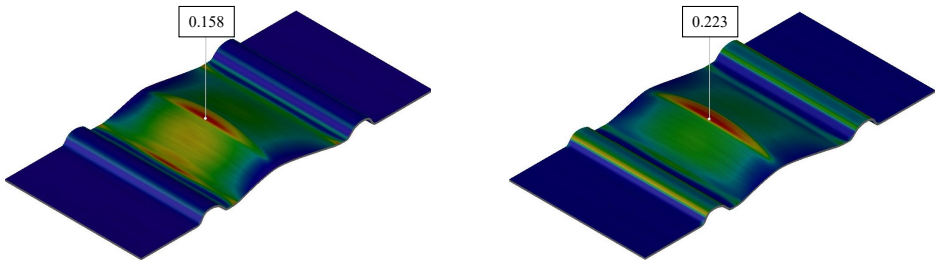

(a) (b)

Figure 6.6: Major strain distribution and local maximum for (a) the membrane layer, and (b) the top layer.

As can be seen from Figure 6.6 there is a significant difference from the maximum strain in the membrane layer to the maximum strain in the top layer, due to the strain gradient across the thickness, caused by the bending effect. Therefore, in order to address these effects, two measures are taken, (I) the limit strain values should be determined at the top layer (as done with DIC) and not transferred to the membrane layer, and (II) the impact of the tool curvature should be taken into consideration. In order to do so, a bending correction of the Forming Limit Curve is performed, using the experimental data obtained for the stretch-bending test presented in Section 5.2. The bending correction is based on determining the limit strain offset $\Delta\varepsilon_1$ between the Forming Limit Curve and the failure strain of the stretch-bending tests, which can be defined as in Eq. 6.5, where $\varepsilon_{1,\,\mathrm{DIC},\,\mathrm{max}}$ is the failure strain of the stretch-bending test, and $\varepsilon_{1\,\mathrm{FLC}}(\varepsilon_{2\,\mathrm{DIC}})$ is the limit strain value form the standard Forming

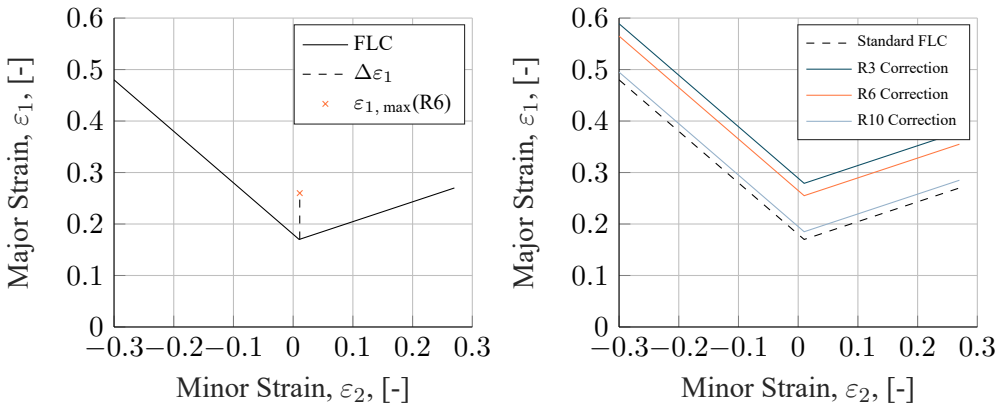

Figure 6.7: Bending correction of the Forming Limit Curve. Figure (a) illustrates the process of identifying $\Delta\varepsilon_1$, and (b) presents the bending corrected limit curves.

Limit Diagram at the minor strain value obtained from DIC for the failure strain, presented in Table 5.1.

$$\Delta\varepsilon_1 = \varepsilon_{1,\,\mathrm{DIC},\,\max} - \varepsilon_{1,\,\mathrm{FLC}}(\varepsilon_{2,\,\mathrm{DIC}}) \tag{6.5}$$

Figure 6.7(a) illustrates the distance $\Delta\varepsilon_1$ for the R6 stretch-bending test. As only one type of test is done for the three radii, a constant offset of the entire Forming Limit Curve will be performed, yielding the curves presented in Figure 6.7(b). In order to be able to distinguish between when to use the four curves, and approximate limits for radii in between the ones used in the experiments, a third dimension is added to the plot - the tool curvature κ. The curvature is defined as in Eq. 6.6, where R is the tool radius, thus yielding the curvature values presented in Table 6.2.

$$\kappa = \frac{1}{R} \tag{6.6}$$

Radius (R)	3	6	10	50
Curvature(κ)	0.3333	0.1667	0.1000	0.0200

Table 6.2: Experimental radii and their corresponding curvature.

With the introduction of the tool curvature, a 3D surface can be fitted to the data points of the FLC, where the uniaxial, plane strain, and eqi-biaxial point has been used as the data points. A polynomial fit has been performed with a second order polynomial fit for the minor strain direction, and a first order polynomial fit for

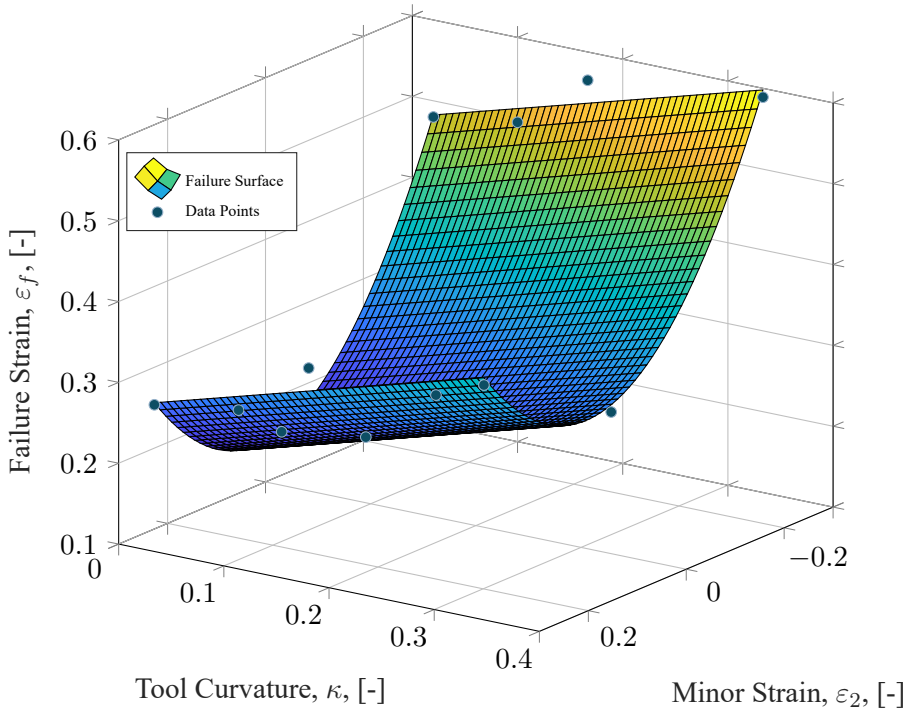

Figure 6.8: Bending Corrected Forming Limit Surface of the AA6016 aluminium alloy. The surface is created from a combination of the curves presented in Figure 6.7(b) and the tool curvatures.

the curvature direction. The fitted Bending Corrected Forming Limit Surface (BCFLS) can be see in Figure 6.8. It should however be noted that the limit surface is only valid in the experimental space i.e. data points that satisfy the conditions $-0.3 \leq \varepsilon_2 \leq 0.3$ and $0.02 \leq \kappa \leq 0.33$.
For an implementation of the failure surface into commercial Finite Element code, the idea of failure measure for each element is applied. A direct comparison of the failure surface and the major strain (at the top layer) in an element can be performed using Eq. 6.7, and once the failure value F reaches unity, the failure limit for the element has been reached.

$$F = \frac{\varepsilon_1}{\varepsilon_f(\varepsilon_2, \kappa)} \tag{6.7}$$

6.4 Components experiencing Edge Effects

The ISO 16630 Hole Expansion Test is the industry standard for material suppliers when describing the edge formability properties of a material. As described

in Section 5.3, the result of the Hole Expansion Test is the Hole Expansion Ratio (HER, λ [%]) and therefore different from other formability measures that are most commonly provided as a strain limit. This to some extent limits the usability of the Hole Expansion test when it comes to failure prediction, as not all issues with edge formability is caused by expansion of holes. One way to use the Hole Expansion Test could be through inverse modeling in Finite Element to determine a limit strain value (as illustrated in Figure 6.9), however one major issue with the Hole Expansion Test prevents this. Over the years, several authors including Schneider et al. 2015 and Larour et al. 2014 have criticized the test for producing a high scatter in experimental results, potentially caused by the vague definition of when the test should be terminated, and the heavily operator reliant post-processing to obtain the λ-values.

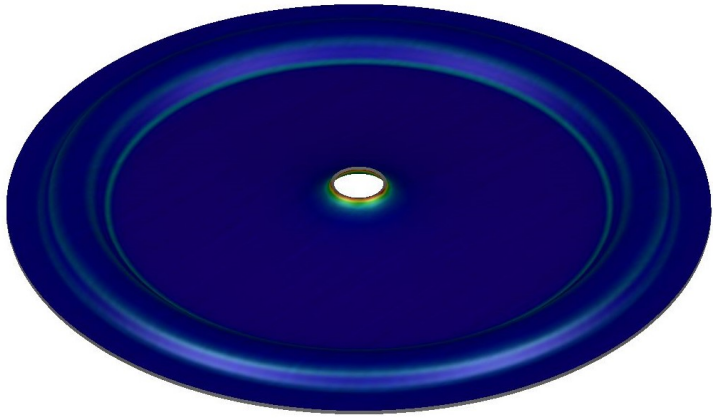

Figure 6.9: Hole Expansion Test simulated in AutoForm R10. The fringe plot on the geometry displays the major strain.

Therefore, the first step in order to be able to determine a limit strain from the Hole Expansion Test is to modify the experimental procedure and setup to produce stable and repeatable results. In an attempt to reduce the scatter, the experimental setup and post-processing procedure presented in 5.3 was developed based on the hypothesis that the high scatter was partially caused by the inability of the setup to restrict material draw-in during the test.
Alternative tests to the ISO standardized Hole Expansion Test does however exist, where one promising test is the KWI test. The two tests builds on the same principle of expanding a shear cut hole in a specimen, but where the Hole Expansion Test utilizes the conically shaped punch, resulting in a 'collar' formation in the test piece, the KWI test utilizes a flat-topped (Marciniack) punch resulting in an in-

plane expansion of the hole. The main benefits of the KWI test is that the flat-topped nature of the test specimen allows for a full DIC analysis of the test, thereby reducing the operator-reliant post-processing to a minimum, as well as eliminating friction between punch and hole edge.

Chapter 7
SUMMARY OF APPENDED PAPERS

7.1 Paper A

Title: On the Failure Prediction of Dual-Phase Steel and Aluminium Alloys Exposed to Combined Tension and Bending

A Barlo, M Sigvant, and B Endelt (2019). *IOP Conference Series: Materials Science and Engineering* 651, p. 012030 DOI: 10.1088/1757-899X/651/1/012030

Summary and relation to the thesis
Paper A serves as a pre-study to Paper B where the, at the time, current implemented failure prediction approaches in AutoForm R8 were investigated to see if they could capture the effect of stretch bending. The paper investigates the standard Forming Limit Diagram (FLD) and the Non-Linear Forming Limit Diagram (now Advanced Formability), and concludes that both approaches fails to accurately predict the onset of necking, thereby outlining the need for further development on failure models targeting stretch-bending. Paper A targets to answer s.RQ. 2.

The author's contribution
The author was responsible for planning and writing the paper along with the calibration of Finite Element models for both the aluminium and dual-phase steel alloy to match the experimental results up to the onset of localized necking. Furthermore, the author was dominant in the evaluation of the two investigated failure prediction methods to capture impact of the stretch-bending phenomenon.

7.2 Paper B

Title: Investigation of a Bending Corrected Forming Limit Surface for Failure Prediction in Sheet Metals

A Barlo, N Manopulo, M Sigvant, B Endelt, and K Trana (2019). *Conference Proceedings, Forming Technology Forum 2019, September 19-20, Munich, Germany*.

Summary and relation to the thesis
Paper B builds on the conclusion from Paper A that further developments of failure models should be done to capture the impact of the stretch-bending phenomenon. The paper investigates a bending correction of the standard forming limit curve by using the failure strain values from three stretch-bending tests with radii of 3, 6, and 10 [mm]. By determining a failure strain difference for one point along the curve, a Δ-value was determined to make a constant offset between the curves. The tool curvature was introduced as a third dimension to be able to distinguish between the curve, transforming the forming limit curve into a forming limit surface. To validate the developed method, a test panel developed at Volvo Cars was used, and it was found that the surface improves the ability to predict failure for components exposed to stretch-bending, and thereby partially answering s.RQ. 2.

The author's contribution
The author was responsible for the planning and writing of the paper along with the development of the methodology, and creation of the forming limit surface. The author was also responsible for implementation of the method into AutoForm R8 as an User Defined Variable (UDV) and for the subsequent evaluation of the test panel.

7.3 Paper C

Title: Failure Prediction of Automotive Components Utilizing a Path Independent Forming Limit Criterion

A Barlo, M Sigvant, N Manopulo, M S Islam, and J Pilthammar (2022). *Key Engineering Materials* 926, pp. 906-916. DOI: 10.4028/p-u6g3p6

Summary and relation to the thesis
Paper C investigates a proposed failure model to predict failure in a highly non-linear strain path (90° turn) in an automotive component that could not be captured by the standard built-in approaches in AutoForm R10 (Forming Limit Diagram and Advanced Formability). The method relies on a transformation of the forming limit

curve from the principal strain space to a space defined by the equivalent plastic strain and the parameter α, and is claimed to be load path independent. The paper targets s.RQ. 1.

The author's contribution
The author was responsible for the planning and writing of the paper along the the transformation of the limits curves using the von Mises and Hill'48 constitutive models. Furthermore, the author was responsible for running simulations of the first generation XC60 wheel house and the evaluation of the critical strain paths in the proposed method.

7.4 Paper D

Title: A Study of the Boundary Conditions in the ISO-16630 Hole Expansion Test

A Barlo, M Sigvant, L Pérez, M S Islam, and J Pilthammar (2022). *IOP Conference Series: Materials Science and Engineering* 1238.1, p. 012031. DOI: 10.1088/1757-899X/1238/1/012031

Summary and relation to the thesis
Paper D investigates the high scatter in results reported in the ISO 16630 Hole Expansion Test and attempts to reduce the said scatter by changing the boundary conditions of the test. This is done by modifying the tooling and test piece geometry of the test, to ensure sufficient clamping force even for high strength steel grades such as DP800. Furthermore, the paper introduces a more robust method for determination of the Hole Expansion Ratio through the use of digital measurements of the images captured by the DIC system as opposed as the current in-standard specified operator reliant method. The paper targets s.RQ. 3.

The author's contribution
The author was responsible for the planning and writing of the paper along with the planning of the experimental work related to the investigation. Prior to the experiments, the author was also responsible for the design of a new punch (including material and heat treatment selection) to fit with the press utilized, and the subsequent procurement of the punch from the vendor. Furthermore, the author was responsible for the analysis of the 62 experimental samples.

Chapter 8

RESULTS

The following chapter presents the results obtained for the failure prediction approaches investigated for the three complex load cases. Each of the three load cases will be handled separately in their own section.

8.1 Non-Linear Strain Paths

Section 6.2 presented the approach for predicting failure in the first generation Volvo XC60 wheel house caused by a highly non-linear strain path. Here it was also presented that the transformation of the limit curve from the principal strain space into the alternative evaluation space defined by $\bar{\varepsilon}^p$ and α could not be decoupled from the constitutive model used for the simulation model. Therefore, the limit curve presented in this section has been transformed based on the BBC2005 constitutive model. One of the reported benefits of the transformation of the evaluation space is that the strain path history can be disregarded, and only the last increment in the simulation needs to be considered. Figure 8.1 presents the critical and arbitrary elements along with the limit curve transformed into the new evaluation space.

As can be observed from the presented results, the approach is not successful in predicting the failure in the critical strain path. Firstly, the explanation for this is to be found in the high α-value of 2.65, which theoretically should not be able to pass $\alpha = 1$ as this indicates equi-biaxial straining. This high value is caused by the change of loading direction, where after the turn, the previous major strain becomes the minor strain and vice versa, and therefore a large step in the minor strain is seen compared to the major strain. In order to be able to accurately predict the failure of this critical strain path, the approach must be expanded to take the bi-directional forming into account, potentially turning the forming curve into at forming locus. A more elaborated discussion of the presented results can be found in Paper C.

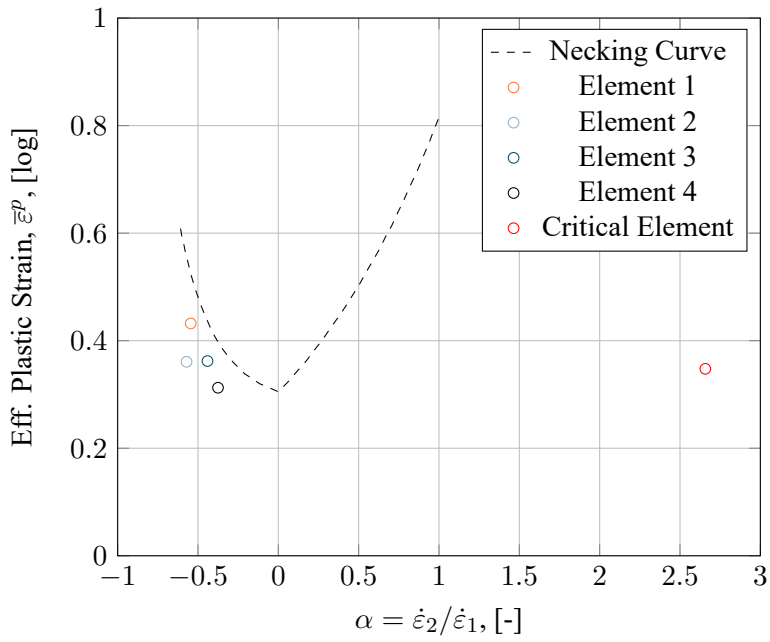

Figure 8.1: Illustration of the arbitrary and critical elements in the transformed evaluation space

8.2 Stretch-Bending

Section 6.3 presented the setup of the Bending Corrected Forming Limit Surface based on experimental stretch-bending tests with tool radii of 3, 6, and 10 [mm] and the standard Forming Limit Curve (tool radius 50 [mm]). For a proper validation of the approach, a component with different tool curvatures than the ones used for the setup of the surface is needed. For this purpose, a test panel developed at Volvo Cars is used. The dimensions and features of the panel is presented in Figure 8.2. The test panel has two different geometries, however for the validation only one of them will be used - the feature resembling a door handle (top and bottom row). Each row has four formed sections where different draw depths are present due to a differentiation in shim amount. Due to the large nature of the panel, a DIC recording of the forming was not possible, and therefore a manual inspection to determine the failure status of each geometry was performed at Volvo Cars. The results of the failure assessment is presented in Figure 8.2.
For the implementation of the method, Equation 6.7 was introduced in AutoForm R8 as an User Defined Variable (UDV). For the implementation, the tool curvature could not be used, why the blank curvature was used instead, as an assumption of the two values being similar was made (further discussion of this can be found in Paper B). With the approach implemented as an UDV, an evaluation of the panel

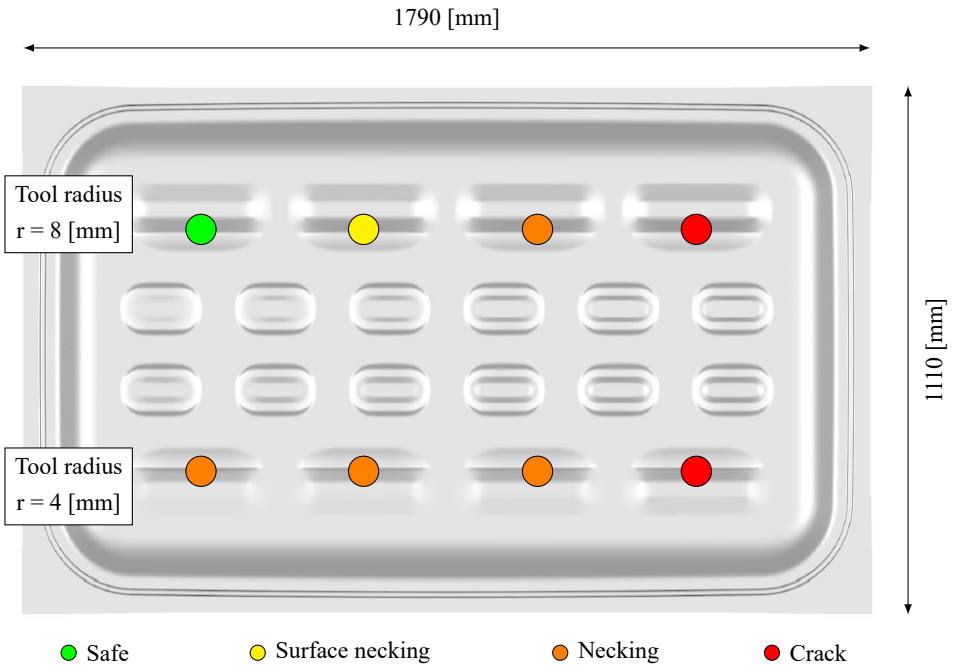

Figure 8.2: Dimensions and features along with results of manual inspection performed of the Volvo Cars test panel.

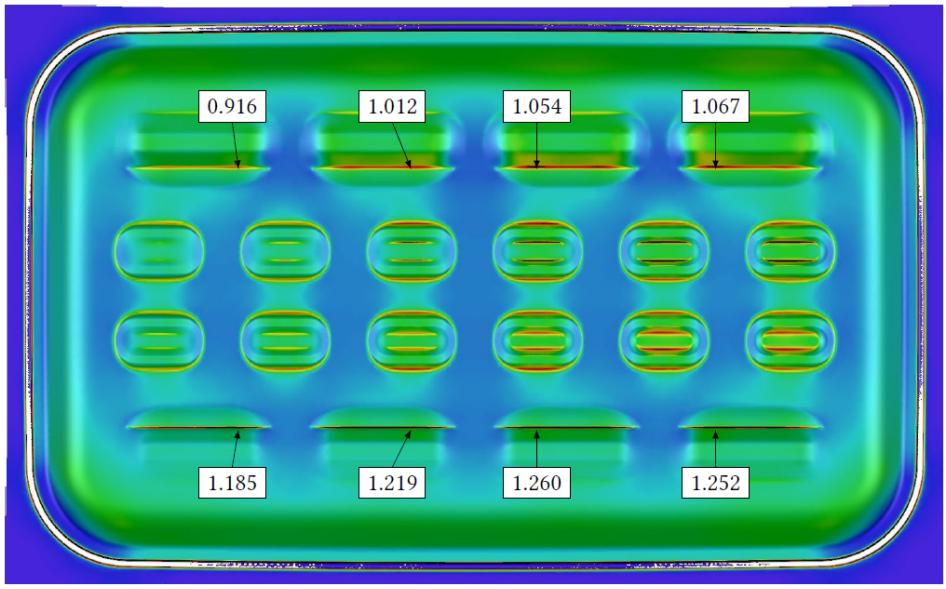

Figure 8.3: Local maximum failure values of the Volvo Cars test panel.

was made. Figure 8.3 presents a out-of-range plot of the local maximum failure, where all elements with a failure value of more than one is represented by a black color in the fringe plot. It can be observed from the results, that the implemented approach captures the failure state of the eight different sections well. Particularly impressive is it that the second geometry from the left on the top row is predicted with a failure value $F = 1.012$, as the manual inspection yielded that the geometry showed surface necking.
Some improvements could however be made to the Bending Corrected Forming Limit Surface. As presented in Section 6.3 the bending correction was performed based on samples in the plane strain region. This constant correction might not be accurate as the effect of stretch-bending might be more or less significant in the uni- and biaxial regions of the Forming Limit Curve. A more elaborated discussion of the results and bending correction can be found in Paper B.

8.3 Edge Effects

The need for an investigation into the high scatter produced in the ISO 16630 Hole Expansion Test was motivated in Section 6.4, and a modified experimental approach and evaluation method was presented in Section 5.3. A total of 62 repetitions was performed of a DP800 dual phase steel in an attempt to produce enough samples to be able to spot any improvements of the scatter. The average hole expansion ratio $\bar{\lambda}$ of the 62 experiments are presented in Figure 8.4. The results presented in this section have also been presented in Paper D.

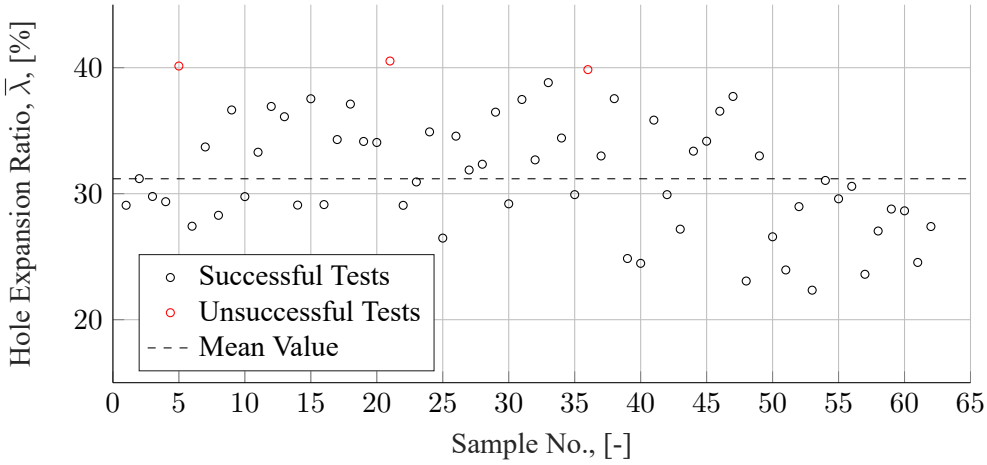

Figure 8.4: Hole Expansion Ratios of the 62 tests conducted. In total three tests were unsuccessful due to no presence of through-thickness cracks.

As presented, a total 59 of the 62 experiments were successfully run, where the

three tests marked unsuccessful are due to the test samples not displaying any through-thickness crack at the time of reaching maximum punch depth. From the reported results it is also apparent that the change in the experimental setup did not result in a stable, repeatable setup. One potential reason for the still high scatter in the test could be the stochastic behaviour of fracture. In all other aspects of sheet metal forming, failure caused by fracture is defined at the onset of fracture, which in the case of the Hole Expansion Test would translate to the onset of surface fracture. It is therefore possible, that with a shift in time for when the evaluation of the test is performed, the scatter could be reduced. Another interesting observation that can be made from the presented results is the downwards turn in $\bar{\lambda}$-values starting from test 47, which could be a result of the punching tool settling into a stable condition. A more elaborate discussion of the results presented can be found in Paper D. Due to the inability of the proposed modifications of the experimental setup to reduce the scatter, it has not been possible to obtain a failure strain limit through inverse Finite Element modeling, and further investigations of the root cause of the scatter is needed.

Chapter 9
CONCLUSIONS

The following chapter presents the conclusions drawn on the research presented in the thesis. Each of the three sub-questions presented in Chapter 1 will be handled separately, and an overall statement on the advancements made on failure prediction of complex load cases will be presented at the end of the chapter.

9.1 Sub-question s.RQ. 1

The first sub-question concerned the topic of non-linear strain paths and was formulated as:

How can failure caused by non-linear strain paths be accurately predicted in manufacturing feasibility studies?

with the accompanying hypothesis:

A transformation of the formability evaluation from the standard $(\varepsilon_2, \varepsilon_1)$-space to a space independent of the load history will increase the prediction accuracy.

On this topic, Section 6.2 presented an approach for the transformation of the standard forming limit diagram into an alternative evaluation space that should be load history independent. An industrial components displaying failure due to highly non-linear strain paths was used as a validation case, and the results were presented in Section 8.1. In total five different elements placed in areas with high plastic strain were evaluated, but non of the evaluated element indicated failure in the component, why the presented method initially failed. However, due to the nature of the critical strain path, it is concluded that the method should not immediately be discarded before further investigations into the phenomenon of radical turns in the strain paths have been conducted. Based on these findings, the thesis has failed to provide an answer to the first sub-question. It should however be noted, that the hypothesis should not yet be refuted until the investigation into radical turns has been conducted.

9.2 Sub-question s.RQ. 2

The second sub-question concerned the topic of stretch-bending and was formulated as:

How can failure caused by combined bending and tension be accurately predicted in manufacturing feasibility studies?

with the accompanying hypothesis:

A bending correction of the standard Forming Limit Diagram will increase the failure prediction accuracy of components experiencing stretch-bending

On this topic Section 6.3 presented an approach for a bending correction of the standard forming limit diagram, based on stretch-bending tests with tool radii of 3, 6, and 10 [mm]. For the validation of the presented approach, a test panel developed at Volvo Cars with tool radii of 4 and 8 [mm] were utilized, and the results were presented in Section 8.2. A failure measure based on the presented approach was implemented in AutoForm R8, and the results from the simulation were compared to a manual inspection of the panel after forming. The implemented approach proved to predict failure in different sections of the panel with high accuracy, even capturing an area failure due to surface necking. Based on these findings, the thesis has confirmed the presented hypothesis thereby providing an answer to the second sub-question.

9.3 Sub-question s.RQ. 3

The third sub-question concerned the topic of edge-effects and was formulated as:

How can failure caused by edge effects by accurately predicted in manufacturing feasibility studies?

with the accompanying hypothesis:

Inverse modelling of the ISO 16630 Hole Expansion Test to obtain a limit strain value will increase the failure prediction accuracy of components experiencing edge effects.

During the review of related work, it was found that the ISO 16630 Hole Expansion Test was experienced to produce high scatter in the results, troubling the process of confirming or refuting the presented hypothesis. Therefore, an attempt to reduce the reported scatter was initially made. Section 5.3 presented a modified experimental setup and post-processing procedure for the Hole Expansion Test, where the operator reliant aspects of the test were reduced. Section 8.3 presented the results

of 62 repetitions of the Hole Expansion Test, showing that even with the modified experimental setup and post-processing, the test still produced a high scatter. Due to the inability of the modified experimental setup to reduced the scatter, the presented hypothesis cannot be either confirmed or refuted, as it has not been possible to calibrate a Finite Element model against the experimental results to perform the inverse modeling.

9.4 Overall Statement

In this thesis, three different approaches were made to predict three different failure phenomena. The first approach was a transformation of the traditional evaluation space to account for non-linear strain paths. Even though the presented approach failed to accurately predict the failure in the industrial components used for validation, the study highlighted the importance of further research into strain paths where the loading direction changes with respect to the rolling direction. The second approach was a bending correction of the traditional forming limit diagram, which showed promising results. Even though the presented approach performed well for the validation case, there is most certainly room for improvement in the approach, but it is deemed a great step in the right direction for the accurate prediction of components exposed to stretch-bending. The third and last approach proposed was never investigated as the 62 repetitions of the Hole Expansion Test still produced a high scatter. Even though the study did not provide an answer to the posted sub-question, the results still bring knowledge to the field of edge cracks, as it raises some new questions about the evaluation of the standardized test.
With the demands for sustainable products rapidly increasing, further research into the field of sheet metal forming is needed more than ever. Smarter, better, faster, and cheaper approaches to both testing and simulation are essential to tackle the challenges of the future.

Chapter 10

FUTURE WORK

The following chapter will present ideas for future work on the approaches presented in this thesis. The three presented approaches will be handled separately in their own section. This will be followed by a general outlook on the topic of failure prediction.

10.1 Evaluation Space Transformation

In the previous chapter, it was concluded the the presented approach did not predict the failure in the industrial component. The expected reason for this is the radical turn in the strain path with respect to the rolling direction. The first step of solving this issue is to identify when the change occurs during the forming process. One solution to this could be to utilize the Schmitt factor, defined as in Eq. 10.1

$$\cos(\phi_d) = \frac{\boldsymbol{d}_1^p : \boldsymbol{d}_2^p}{||\boldsymbol{d}_1^p||||\boldsymbol{d}_2^p||} \tag{10.1}$$

where $\boldsymbol{d}^p$ is the plastic rate-of-deformation tensor, which is defined as:

$$\boldsymbol{d}^p = \dot{\lambda}\frac{\partial \boldsymbol{f}}{\partial \boldsymbol{\sigma}} \tag{10.2}$$

With the identification of the point of turning (either during the numerical solution or as a post-processing operation) measures can be taken to reverse the major and minor strain, thereby avoiding the high α-values.
Identifying the point of turn is not enough though. As all materials used in sheet metal forming to some degree are ansiotropic, it must also be investigated how the anisotropy influences the Forming Limit Curve, and if this impact is not negligible, an approach for how to implement the different Forming Limit Curves, and the differentiation between them must be investigated.

10.2 Bending Correction

The presented approach for a bending correction of the Forming Limit Curve showed promising results, however there is room for improvement. One of the areas that must be further investigated is the offset of the Forming Limit Curve. In the presented approach, a constant offset is done based on each stretch-bending test, however this might not accurately represent the real behaviour of the material. The constant offset is based on a $\Delta\varepsilon_1$ values determined in the plane strain region of the curve. For this approach to be generally accepted, an investigation should be launched into how stretch-bending influences the formability in the uni- and biaxial areas of the Forming Limit Curve. Based on this, a potential differentiated bending correction of the curve could be the correct approach.
Besides the potential need for a differentiated bending correction, the implementation method needs to be considered. In the presented approach, and with the implementation as an user defined variable, the method performs well with convex bends, however its performance when concave bends are present is unknown. Therefore, this needs to be investigated further.

10.3 Hole Expansion Test

The modified experimental setup and post-processing approach presented for the ISO 16630 Hole Expansion Test still produced high scatter for the 62 tests. Moving forward, a discussion should be opened on where the test should be evaluated. In the standard it is specified that the test should be evaluated at the appearance of a through-thickness crack, but this contradicts all other best practices when it comes to failure evaluation. Normally, the onset of either a neck or a crack is seen as the point of failure, as anything past this point will result in a non-conforming part in industry. Besides not following best practice, the high scatter in the test could also be caused by the stochastic behaviour of fracture, why in the future, an investigation should be made looking at the scatter in the test if the evaluation point is moved from the point of a through-thickness crack to the onset of a surface crack, or even the onset of necking if this phenomenon occurs.

10.4 Overall Outlook on Sheet Metal Forming Research

The outlook of research on sheet metal forming is naturally not limited to the three presented load cases. As in many other research areas, machine learning is also making its entry into the research community. The application potential of neural networks in sheet metal forming is wide, ranging from fracture detection in experiments as recently presented by e.g. Müller et al. 2021, to the prediction of forming limits for bi-linear strain paths as presented by e.g. Bonatti and Mohr 2021 and

modeling of elasto-plastic behaviour recently presented by e.g. Gorji et al. 2020 and Zhang and Mohr 2020. With the introduction of machine learning and neural networks into the research useful tools such as meta-models can be developed faster and cheaper without the need for a large number of experiments. This could potentially be very valuable when developing phenomenological failure models, like the GFLC approach presented earlier in this Thesis.
Another area that is getting attention is on the topic of Material Testing 2.0 where new mechanical tests are developed to identify the constitutive parameters of a material based on full-field measurements. In the Material Testing 2.0 era, the goal is to develop new and complex test geometries, targeting to determine multiple constitutive parameters from a single test, thereby reducing the number of tests needed. According to Pierron and Grédiac 2021 this new era is spearheaded by the maturity levels reached by the full-field measurements techniques such as Digital Image Correlation.

REFERENCES

A Good Practice Guide for Digital Image Correlation (Oct. 2018). Guide. International Digital Image Correlation Society.

Ablat, M A and A Qattawi (2017). "Numerical simulation of sheet metal forming: a review". In: *International Journal of Advanced Manufacturing Technology* 89, pp. 1235–1250. DOI: 10.1007/s00170-016-9103-5.

Andrade, F X C et al. (2016). "An incremental stress state dependent damage model for ductile failure prediction". In: *International Journal of Fracture* 200, pp. 127–150. DOI: 10.1007/s10704-016-0081-2.

Atzema, E H et al. (2010). "The influence of curvature on FLCs of mild steel, (A)HSS, and aluminium". In: *Conference Proceedings, International Deep Drawing Research Group (IDDRG), May 31 - June 2, 2010, Graz, Austria*.

Banabic, D (2010). *Sheet Metal Forming Processes - Constitutive Modelling and Numerical Simulation*. 1st edn. ISBN: 978-3-540-88112-4. Springer London.

Banabic, D and M Sester (2012). "Influence of Material Models on the Accuracy of the Sheet Forming Simulation". In: *Materials and Manufacturing Processes* 27:3, pp. 273–277. DOI: 10.1080/10426914.2011.578005.

Bandpay, M G (2015). "Instability and Fracture Models to Optimize the Metal Forming and Bending Crack Behaviour of Al-Alloy Composites". PhD thesis. ETH Zurich.

Barlo, A (2019). "Investigation of Alternative Evaluation Spaces for Failure Prediction in Sheet Metals". MA thesis. Aalborg University.

Barlo, A et al. (Sept. 2019). "Investigation of a Bending Corrected Forming Limit Surface for Failure Prediciton in Sheet Metals". In: *Conference Proceedings, Forming Technology Forum 2019, September 19-20, Munich, Germany*.

Basaran, M et al. (2010). "An extension of the GISSMO damage model based on lode angle dependency". In: *Conference Proceedings of the 9th LS-Dyna Anwenderforum*.

Blessing, L T M and A Chakrabarti (2009). *DRM, a Design Research Methodology*. 1st edn. ISBN: 978-1-84882-587-1. Springer London.

Bonatti, C and D Mohr (2021). "Neural network model predicting forming limits for Bi-linear strain paths". In: *International Journal of Plasticity* 137, p. 102886. DOI: 10.1016/j.ijplas.2020.102886.

Bylund, N (2004). “Simulation Driven Product Development Applied to Car Body Design”. PhD thesis. Luleå University of Technology.

Cook, R D et al. (2002). *Concepts and Applications of Finite Element Analysis*. 4th edn. ISBN:978-0-471-35605-9. Wiley.

Corres, A B F d (2022). “Development of a New Methodology to Determine the Forming Limit Diagram”. Bachelor Thesis. Mondragon University.

Ertürk, S, M Sester, and M Selig (2018). “Limitations of Forming Limit Diagrams: Consideration of Bending Strain, Surface and Edge Cracks”. In: *Conference Proceedings, Forming Technology Forum 2018, July 2-3, Zurich, Switzerland*.

Gorji, M B et al. (2020). “On the potential of recurrent neural networks for modeling path dependent plasticity”. In: *Journal of the Mechanics and Physics of Solids* 143, p. 103972. DOI: 10.1016/j.jmps.2020.103972.

Graf, A and W Hosford (1993). “Effect of changing strain paths on forming limit diagrams of Al 2008-T4”. In: *Metallurgical and Materials Transactions A* 24.671.

Hol, J et al. (2012). “Advanced friction modeling for sheet metal forming”. In: *Wear* 286-287, pp. 66–78. DOI: 10.1016/j.wear.2011.04.004.

Metallic materials – Sheet and strip – Determination of forming-limit curves (Oct. 2008). Standard. Geneva, CH: International Organization for Standardization.

Metallic materials – Sheet and strip – Hole expanding test (Aug. 2018). Standard. Geneva, CH: International Organization for Standardization.

Keeler, S and W Backofen (1964). “Plastic instability and fracture in sheet stretched over rigid punches”. In: *AMS Transactions Quarterly* 56, pp. 25–48.

Larour, P et al. (2014). “Evaluation of alternative stretch flangeability testing methods to ISO 16630 standard”. In: *Conference Proceedings, International Deep Drawing Research Group (IDDRG), June 1-4, 2014, Paris, France*.

Liewald, M and M Gall (2013). “Experimental Investigation of the Influence of Shear Cutting Parameters on the Edge Crack Sensitivity of Dual Phase Steels”. In: *Conference Proceedings, International Deep Drawing Research Group (IDDRG), June 2 - 5, 2013, Zurich, Switzerland*.

Manopulo, N and B Carleer (2019). “On the way towards a comprehensive failure modelling for industrial sheet metal stamping processes”. In: *IOP Conference Series: Materials Science and Engineering* 651, p. 012004. DOI: 10.1088/1757-899X/651/1/012004.

— (2020). “A new workflow for the effective distinction between necking induced spilts and direct fracture phenomena”. In: *IOP Conference Series: Materials Science and Engineering* 967, p. 012066. DOI: 10.1088/1757-899X/967/1/012066.

Mattiasson, K, J Jergéus, and P DuBois (2014). “On the prediction of failure in metal sheets with special reference to strain path dependence”. In: *International Journal of Mechanical Sciences* 88, pp. 175–191. DOI: 10.1016/j.ijmecsci.2014.08.006.

Müller, A et al. (2021). “Machine Learning Classifiers for Surface Crack Detection in Fracture Experiments”. In: *International Journal of Mechanical Sciences* 209, p. 106698. DOI: 10.1016/j.ijmecsci.2021.106698.

Needleman, A and V Tvergaard (1977). “Necking of biaxially stretched elastic-plastic circular plates”. In: *Journal of the Mechanics and Physics of Solids*, pp. 159–183.

Neukamm, F, M Feucht, and A Haufe (2008). “Consistent damage modelling the the process chain of forming to crashworthiness simulations”. In: *Conference Proceedings of the 7th LS-Dyna Anwenderforum*.

Norz, R et al. (2022). “Prediction of Necking Initiation in Case of Abrupt Changes in the Loading Direction”. In: *The Minerals, Metals & Materials Series: NUMISHEET 2022*, pp. 617–625. DOI: 10.1007/979-3-031-06212-4_56.

Olofsson, E and M Al-Fadhli (2022). “Pre-Straining Operation: Prediction of Strain Paths Within a Forming Limit Diagram”. Master Thesis. Blekinge Institute of Technology.

Pierron, F and M Grédiac (2021). “Towards Material Testing 2.0. A review of test design for identification of constitutive parameters from full-field measurements”. In: *Strain* 57, p. 12370. DOI: 10.1111/str.12370.

Pilthammar, J (2017). “Elastic Press and Die Deformations in Sheet Metal Forming Simulations”. Licentiate Thesis. Blekinge Institute of Technology.

Schneider, M et al. (2015). “Overview and comparison of various test methods to determine formability of a sheet metal cut-edge and approaches to the test results application in forming analysis”. In: *Materialwissenschaft und Werkstofftechnick* 46 (12), pp. 1196–1217. DOI: 10.1002/mawe.201500446.

Sigvant, M, K Mattiasson, and M Larsson (2008). “The Definition of Incipient Necking and its implication on Experimentally or Theoretically Determined Forming Limit Curves”. In: *Conference Proceedings, International Deep Drawing Research Group (IDDRG), 16-18 June, 2008, Olofström, Sweden*.

Sigvant, M and J Pilthammar (2019). *Sheet Metal Forming Simulations at Volvo Cars: The past, the present and the future*. Keynote presentation, Forming Technology Forum, 19-20 September 2019, Munich, Germany.

Sigvant, M, J Pilthammar, et al. (2018). “Smart Stamping: Improved Quality in Stamping by Model Drive Control”. In: *Conference Proceedings, Forming Technology Forum 2018, July 2-3, Zurich, Switzerland*.

Sowerby, R and J L Duncan (1971). “Failure in sheet metal in biaxial tension”. In: *International Journal of Mechanical Sciences* 13, pp. 217–229.

Sriram, S et al. (2003). “Stretch Bendability of Advanced High Strength Steels”. In: *SAE Transactions* 112, pp. 641–649. ISSN: 0096736X, 25771531.

Stoughton, T (2000). “A general forming limit criterion for sheet metal forming”. In: *International Journal of Mechanical Sciences* 42 (1), pp. 1–27. DOI: 10.1016/S0020-7403(98)00113-1.

United Nations (2023). *The 17 Goals*. URL: https://www.globalgoals.org/goals/ (visited on 01/21/2023).

Volk, W and J Suh (2013). "Prediction of formability for non-linear deformatino history using generalized forming limit concept (GFLC)". In: *AIP Conference Proceedings* 1567 (1), pp. 556–561. DOI: 10.1063/1.4850035.

Wang, K, L Greve, and T Wierzbicki (2015). "FE simulation of edge fracture considering pre-damage from blanking process". In: *International Journal of Solids and Structures* 71, pp. 206–218. DOI: 10.1016/j.ijsolstr.2015.06.023.

Yoon, J I et al. (2016). "Factors governing hole expansion ration of steel sheets with smooth sheared edge". In: *Metals and Materials International* 22, pp. 1009–1014. DOI: 10.1007/s12540-016-6345-5.

Zeng, D et al. (2009). "A Path Independent Forming Limit Criterion for Sheet Metal Forming Simulations". In: *SAE International Journal of Materials and Manufacturing* 1.1, pp. 809–817. ISSN: 19463979, 19463987.

Zhang, A and D Mohr (2020). "Using neural networks to represent von Mises plasticity with isotropic hardening". In: *International Journal of Plasticity* 132, p. 102732. DOI: 10.1016/j.ijplas.102732.

PAPER A

A Barlo, M Sigvant, and B Endelt (2019). ”On the Failure Prediction of Dual-Phase Steel and Aluminium Alloys Exposed to Combined Tension and Bending”. In: *IOP Conference Series: Materials Science and Engineering* 651, p. 012030 DOI: 10.1088/1757-899X/651/1/012030

IOP Conf. Series: Materials Science and Engineering **651** (2019) 012030 doi:10.1088/1757-899X/651/1/012030

On the Failure Prediction of Dual-Phase Steel and Aluminium Alloys Exposed to Combined Tension and Bending

Alexander Barlo[1,2*], Mats Sigvant[1,3], and Benny Endelt[2]

[1]Volvo Cars Dept. 81110 Strategy & Concept, Olofström, Sweden
[2]Department of Materials and Production, Aalborg University, Aalborg, Denmark
[3]Department of Mechanical Engineering, Blekinge Institute of Technology, Karlskrona, Sweden

E-mail: Alexander.Barlo@volvocars.com

Abstract. The interest in accurate prediction of failure of sheet metals in the automotive industry has increased significantly over the last two decades. This paper aims to evaluate two failure prediction approaches implemented in the commercial Finite Element code AutoForm^{plus} R7.04; (i) the standard Forming Limit Diagram (FLD), and (ii) the Non-linear Forming Limit Diagram. The evaluation will be testing the two approaches accuracy on predicting failure of both an AA6016 aluminium alloy and a CR440Y780T-DP dual-phase steel alloy specimen exposed to combined tension and bending. Based on the findings of this study, it is concluded that neither of the evaluated approaches is able to accurately predict failure in both cases presented.

1. Introduction

In the automotive industry today, a lot of effort is put into the failure prediction of sheet metal parts to ensure stamping process feasibility. Even though a large variety of failure prediction approaches have been proposed during the last decade, none of these have been able to replace the Forming Limit Diagram (FLD) as the industry standard within the sheet metal forming community.

At Volvo Cars Body Components, the focus on accurate failure prediction has increased over the years, and several experiments of AA6016 aluminium and CR440Y780T-DP dual-phase steel alloy specimens, exposed to combined tension and bending, have been performed. The research presented in this paper aims to evaluate two failure prediction methods implemented in the commercial Finite Element code AutoForm^{plus} R7.04:

(i) The standard Forming Limit Diagram (FLD).
(ii) The Non-linear Forming Limit Diagram.

For clarification, the term FLD is used as a description of the complete Forming Limit Diagram, containing both Forming Limit Curves (FLC) and strain fields.

The evaluation of said methods will be based on numerical models calibrated towards experiments recorded with Digital Image Correlation (DIC) to obtain the history of the forming operation.

2. Experimental Work

2.1. Experimental Setup

Experiments with punch radii of 3, 6, and 10 mm have been conducted in the setup presented in Figure 1. In the setup, the punch is moved 6 mm to the right of the model in order to eliminate the stochastic fracture location, that otherwise would be with the punch located in the centre. All tests have been run to failure, and the applied DIC is used to go back in operation history to investigate the strain development. The focus of this paper will be on the setup with a punch radius of 6 mm.

The experiments are performed as single-action draw operations with a ram velocity of 25 mm/s.

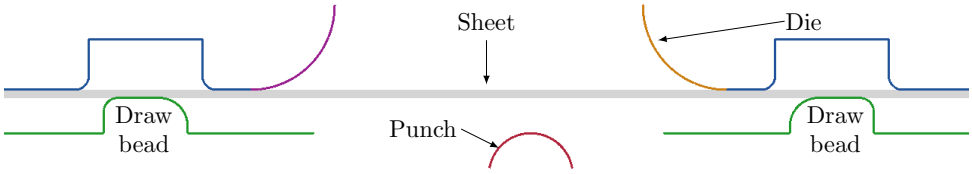

Figure 1. Cross-sectional view of the experimental setup geometry.

2.2. Experimental Repeatability

The repeatability of the AA6016 aluminium alloy is tested, to ensure the experimental data used is not an outlier.

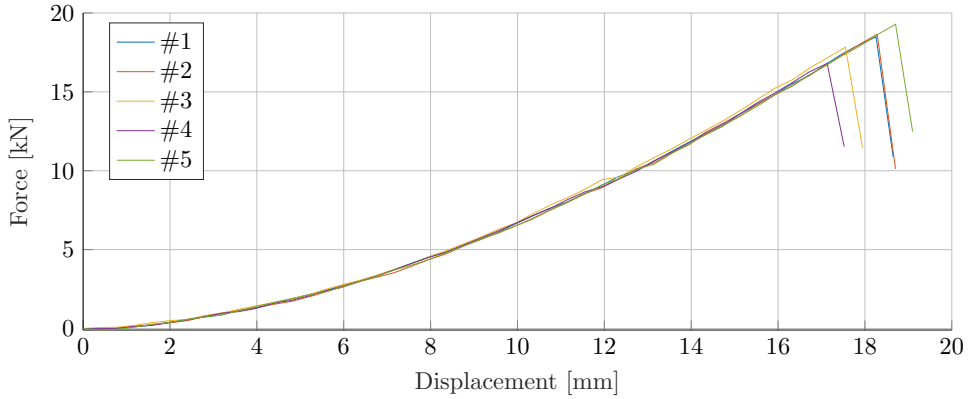

Figure 2. Force-displacement curves of the AA6016 aluminium alloy. Five tests have been conducted in order to determine repeatability.

As presented in Figure 2, the force-displacement curves of the repeated experiments align well on the force levels, but show a deviation between lowest and highest punch depth of approximately 2 mm at the point of fracture.

2.3. Neck Detection of Specimens

An undesirable phenomenon in the sheet metal forming process is failure caused by fracture. To detect if the fracture of the specimens is neck initiated, a test has been terminated approximately

0.5 mm before the fracture should occur. The punch depth of this test is based on the experiment with the lowest displacement (experiment # 4 in Figure 2). Figure 3 presents the result of this test, where a section has been examined and measured under a microscope. The outcome of the examination is that a neck in the specimen is present, why it can be concluded that the fracture is initiated by necking.

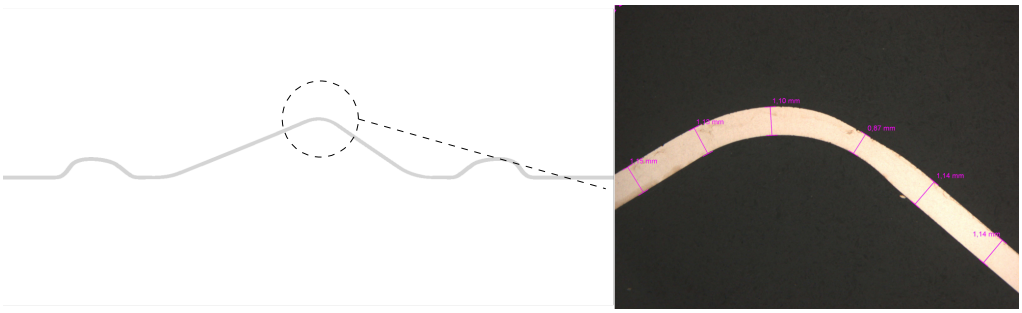

Figure 3. Cross section of an AA6016 specimen. The test has been terminated approximately 0.5 mm before fracture depth. The specimen clearly shows signs of necking.

3. Numerical Reproduction of Experiments

In order to evaluate the two failure criteria proposed, numerical reproductions of the experimental tests have been made in the commercial Finite Element code AutoForm^{plus} R7.04. Models for both the AA6016 aluminium and CR440Y780T-DP dual-phase steel alloy have been created using the elasto-plastic shell element with 11 integration points through the thickness.

3.1. Material Models

The hardening curves of the material models have been created from a combination of tensile tests and bulge tests. The applied hardening curves can be found in Figures 4 and 5.

The anisotropic behaviour is modelled using the Banabic-Balan-Comsa (BBC) yield criterion for both materials. This is done as more than 10 years of experience at Volvo Cars proves this to perform well. The same experience does however show, that the standard values for the exponent M ($M = 2 \cdot k$, 6 for BCC structure, and 8 for FCC structure [1]) need to be calibrated. The calibration of the exponent is performed by inverse modelling of the Limiting Dome Height (LDH) test.

3.2. Strain Predictions

In order to be secure accurate numerical reproductions of the experiments, a comparison of simulated and experimental major strain values is performed. The comparison is carried out by applying the DIC software ARAMIS^{TM} by GOM, where a stochastic pattern has been applied to the surface of the experimental specimens prior to testing.

Figures 6 and 7 present the major strain comparison of the numerical models and the experiments. The full lines represent the experimental data, and the dashed lines represent the numeric results. The vertical line at X = 6 mm indicates the center of the punch, and the distances in the legend describe the punch displacement distance from fracture. The predictions

Table 1. Material models used for the numerical reproduction of both the AA6016 aluminium alloy and the CR440Y780T-DP dual-phase steel alloy.

Parameter	**AA6016**	**CR440Y780T-DP**
σ_0	110.3 [MPa]	309.5 [MPa]
σ_{45}	105.9 [MPa]	307.8 [MPa]
σ_{90}	106.5 [MPa]	313.4 [MPa]
σ_b	98.3 [MPa]	307.5 [MPa]
r_0	0.732	0.678
r_{45}	0.535	0.875
r_{90}	0.677	0.848
r_b	1.01	1.02
Exponent (M)	5.7	6.2
Yield Criteria	BBC	BBC
Thickness Stress	ON	ON

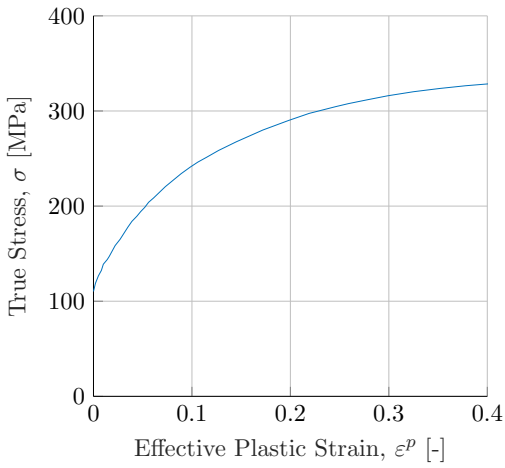

Figure 4. Hardening curve of the AA6016 aluminium alloy.

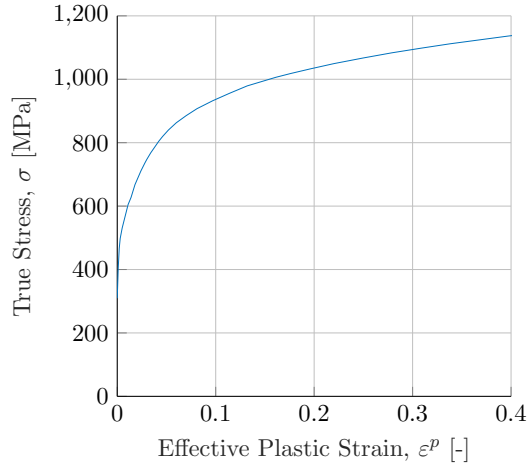

Figure 5. Hardening curve of the CR440Y780T-DP dual-phase steel alloy.

of the numerical models presented corresponds well with those of the experiments up until the last data extracted. This is believed to be due to the initialization of unstable necking, as the last data presented (red lines) are located less than 0.5 mm from fracture. The underprediction of the simulated major strain in the last stages could result in numerical models that do not indicate failure.

4. Failure Prediction

Having obtained numerical models with acceptable accuracy, the two specified failure prediction approaches can now be evaluated.

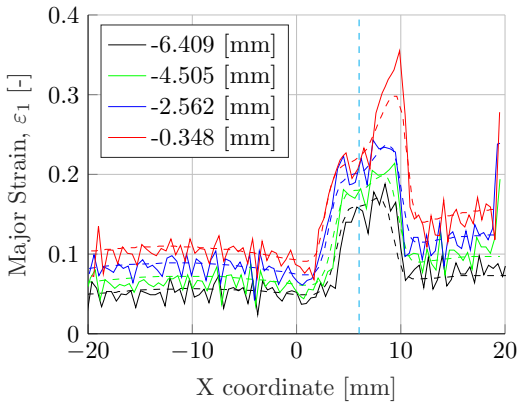

Figure 6. Major strain prediction of the AA6016 aluminium alloy numerical model. The distances presented in the legend cover both the experimental and numerical results.

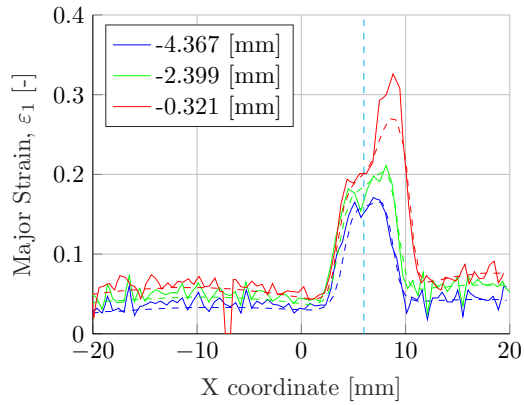

Figure 7. Major strain prediction of the CR440Y780T-DP dual-phase steel alloy numerical model. The distances presented in the legend cover both the experimental and numerical results.

4.1. Standard Forming Limit Diagram (FLD)

The Forming Limit Diagram (FLD) initially proposed by [2], has for the past many years been the industry standard within the automotive industry for predicting failure in sheet metal parts. The FLD does however require proportional loading to be applicable [3][4]. From a theoretical point of view, this would instantly reject the FLD as a suitable approach for failure prediction in specimens exposed to combined tension and bending. However, from an engineering point of view, the FLD approach is tested to investigate if the bending-under-tension load situation in the specimens could be evaluated accurately with the FLD option implemented in AutoForm^{plus} R7.04.

Figures 8 and 9 present the strain paths of the two alloys in the element with the highest major strain value at the end of the simulation. Strain paths in the bottom (blue), membrane (green), and top (black) layer are presented. As seen, the strain path in both models is far from linear in all layers included. Furthermore, indications of fracture in the top layer of both models is present, despite the numerical model underpredicting the major strain of a point in time where the specimen has not yet fractured. This leads to the conclusion that the standard FLD can not be applied to specimens exposed to combined tension and bending.

4.2. Non-linear Forming Limit Diagram

The evaluation of non-linear strain paths for failure prediction in metal sheets, is a topic that has been discussed for many years. The approach investigated in this paper, is the Non-linear Forming Limit Diagram implemented in AutoForm^{plus} R7.04 based on [5] and [6]. In short, the approach is expressed by a metamodel of a the total strain path length ratio λ, as presented in Equation 1.

$$\lambda = f(l_{pre}, \beta_{pre}, l_{post}, \beta_{post}) = \lambda_{pre} + \lambda_{post} = \frac{l_{pre}(\beta_{pre})}{l_{FLC}(\beta_{pre})} + \frac{l_{post}(\beta_{post})}{l_{FLC}(\beta_{post})} \quad (1)$$

The Non-linear Forming Limit Diagram is used to predict the onset of necking in sheets. To determine the point where an instability is introduced in the experiments, the approach proposed

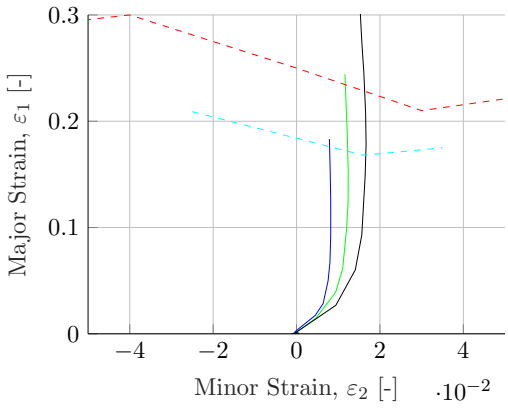

Figure 8. The strain paths of one element in the numerical model of the AA6016 aluminium alloy.

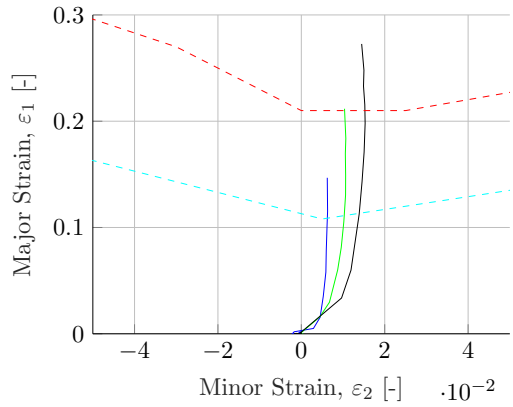

Figure 9. The strain paths of one element in the numerical model of the CR440Y780T-DP dual-phase steel alloy.

by [7], using the first derivative of the major strain with respect to time (strain rate), is applied. The instability point, determined in ARAMIS^{TM}, is then reproduced in the numerical model, and comparisons of the standard Forming Limit Diagram and the Non-linear Forming Limit Diagram can be performed. Figures 10 and 11 present the Forming Limit Diagram and the Non-linear Forming Limit Diagram of the AA6016 aluminium alloy.

The Forming Limit Diagram presented in Figure 10 reveals that the point of instability has been passed. This is in line with the findings in Section 4.1.

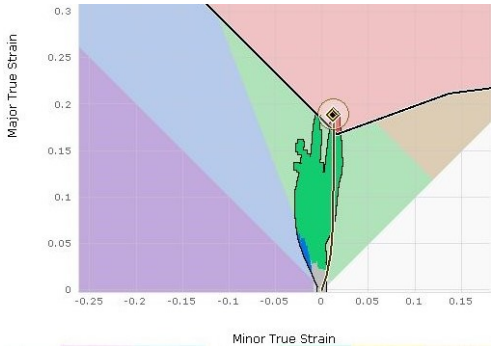

Figure 10. Forming Limit Diagram of the AA6016 aluminium alloy.

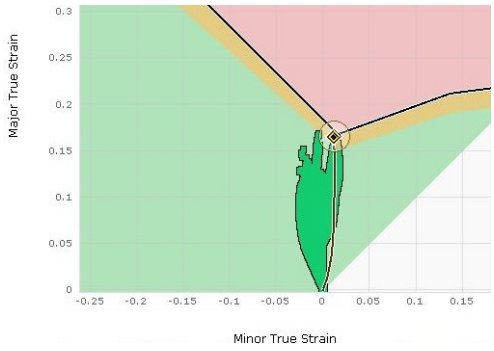

Figure 11. Non-linear Forming Limit Diagram of the AA6016 aluminium alloy.

Turning to the Non-linear Forming Limit Diagram (Figure 11), the model implemented in AutoForm^{plus} R7.04 yields a result that is acceptable, where indication of being on the border of instability is presented. This means that the Non-linear Forming Limit Diagram is an applicable approach in the case of the AA6016 aluminium alloy, but in order to accept it as a general

approach, it must also perform well for other materials and radii.

Figures 12 and 13 present the standard Forming Limit Diagram and Non-Linear Forming Limit Diagram of the CR440Y780T-DP dual-phase steel alloy. The same approach for detection of the point of instability as used in the AA6016 aluminium alloy case is applied for this case.

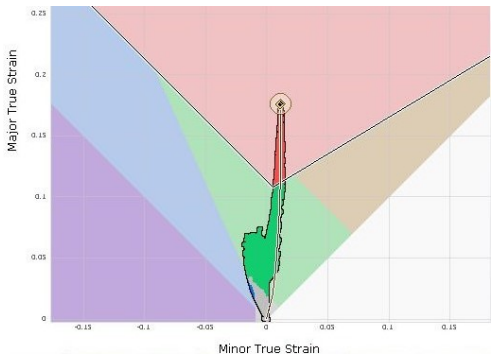

Figure 12. Forming Limit Diagram of the CR440Y780T-DP dual-phase steel alloy.

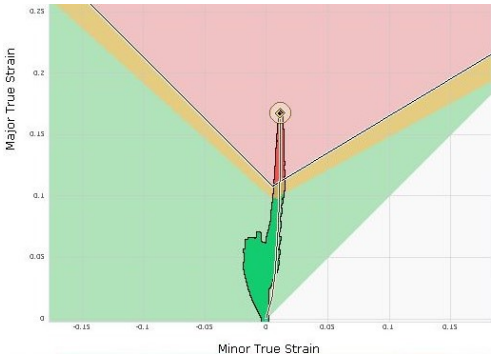

Figure 13. Non-linear Forming Limit Diagram of the CR440Y780T-DP dual-phase steel alloy.

The standard Forming Limit Diagram (Figure 12) yields that the point of instability is passed. What is interesting is that the Non-linear Forming Limit Diagram (Figure 13) also indicates that the point of instability has been passed. Furthermore, the magnitude of the strain level above the instability limit is significant and is believed not to be due to experimental uncertainties.

As the approach has not been able to predict the point of instability in both cases (both the AA6016 aluminium and CR440Y780T-DP dual-phase steel alloy), the authors of this paper can not accept the Non-linear Forming Limit Diagram as a general approach in its current implementation.

5. Conclusion

The work presented in this paper aimed to evaluate the following two failure prediction approaches implemented in the commercial Finite Element code AutoForm^{plus} R7.04 in regards to handle specimens exposed to combined tension and bending:

(i) The standard Forming Limit Diagram (FLD)
(ii) The Non-linear Forming Limit Diagram

Through comparison of experiments and numerical models, the industry standard Forming Limit Diagram proved to be not applicable due to its inability to handle the non-linear strain paths during the forming operation. The Non-linear Forming Limit Diagram yielded an accurate prediction of the AA6016 aluminium alloy, but performed poorly for the CR440Y780T-DP dual-phase steel alloy. Due to the unstable performance of the approach, the Non-linear Forming Limit Diagram is, in this paper, not accepted as a general approach.

Based on the research presented in this paper, it can be concluded that none of the evaluated approaches can be accepted as general approaches to failure prediction of specimens exposed to combined tension and bending.

6. Future Work

As presented in this paper, the two approaches evaluated were not able to accurately predict failure for all cases and failure modes. In both the stamping and crash community, a general accurate approach for predicting different failure modes is of great interest.

An interesting approach to reduce the sensitivity to non-linear strain paths in failure prediction of metal sheets, is to investigate the stress based FLD presented in e.g. [10], where the FLD in the principal strain space is transformed into the principal stress space.

Another interesting approach is the damage accumulation model GISSMO. The GISSMO model relies on tracking the damage state in different stages of the simulation in form of the plastic strain, and comparing it to a specified failure strain value dependent on both the triaxiality [8] and the Lode angle [9]. This approach will be the starting point for further research on this topic by the authors.

Yet another interesting question to raise, is where numerical models are evaluated. Both the standard Forming Limit Diagram and the Non-linear Forming Limit Diagram evaluates the models in the membrane layer, but Figures 8 and 9 present steep strain gradients across the thickness of the blank. Therefore, failure prediction approaches evaluating the blank at the top layer of the model, when exposed to combined tension and bending, is believed to be an interesting approach.

Acknowledgments

The authors of this report would like to thank Dr. Niko Manopulo from AutoForm Engineering GmbH for the interesting discussions about the Finite Element models concerning the AA6016 aluminium alloy. Furthermore, the authors would like to show their gratitude towards Prof. Dr. Wolfram Volk and Mr. Roman Norz from the Lehrstuhl für Umformtechnik und Geißereiwesen at Techniches Universität München for their assistance regarding the Non-linear Forming Limit Diagram approach.

References

[1] Banabic,D. & Sester,M.(2012), 'Influence of material models on the accuracy of the sheet metal simulations', *Material and Manufacturing Processes* **27**, 304-8.
[2] Keeler,S. & Backofen,W.(1964), 'Plastic instability and fracture in sheet stretched over rigid punches',*ASM Trans. Quart.* **56**, 25-48.
[3] Hosford,W.F. & Cadell,R.M.(2007), *Metal Forming - Mechanics and Metallurgy*, ISBN 9780521881210, 3rd edn., Cambridge University Press.
[4] Banabic,D.(2010), *Sheet Metal Forming Processes - Constitutive Modelling and Numerical Simulations*, ISBN 9783540881124, 1st edn., Springer.
[5] Volk,W. et al.(2012), 'Failure prediction for nonlinear strain paths in sheet metal forming', *CIRP Annals - Manufacturing Technology* **61**, 259-262.
[6] Volk,W. et al.(2013), 'Phenomenological and numerical description of localized necking using generalized forming limit concept', *IDDRG Proceedings 2013*, 16-21.
[7] Sigvant,M. et al.(2008), 'The definition of incipient necking and its impact on experimentally or theoretically determined forming limit curves', *Proceedings of the IDDRG2008 Conference*, Olofström, Sweden.
[8] Neukamm,F. et al.(2008), 'On closing the constitutive gap between forming and crash simulation', *10^{th} International LS-DYNA Users Conference*, 12-21.
[9] Basaran,M. et al.(2010), 'An extension of the GISSMO damage model based on lode angle dependence', *9. LS-DYNA Anwenderforum.*
[10] Stoughton, T.B. & Yoon, J.W.(2010), 'A new approach for failure criterion for sheet metals', *International Journal of Plasticity* **27**, 440-459.

PAPER B

A Barlo, N Manopulo, M Sigvant, B Endelt, and K Trana (2019). ”Investigation of a Bending Corrected Forming Limit Surface for Failure Prediction in Sheet Metals”. In: *Conference Proceedings, Forming Technology Forum 2019, September 19-20, Munich, Germany*.

INVESTIGATION OF A BENDING CORRECTED FORMING LIMIT SURFACE FOR FAILURE PREDICTION IN SHEET METALS

Alexander Barlo[1,3*], Niko Manopulo[2], Mats Sigvant[1,4], Benny Endelt[3], Kristoffer Trana[1]

[1]Volvo Cars Stamping Engineering, Olofström, Sweden
[2]AutoForm Engineering GmbH, Zürich, Switzerland
[3]Department of Materials and Production, Aalborg University, Aalborg, Denmark
[4]Department of Mechanical Engineering, Blekinge Institute of Technology, Karlskrona, Sweden

ABSTRACT: Ensuring process feasibility is a high priority in the automotive industry today. Within the CAE departments concerning the manufacturing of body components, one of the most important areas of interest is the accurate prediction of failure in components through Finite Element simulations. This paper investigates the possibility of introducing the component curvature as a parameter to improve failure prediction. Bending-under-tension specimens with different radii are used to create a Bending Corrected Forming Limit Surface (BC-FLS), and a test die developed at Volvo Cars, depicting production-like scenarios by exposing an AA6016 aluminium alloy blank to a stretch-bending condition with biaxial pre-stretching, is used to validate the proposed model in the commercial Finite Element code AutoForm^{TM} R8. The findings of this paper showed that the proposed BC-FLS approach performed well in the failure prediction of the test die compared to the already in AutoForm^{TM} R8 implemented max failure approach.

KEYWORDS: Sheet Metal Forming, Failure Prediction, Formability, Curvature Dependency

1 INTRODUCTION

In the automotive industry today, one of the top priorities is to ensure process feasibility. One of the areas where this is seen, is within the Computer Aided Engineering (CAE) departments concerning the design and manufacturing of body components. Over the past years, more complex lightweight materials, such as AHSS and aluminium alloys, have been introduced along with increased component complexity. One of the great challenges the automotive industry faces today in regard to ensuring process feasibility, is the accurate prediction of failure of parts during the engineering phase. Between different industries, the term 'failure' has different meanings, but within the stamping department at Volvo Cars, failure is defined as *the onset of necking*.

For the past decades, the standard way of predicting failure in sheet metal forming simulations has been to apply the Forming Limit Diagram (FLD) originally proposed by Keeler & Backofen [1]. As the research on formability of sheet metals has advanced, the FLD approach has at several occasions been proven to perform poorly e.g. for components experiencing non-linear strain paths, or components where the stamping operation includes bending over a sharp radius.

The latter case has been investigated by e.g. Barlo et al. [2] presenting an evaluation of the performance of the FLD and the Non-Linear Forming Limit Diagram for failure prediction in dual-phase steel and aluminium alloys exposed to bending under tension. This evaluation of the FLD showed that it was indeed not able to accurately predict the onset of necking in a numerical model of the tested components.

Based on these observations, this paper aims to investigate how a bending correction of the standard Forming Limit Curve (FLC) could aid in the accurate failure prediction of components exposed to bending under tension for components of an AA6016 aluminium alloy.

2 EXPERIMENTAL WORK

In this paper two different experimental setups are used other than the Nakajima test setup used to determine the standard FLC:

* Corresponding author: Bruksgatan 1, SE-293 38 Olofström, Sweden, Alexander.Barlo@volvocars.com

1. Bending-under-tension experimental setup
2. Volvo Cars bending-under-tension test die

2.1 BENDING-UNDER-TENSION EXPERIMENTAL SETUP

The bending-under-tension experiments are used to perform the bending correction of the FLC. An experimental setup with three changeable double-curved punches with three different major radii of 3, 6, and 10 mm, and a minor punch radius of 100 mm is used. The reasoning for applying double-curved punches is to reduce the risk of a stochastic fracture location, and for the same reason the punch centre has been offset 6 mm to one side. An illustration of the experimental setup is presented in Figure 1.

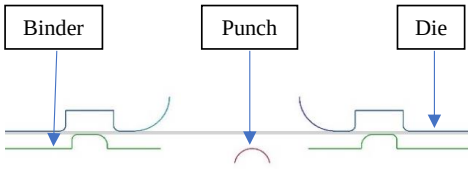

Fig. 1 *Illustration of the bending-under-tension experimental setup. The punch in the setup is changeable between punches of 3, 6, or 10 mm.*

To ensure the stretch-bending condition being present, locking beads (see Figure 2) are used to prevent material flow towards the area exposed to the actual bending operation.

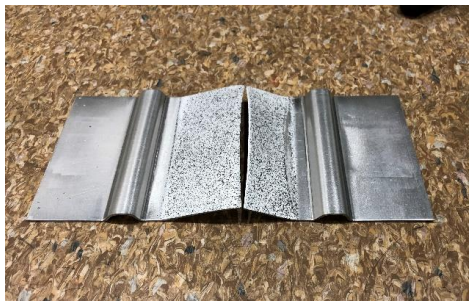

Fig. 2 *Post operation bending-under-tension specimen. The stochastic pattern applied to the surface is used for the DIC analysis.*

The experiments are performed in a single-action mechanical press using the die as the displacing tool, and with a ram velocity of 25 mm/s. The actual experimental setup is presented in Figure 3.

Fig. 3 *Setup for the bending-under-tension experiments.*

On top of the die, two cameras are mounted enabling 3D Digital Image Correlation (DIC) and strain history analysis through the software ARAMIS™ developed by GOM.

2.2 VOLVO CARS BENDING-UNDER-TENSION TEST DIE

The Volvo Cars Bending-Under-Tension Test Die has been developed to depict a more production-like scenario, as the blank during stamping is exposed to a stretch-bending condition with biaxial pre-stretching as encountered in critical features such as door handles or fenders.

Fig. 4 *Volvo Cars Bending-Under-Tension Test Die panel. The die produces two different geometries, using punch nose radii of 4 and 8 mm.*

The panel produced by the test die is presented in Figure 4. The die produces two different geometries, and each geometry is repeated two times – one time with punch nose radius 4 mm and one with punch nose radius 8 mm. Furthermore, each of the geometries are then repeated a number of times with different feature depths to capture the actual forming limits. For the validation of the proposed failure prediction approach, only one of the geometries is initially of interest.

No DIC measurements has been recorded on this panel, why a manual inspection has been performed instead. The outcome of the manual inspection is presented in Figure 5.

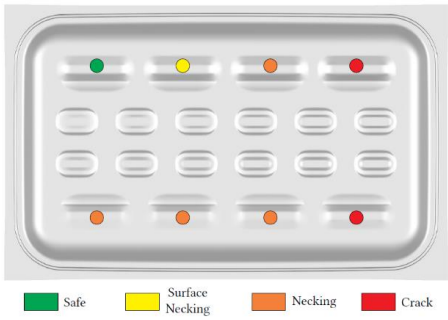

Fig. 5 *Outcome of the manual inspection of the stamped panel. Results for only one geometry is presented as this is initially the only one used for failure prediction approach validation.*

3 MATERIAL CHARACTERIZATION

For a validation of the proposed failure prediction approach, a numerical model of the Volvo Cars Bending-Under-Tension Test Die will be applied.

Table 1: *Material parameters for de modelling of the AA6016 aluminium alloy with the BBC05 yield surface.*

Material Parameter	Value	Unit
R_0	0.732	-
R_{45}	0.535	-
R_{90}	0.677	-
R_b	1.007	-
σ_0	110.3	MPa
σ_{45}	105.9	MPa
σ_{90}	106.5	MPa
σ_b	98.3	MPa
M	5.7	-

To ensure valid numerical results, an important factor is the applied material model. As experience throughout the years at Volvo Cars have shown the BBC05 material model to perform well, this material model will also be applied in this case. Material parameters of the AA6016 aluminium alloy used for the material model are listed in Table 1, and the applied hardening curve is presented in Figure 6.

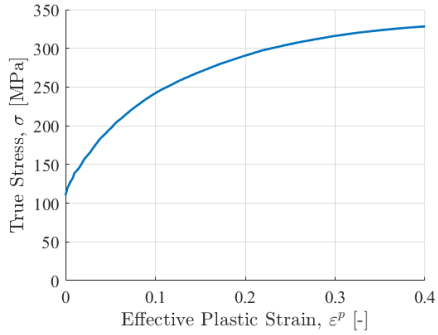

Fig. 6 *Hardening curve of the AA6016 aluminium alloy.*

4 DETERMINING THE EXPERIMENTAL ONSET OF NECKING

As defined in the introduction of this paper, the term failure is defined as onset of necking. Approaches to determine the onset of necking in experiments is something that has been discussed for several years and has still not been defined. Several approaches have been proposed e.g. the time dependent method proposed by Volk et al. [3] and a major strain rate based method proposed by Sigvant et al. [4]. To determine the initial FLC for onset of necking, as well as the onset of necking in the bending-under-tension experiments, an approach based on the development of the first derivative with respect to time of the major strain ($\dot{\varepsilon}_1$) proposed by Sigvant et al. [4] is applied. The major strain rate is calculated based on a statistical area introduced to the DIC measurement. The derivative is found using both the previous and next point in time as presented in Equation (1).

$$\dot{\varepsilon}_1 = \frac{\varepsilon_1(t_{n+1}) - \varepsilon_1(t_{n-1})}{t_{n+1} - t_{n-1}} \quad (1)$$

Figure 7 presents an example of how this analysis could turn out. In the method applied, the onset of necking is defined to occur when the maximum measured major strain rate exceeds the predicted average plus three standard deviations.

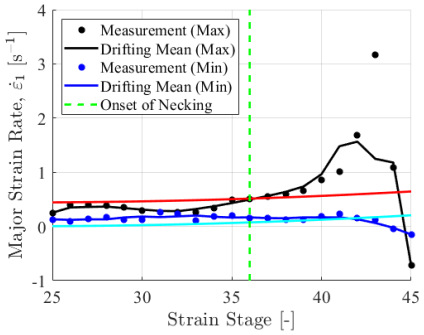

Fig. 7 *Illustration of determination of the onset of necking in a bending-under-tension R6 specimen. The onset of localized necking is passed once the drifting mean exceeds the predicted average (red line) plus three standard deviations.*

5 INFLUENCE OF BENDING ON SHEET FORMABILITY

The influence of bending on the formability of sheet materials is something that has been previously investigated by e.g. Atzema et al. [5] and Vallellano et al. [6]. A format often used to visualize the bending effect on sheet formability is to consider the outer surface maximum major strain at maximum force as a function of the thickness / tool radius ratio (α). Performing this check for the AA6016 aluminium alloy bending-under-tension experiments, Figure 8 show an increase in failure strain with the decrease of tool radius.

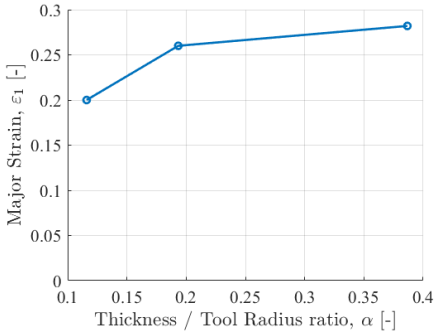

Fig. 8 *Bending influence on the outer surface maximum major strain for the AA6016 aluminium alloy bending-under-tension experiments. The values have been obtained from the DIC analysis.*

The increase of the major strain at the outer surface with a decrease in tool radius illustrates quite well why the FLD performs poorly for bending over sharp radii. The Nakajima test used to determine the standard FLC employs a hemispherical punch with a radius of 50 mm. With this observation, a bending correction of the standard FLC now seems even more interesting.

6 BENDING CORRECTION OF THE STANDARD FLC

In this first attempt to create a bending correction in this paper, the entire FLC will be corrected by an offset ($\Delta\varepsilon_1$). To determine this offset, the DIC measurements of the bending-under-tension experiments are used to find the delta value between the outer surface maximum major strain, and the standard FLC. This delta value is determined as presented in Equation (2) and illustrated in Figure 9.

$$\Delta\varepsilon_1 = \varepsilon_{1,DIC,max} - \varepsilon_{1,FLC}(\varepsilon_{2,DIC}) \quad (2)$$

Table 2 presents a nomenclature of the variables presented in Equation (2), and Table 3 presents the data determined from the DIC measurements of the bending-under-tension experiments. Using Equation (2) the bending corrected curves are determined and presented in Figure 10. The idea of creating a bending corrected FLC has previously been presented by e.g. Ertürk et al. [7] proposing a bending correction of the FLC in the membrane layer of a numerical model.

Table 2: *Nomenclature of variables used in Equation (2).*

Variable	Definition	Unit
$\varepsilon_{1,DIC,max}$	Experimental global maximum major strain	-
$\varepsilon_{2,DIC}$	Experimental minor strain at $\varepsilon_{1,DIC,max}$	-
$\varepsilon_{1,FLC}(\varepsilon_{2,DIC})$	FLC limit strain at $\varepsilon_{2,DIC}$	-

Table 3: *Values necessary to calculate the $\Delta\varepsilon_{11}$ values for the bending correction.*

Radius	$\varepsilon_{1,DIC,max}$	$\varepsilon_{2,DIC}$	$\varepsilon_{1,FLC}(\varepsilon_{2,DIC})$
3	0.282	0.022	0.173
6	0.260	0.011	0.175
10	0.200	0.001	0.185

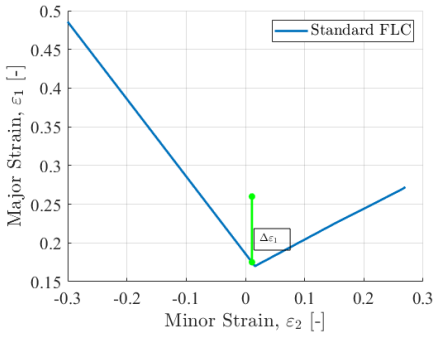

Fig. 9 *Illustration of the determination of the $\Delta\varepsilon_{11}$ value. The illustration exemplifies the R6 experiment, and the values presented in Table 3 have been used.*

To determine when to use which of the in Figure 10 presented curves, an additional parameter is introduced. In the work presented by Atzema et al. [4] the curvature (κ) on the concave side of the bend (tool curvature) was used as a measure to distinguish between the limit curves. This paper introduces the curvature to distinguish between limit curves, and thereby creating a limit surface. This surface will be called the Bending Corrected Forming Limit Surface (BC-FLS).

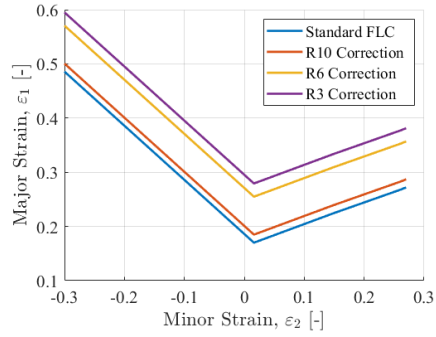

Fig. 10 *Bending corrected forming limit curves of the AA6016 aluminium alloy.*

As in [4], the curvature of the bend will be defined on the concave side i.e. it is calculated directly from the tool radius as presented in Equation (3)

$$\kappa = \frac{1}{R} \tag{3}$$

where R is the tool radius. This definition of the curvature yields the values presented in Table 4. The introduction of the curvature transfers the two-dimensional FLC into the three-dimensional space. A polynomial fitting of a surface to the data points, based on the best fit method, a BC-FLS ($\varepsilon_f(\varepsilon_{22}, \kappa)$) is performed, and yields a surface with an adjusted R^2 value of 0.9690. This limit surface is presented in Figure 11.

Table 4: *Curvature values at the concave side of the bend of the bending-under-tension specimens as well as for the Nakajima test.*

Radius:	3	6	10	50
Curvature:	0.3333	0.1667	0.1	0.02

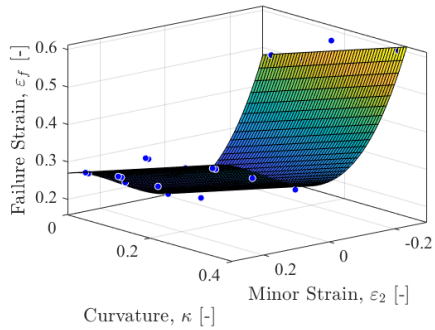

Fig. 11 *Bending corrected forming limit surface of the AA6016 aluminium alloy. The surface is created from a combination of the curves presented in Figure 10 and the curvatures presented in Table 4.*

The created BC-FLS does however have its limitations. Since the surface is fitted to data points, the presented failure strain definition should not be used outside of the experimentally defined space i.e. when the data points do not satisfy the conditions $-0.3 \leq \varepsilon_2 \leq 0.3$ and $0 \leq \kappa \leq 0.35$.

7 NUMERICAL EVALUATION

To validate the proposed BC-FLS approach, a numerical model of the Volvo Cars Bending-Under-Tension Test Die is used. The model is run in the commercial Finite Element code AutoForm™ R8. The model is created using the Elasto-Plastic Shell (EPS) element formulation with 11 integration points through the thickness, as well as an active consideration of surface pressure as a result of tool reactions and binder pressure. A simple friction model is applied using a global Coulomb friction coefficient of 0.12.

In this model, the draw beads have been of significance to ensure the presence of the stretch-bending phenomenon. Therefore, to reduce material flow in the model geometrical draw beads have been used.

To increase the possibility of capturing the onset of necking in the numerical model, a fine mesh is

applied in the zones exposed to bending with a minimum element size of 0.62 mm and a maximum allowed element angle of 10°.

To assess the state of the elements in the models, the idea of failure measure (F) to each element is introduced. The idea of failure in this model, is a direct relationship between the failure strain ($\varepsilon_f(\varepsilon_2, \kappa)$, graphically presented in Figure 11) and the element major strain at the convex side of the bend (ε_1) as presented in Equation (4). Once the failure measure reaches unity, the onset of necking has been reached for the element.

$$F = \frac{\varepsilon_1}{\varepsilon_f(\varepsilon_2, \kappa)} \tag{4}$$

Having a numerical model of the component, additional options regarding the definition of the curvature have become available. Evaluating the component at the convex side of the bended zones, the curvature is also found at this point. As the curvature could possibly variate within a single element, as exemplified in Figure 12, a choice must be made on which curvature definition should be used for the validation. As previously presented in Figure 8, the failure strain increases with an increase in curvature but due to the definition of the curvature on the concave side of the bend in the creation of the BC-FLS, the curvatures are lower than they should be from the DIC surface measurement. An initial attempt to account for this is to use the mean curvature (as defined in Equation (5)) of the element, thereby also lowering the curvature used for the validation.

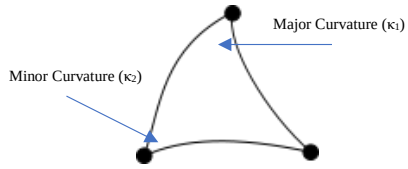

Fig. 12 *Example of curvatures on a triangular shell element. The indicated minor and major curvatures are used to calculate the mean curvature in the FE model used for the validation of the BC-FLS approach.*

$$\text{Mean Curvature} = \frac{\kappa_1 + \kappa_2}{2} \tag{5}$$

Having defined the curvature to be used in the numerical model, the validation can be performed. For the purpose of visualising the BC-FLS approach, Equation (4) has been implemented as a User Defined Variable (UDV) in AutoForm™ R8. Figures 13 (a) and (b) present the top and bottom rows of the Volvo Car Bending-Under-Tension Test Die component respectively.

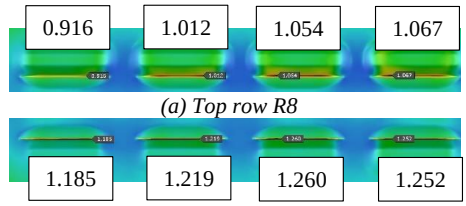

(a) Top row R8

(b) Bottom row R4

Fig. 13 *Local failure maxima for one geometry.*

The fringe plots presented for the two rows are so-called 'out of range' plots, meaning all elements having passed a certain threshold are presented without colour. In the case of the BC-FLS the threshold value is set to 1, resulting in all elements having passed the onset of necking is presented without colour in the fringe plots. The results presented seems to accurately predict the failure state observed in the manual inspection of the panel presented in Figure 5.

To support a claim of this application to perform better than the standard FLD, the Max Failure approach implemented in AutoForm™ R8 is used as a reference. The local max failure maxima are presented in Figures 14 (a) and (b).

Comparing the results from Figures 13 and 14, it can be seen that the proposed BC-FLS approach predicts the onset of necking more accurately than the Max Failure approach implemented in AutoForm™ R8.

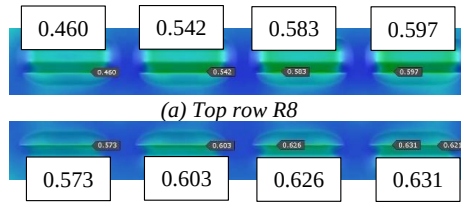

(a) Top row R8

(b) Bottom row R4

Fig. 14 *Local max failure maxima for one geometry.*

8 CONCLUSIONS

This paper presented an approach for failure prediction in sheet metal components exposed to bending over sharp radii during the forming operation. This approach is based on performing a bending correction of the standard Forming Limit Curve (FLC) based on tool curvature, thereby transforming the standard Forming Limit Diagram (FLD) into a Bending Corrected Forming Limit Surface (BC-FLS). The surface was created using experimental data from a series of bending-under-tension tests, where global maximum strain values were used to correct the FLC. From these corrected curves, and the major punch curvature, the BC-FLS

was fitted using a best fit approach. An evaluation of the Volvo Cars Bending-Under-Tension Test Die with an AA6016 aluminium alloy blank was performed in the commercial Finite Element code AutoForm™ R8.

The numerical model validated the proposed failure prediction approach, and a comparison of the proposed approach and the already implemented Max Failure approach in AutoForm™ R8 aided to support the claim that the BC-FLS is a step towards a more accurate failure prediction of components exposed to bending-under-tension.

9 FUTURE WORK

The work presented in this paper, is at an early stage why several points of improvements can be pointed out. In its current form, the BC-FLS approach presented in this paper, is a post-processing tool. For the Volvo Cars Bending-Under-Tension Test Die component, the maximum failure (failure as defined by Equation (4)) is fortunately located at the very end of the simulation. However, scenarios of changing strain paths during one or multiple stamping operations could cause onset of necking at an arbitrary point in the process time without the user noticing it. Based on this, the first improvement that must be done to the approach is to introduce the principle of a process maximum failure, where the maximum failure obtained in a specific element is kept, even if this is reduced due to changes in strain paths.

Also, the bending correction of the FLC must be improved. As presented in Table 1, the major strains used for the bending correction is in very near proximity of the plain strain loading condition. During their investigation Atzema et al. [4] concluded that the effect of an increased curvature was close to negligible in the proximity of the uniaxial loading condition, moderate in the proximity of the biaxial loading condition and large in the proximity of the plain strain loading condition. This indicates that the bending corrected curves presented in Figure 10, and the BC-FLS presented in Figure 11, heavily overpredict the failure strain limit on parts of the left-hand side of the FLD, while a moderate overestimation is suspected to be present on parts of the right-hand side.

As presented in this paper, the BC-FLS approach has performed well for the Volvo Cars Bending-Under-Tension Test Die with an AA6016 aluminium alloy blank. To verify the approach as being general, the study must initially be extended to investigate multiple grades of aluminium and eventually also to include other material types e.g. dual-phase steel alloys.

REFERENCES

[1] Keeler S. & Backofen W.: *Plastic Instability and Fracture in Sheet Stretched over Rigid Punches*. In: ASM Trans. Quart **56**, 25-48, 1964.

[2] Barlo A., Sigvant M., & Endelt B.: *On the Failure Prediction of Dual-Phase Steel and Aluminium Alloys Exposed to Combined Tension and Bending*. In: The 38th International Deep Drawing Research Group Annual Conference, 2019.

[3] Volk W., Weiss H., Jocham D., & Suh J.: *Phenomenological and Numerical Description of Localized Necking using Generalized Forming Limit Concept*. In: 2013 IDDRG Conference Proceedings, 2013.

[4] Sigvant M., Mattiasson K. & Larsson M.: *The Definition of Incipient Necking and its implication on Experimentally or Theoretically Determined Forming Limit Curves.* In: 2008 IDDRG Conference Proceedings, 2008.

[5] Atzema E. H., Frictorie E., van den Boogard A. H. & Droog J. M. M.: *The Influence of Curvature on FLCs of Mild Steel, (A)HSS and Aluminium.* In: The 28th International Deep Drawing Research Group Annual Conference, 519-528, 2010.

[6] Vallellano C., Morales D., Martinez A.J., & Garcia-Lomas F. J.: *On the use of the Concave-Side Rule and Critical-Distance Methods to Predict the Influence of Bending on Sheet-Metal Formability.* In: Int J Mater Form **3**, 1167-1170, 2010.

[7] Ertürk S., Sester M., & Selig M.: *Limitations of Forming Limit Diagrams: Consideration of Bending Strain, Surface and Edge Cracks.* In: FTF 2018 Conference Proceedings, 2018.

PAPER C

A Barlo, M Sigvant, N Manopulo, M S Islam, and J Pilthammar (2022). ”Failure Prediction of Automotive Components Utilizing a Path Independent Forming Limit Criterion”. In: *Key Engineering Materials* 926, pp. 906-916. DOI: 10.4028/p-u6g3p6

Key Engineering Materials
ISSN: 1662-9795, Vol. 926, pp 906-916
doi:10.4028/p-u6g3p6

Submitted: 2021-12-05
Revised: 2022-01-17
Accepted: 2022-02-04
Online: 2022-07-22

Failure Prediction of Automotive Components Utilizing a Path Independent Forming Limit Criterion

Alexander Barlo[1,a*], Mats Sigvant[1,2,b], Niko Manopulo[3,c], Md Shafiqul Islam[1,d], and Johan Pilthammar[1,2,e]

[1]Department of Mechanical Engineering, Blekinge Institute of Technology, Karlskrona, Sweden

[2]Volvo Cars Dept. 81110 Strategy & Concept, Olofström, Sweden

[3]AutoForm Development GmbH, Zurich, Switzerland

[a]Alexander.Barlo@bth.se, [b] mats.sigvant@volvocars.com, [c]niko.manopulo@autoform.ch, [d]mdm@bth.se, [e]johan.pilthammar@volvocars.com

Keywords: Formability, Failure Prediction, Path Dependency, Non-Linear Strain Paths

Abstract. An area in the automotive industry that receives a lot of attention today is the introduction of lighter and more advanced material grades in order to reduce carbon emissions, both during production and through reduced fuel consumption. As the complexity of the introduced materials and component geometries increases, so does the need for more complex failure prediction approaches. A proposed path-independent failure criterion, based on a transformation of the limit curve into an alternative evaluation space, is investigated. Initially, the yield criterion used for this transformation of the limit curve was investigated. Here it was determined that the criterion for the transformation could not be decoupled from the material model used for the simulation. Subsequently, the approach using the transformed limit curve was tested on an industrial case from Volvo Cars, but a successful failure prediction was not obtained.

Introduction

An area of automotive engineering that receives a large amount of attention today is how to reduce the carbon footprint of a vehicle throughout its entire lifetime. Within the departments that concerns the manufacturing of automotive body components, one approach to meet these demands is to introduce lighter and more advanced material grades into the production lines. It can be noted that lighter and stronger materials are often less formable. So, using these advanced materials plus the demand for more complex shaped parts push recent designs to reach very close to the forming limit of the materials in some regions of the part. This naturally makes accurate failure prediction crucial. The study presented in this paper will investigate a path independent failure criterion, originally proposed by Zeng et al. [1] on a component from Volvo Cars that has proven to fail due to non-linear strain paths (NLSP). This paper will start out with a walk-through of the investigated approach.

Method

The path independent failure criterion investigated in this paper was originally proposed by Zeng et al. [1] as an alternative to the stress-based forming limit diagram proposed by Stoughton [2]. The investigated approach relies on a transformation of the evaluation space for failure from the traditional principal strain space, defined by coordinates in minor and major strain, to a space defined by the material flow direction α at the end of forming and the effective plastic strain $\bar{\varepsilon}^p$. The foundation for the approach is, that the parameter α, defined as the relationship between the increment in minor and major strain for the last stage in simulation (see Eq. 1), is uniquely related to the stress ratio σ_2/σ_1 for an associated flow rule.

$$\alpha = \dot{\varepsilon}_2/\dot{\varepsilon}_1 \tag{1}$$

Industrial Case

For the investigation of the approach, an industrial case manufactured from a VDA239 CR4 mild steel is used. A component from Volvo Cars has been chosen (see Fig. 1), as the component has proven to fail partially due to NLSP without this being detected in the simulations using the standard failure prediction approaches in an industrial setting.

Fig. 1: Volvo Cars component showing failure due to Non-Linear Strain Path.

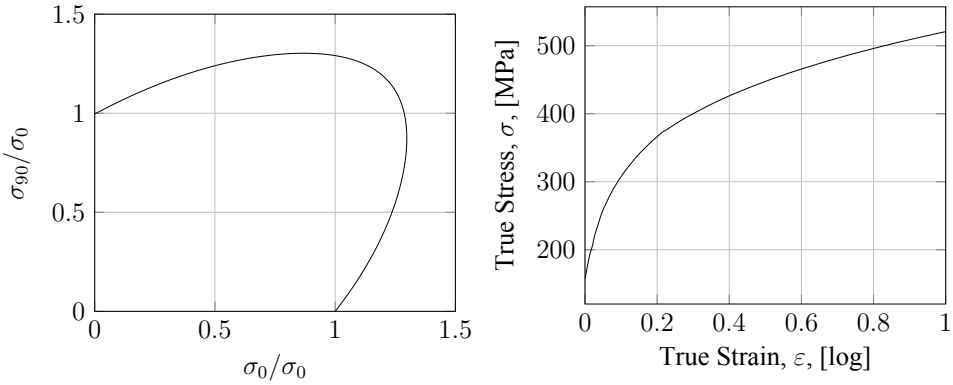

Fig. 2: Yield locus and hardening curve of the VDA239 CR4 mild steel.

Table 1: Parameters for the BBC 2005 Material Model

r_{00}	r_{45}	r_{90}	r_b	σ_0/σ_0	σ_{45}/σ_0	σ_{90}/σ_0	σ_b/σ_0	M
1.805	1.336	1.876	0.982	1	1.0214	0.9959	1.1938	4.5

The component has been modelled in the Finite Element (FE) software AutoForm™ R10 with a BBC 2005 material model. Figure 2 presents the yield locus and hardening curve, and Table 1 presents the parameters for the BBC 2005 material model. In the FE software, the component was checked with the standard failure prediction tools. In AutoForm™ R10 an advanced version of the standard Forming Limit Diagram (FLD), based on the method proposed by Volk and Suh [3], is available. This advanced FLD should be able to account for NLSP, however when evaluating the industrial case with this tool, the component is marked safe (see Fig. 3), even if the necking curve is entered as the limiting

criteria. The strain path presented in Figure 3 is that of the critical element where the crack appears. What should be noted is that the loading path changes with respect to the rolling direction. One of the requirements for the application of the advanced FLD is that such change does not occur. This results in a change from uniaxial load condition in the rolling direction to a plane strain load condition in the rolling direction is assumed to be the same as a change from uniaxial load condition in the rolling direction to a plane strain load condition in the transverse direction. In the industrial case presented in this paper, we can perform a check of the standard FLC and advanced FLC by looking at the Max Failure feature in AutoForm™ R10. The Max Failure feature measures how close one is to the limit curve of the standard FLC and the advanced FLC. The Max Failure value for the critical element for the standard FLC is 0.822, and for the advanced FLC it is 0.854. This indicates, that the advanced FLC do account for the non-linearity of the strain path, but it is ignoring the change with respect to rolling direction, and therefore does not mark the critical element as critical. This challenging aspect of predicting failure in components exposed to changes in load path with respect to the rolling direction further strengthens the argument for research into prediction of failure due to NLSP.

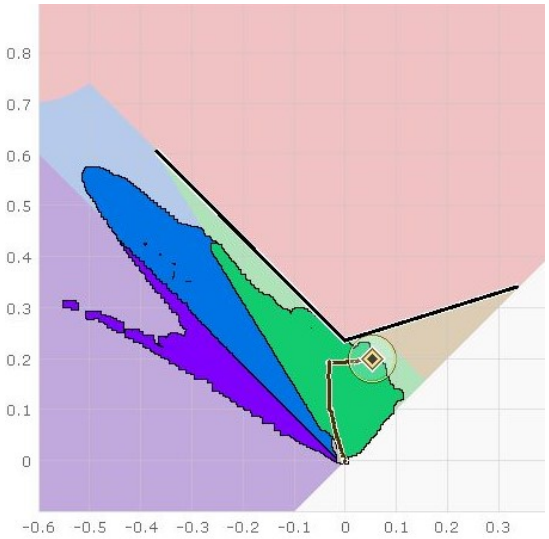

Fig. 3: Evaluation of the industrial case using the Advanced Forming Limit Diagram available in AutoForm™ R10. The strain path of the critical element is highlighted

Limit Curve Transformation

An integral part of the method by Zeng et al. [1] is the transformation of the standardized Forming Limit Curve (FLC) into the new evaluation space. In their paper, the transformation is performed using a Hill'48 material model for the calculation of the limit strain $\bar{\varepsilon}^p$. It is well known that the choice of yield criterion highly influences the calculation of i.e., the equivalent plastic strain. Since the industrial case is modelled with a BBC 2005 yield criterion, a study of how large the impact of the selected yield criterion for the transformation is on the limit strain will be conducted. Three different yield criteria will be looked into: von Mises, Hill'48, and BBC 2005.

The FLC used in the industrial case has been experimentally determined in compliance with ISO 12004-2 [4] and was recorded with the 3D DIC system ARAMIS from GOM. In the industrial case, the term 'failure' will be defined as the onset of localized necking. Therefore, the FLC is in this case describing the onset of localization. To accurately determine the point in the test where the onset of localization occurs, the method proposed by Sigvant et al. [5] was used. The FLC for the VDA 239 CR4 mild steel can be seen in Figure 4.

In order to perform the transformation, an assumption of linear (and proportional) deformation from zero to limit strain is made so that $d\varepsilon_i = \varepsilon_i$. Table 2 presents the experimental points of the FLC.

Table 2: Experimental Forming Limit Curve points.

FLC Point [-]	**Major Strain, ε_1, [log]**	**Minor Strain, ε_2, [log]**
Uniaxial Tension	0.608	-0.370
Plane Strain	0.235	0.000
Equi-biaxial Tension	0.341	0.340

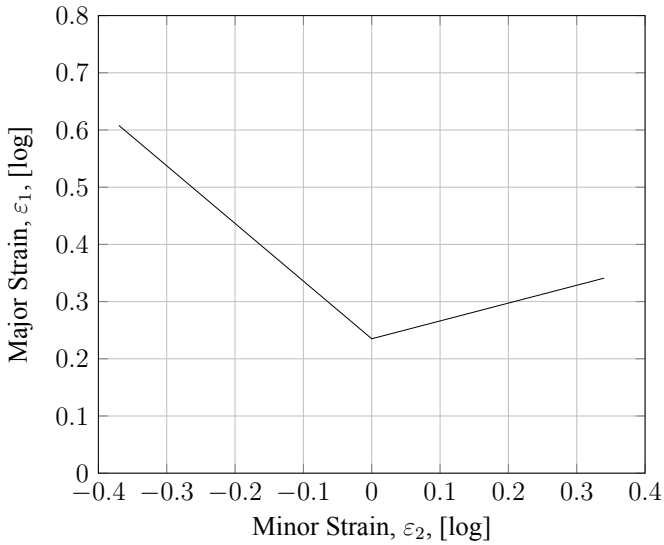

Fig. 4: Necking limit of the VDA239 CR4 mild steel. The curve is determined experimentally in compliance with ISO 12004-02 [4] and the onset of localized necking is determined according to the method proposed by Sigvant et al. [5].

For the transformation, the number of data points in the FLC has been expanded from 3 to 49 by evenly distributing 25 points between the uniaxial and plane strain points, and another 24 between the plane strain and equi-biaxial point. This is done due to observations made in the transformed curves of Zeng et al. [1] and Mattiasson et al. [6] where the limit curve cannot be defined by two linear sections between the uniaxial and plane strain point and the plane strain point and the equi-biaxial point. For the first transformation, the von Mises yield criterion is used. For the calculation of the von Mises equivalent plastic strain, an assumption of associated flow rule and plane stress is made, leading to the expression presented in Eq. 2 can be used.

$$\bar{\varepsilon}^p = \sqrt{\frac{4}{3} \cdot (\varepsilon_1^2 + \varepsilon_2^2 + \varepsilon_1 \cdot \varepsilon_2)} \tag{2}$$

For the transformation using the Hill'48 yield criterion, Eq. 3 is used to calculate the equivalent plastic strain [7]. For this calculation an assumption of linear deformation ($d\varepsilon_i = \varepsilon_i$) and plane strain ($\varepsilon_{12} = 0$) is made.

$$\bar{\varepsilon}^p = \sqrt{\frac{1}{F \cdot H + F \cdot G + G \cdot H} \cdot [(F+H) \cdot \varepsilon_1^2 + 2 \cdot H \cdot \varepsilon_1 \cdot \varepsilon_2 + (G+H) \cdot \varepsilon_2^2]} \tag{3}$$

For the Hill'48 determination, the three constants F, G, and H can be determined based on the r-values according Eq. 4 [8].

$$
\begin{aligned}
R_{22} &= \sqrt{\frac{r_{90}\cdot(r_{00}+1)}{r_{00}\cdot(r_{90}+1)}} \\
R_{33} &= \sqrt{\frac{r_{90}\cdot(r_{00}+1)}{r_{00}+r_{90}}} \\
F &= \frac{1}{2}\cdot\left(\frac{1}{R_{22}^2}+\frac{1}{R_{33}^2}-1\right) \\
G &= \frac{1}{2}\cdot\left(-\frac{1}{R_{22}^2}+\frac{1}{R_{33}^2}+1\right) \\
G &= \frac{1}{2}\cdot\left(\frac{1}{R_{22}^2}-\frac{1}{R_{33}^2}+1\right)
\end{aligned}
\tag{4}
$$

For the transformation of the curve using the BBC 2005 yield criteria this is not possible to do analytically why a numerical approach must be adapted. For this, the approach presented by Bandpay [9] is used to calculate the equivalent plastic strain of the different points of the standard FLC.

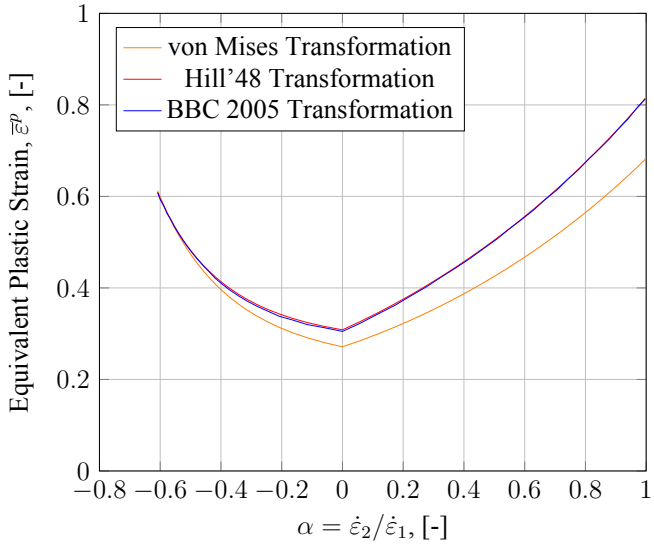

Fig. 5: Forming Limit Curve transformed from the traditional principal strain space into the new evaluation space based on three different yield criteria.

Figure 5 presents the transformed curves based on the three different yield criteria. As expected, the limit curve generated based on the von Mises yield criterion performs way different that those of the Hill'48 and BBC 2005 criteria. Focusing on the other two limit curves, they are highly similar, with the limit curve transformed based on BBC 2005 slightly lower, most prominent in the area of plane strain ($\alpha \approx 0$). This behavior seems to be in line with how the yield locus behaves with the two different criteria. Figure 6 presents a comparison of the yield loci when applying the Hill'48 and BBC 2005 criteria. From this, it can be seen that the two loci correspond very well to each other except in the region describing the plane strain behavior of the material. Therefore, to make an educated decision on which model to choose in this case, experimental data from a Limiting Dome Height (LDH) test is compared to simulations using a Hill'48 and BBC 2005 yield criteria.

Figure 7 presents a comparison of the major and minor strain profiles over a cross section of the experimental data (experiments of same batch of material as for the industrial case) and simulations run with Hill'48 and BBC 2005 yield criteria presented by Sigvant and Pilthammar [10]. This clearly shows that the BBC 2005 yield criteria predicts the strains better than the Hill'48. Due to this, the limit curve determined using the BBC 2005 yield criteria will be used for the post-processing.

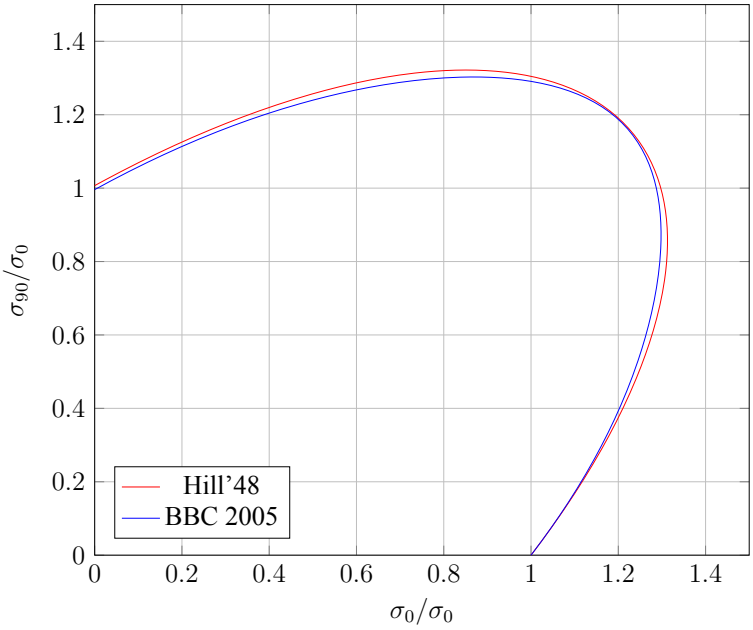

Fig. 6: Comparison of the yield loci for the VDA239 CR4 mild steel when applying a Hill'48 and BBC 2005 material model.

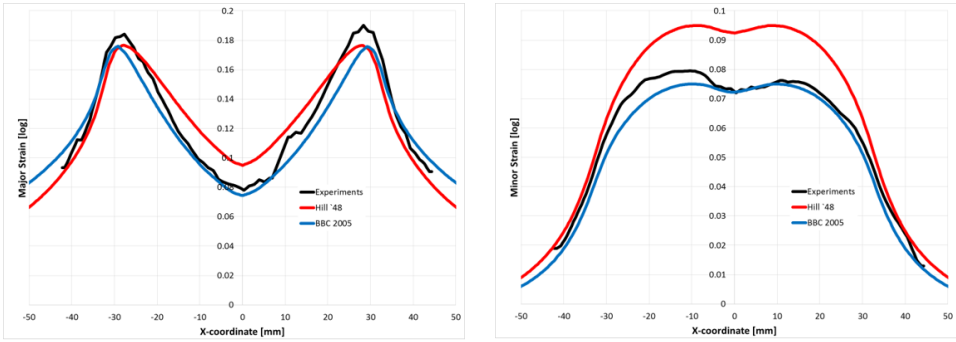

Fig. 7: Strain profile over a cross-section of a LDH-test of the VDA239 CR4 mild steel. Experimental results compared to simulations using Hill'48 and BBC 2005 yield criteria [10]

Post-Processing

The chosen curve based on the BBC 2005 yield criteria is applied to the industrial case from Volvo Cars. In order to do so, the strain paths of 5 different elements in the simulation are chosen to test the approach – one strain path from a critical element in the split area, and four arbitrary elements chosen in areas with high plastic strain values. The four arbitrary elements can be seen in Figure 8. These five different elements yield different strain paths – some highly non-linear and some resembling more linear strain paths (Figure 9). This mix of strain paths is deemed to be a good fit for a first test of the method, as it is important that the method does not create 'false positives' of failure where other approaches mark the point safe (*concept of primum non nocere – first do no harm* [11]). Especially interesting is the strain path for the critical element.

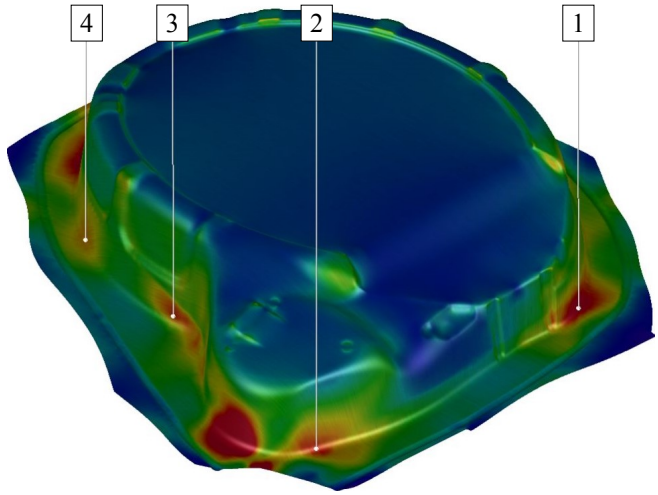

Fig. 8: Arbitrary control elements in areas with high plastic strain values.

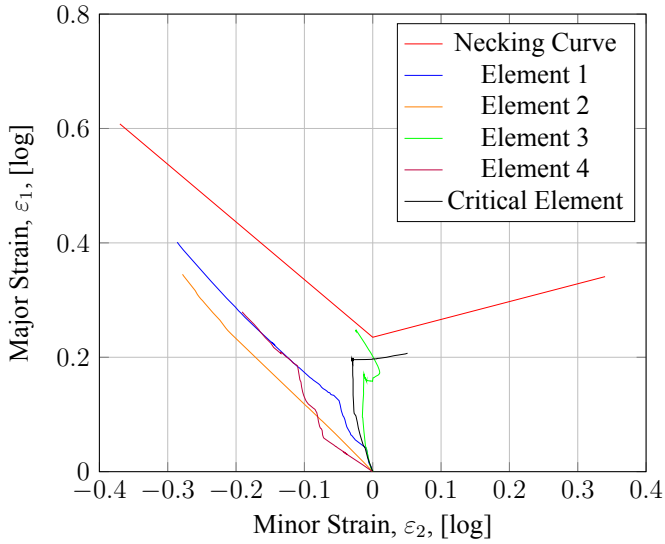

Fig. 9: Strain paths of the critical element and the four arbitrary control points in the principal strain space.

The critical points start out by being formed under plane strain condition up to roughly 20%. From here the strain path does a near 90° turn and proceeds to have a very small increase in major strain value in the principal strain space. The critical element ends up being relatively far away from the necking curve, especially compared to element 3. However, in reality element 3 does not fail, and the critical element not only show sign of onset of necking, it produces a through-thickness crack as presented in Figure 1.

As with the limit curve, the 5 elements investigated also needs to be transformed from the principal strain space. The equivalent plastic strain in the element is simply obtained from the simulation and exported so a post-processing can occur outside the FE software. The calculation of the α value is based on major and minor strains also exported from the FE software. According to Zeng et al. [1] and Mattiasson et al. [6], the path independence of the approach comes from the strong link to the stress-based forming limit diagram. This is backed up by Stoughton and Zhu [12] arguing that this is due to the path-independent constitutive laws governing the evolution of stresses and strains. Therefore, for the evaluation, the full strain path need not to be considered, but only the last step of the simulation. The data for the arbitrary and critical elements both in the principal strain space and the transformed evaluation space can be found in Table 3, and a plot of evaluation space can be seen on Figure 10.

Table 3: Data for the arbitrary and critical elements in the principal strain space and the transformed evaluation space.

Parameter	Element 1	Element 2	Element 3	Element 4	Critical Element
ε_1(i) [log]	0.4012	0.3451	0.2473	0.2794	0.2071
ε_1(i-1) [log]	0.4003	0.3446	0.2465	0.2791	0.2069
ε_2(i) [log]	-0.2861	-0.2783	-0.0255	-0.1912	0.0509
ε_2(i-1) [log]	-0.2856	-0.2780	-0.0251	-0.1911	0.0503
α [-]	-0.5453	-0.5712	-0.4407	-0.3754	2.6576
$\bar{\varepsilon}^p$ [log]	0.4320	0.3608	0.3621	0.3125	0.3477

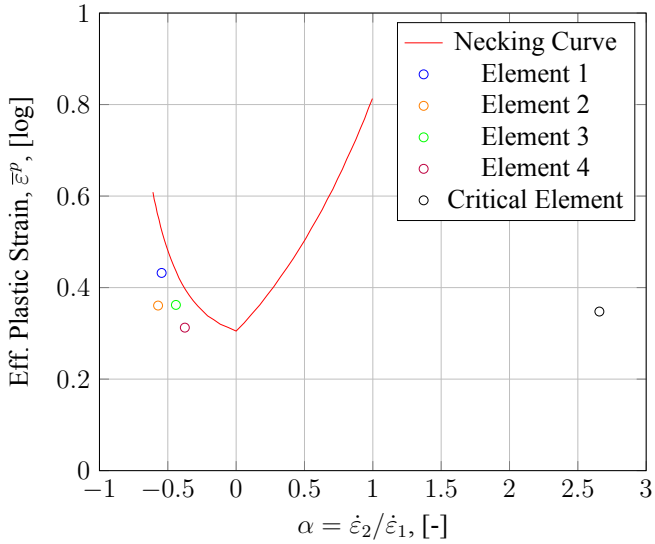

Fig. 10: Illustration of the arbitrary and critical elements in the transformed evaluation space

From Figure 10 it is clear that the approach highly overpredicts the α-value of the critical element. The α-value in the plot should not be able to pass the value of 1 since this indicates an equi-biaxial

strain state. What is seen here could be the result of the near 90° turn in the critical strain path, which could be an extremely rare phenomenon that needs to be discussed further. The positive outcome of the investigation is that for the four arbitrary control elements selected, no false positives are detected.

Discussion

As presented, the investigated approach was not able to predict the failure in the critical strain path of the industrial case. This does not necessarily mean that the approach should be discarded immediately. Taking a closer look at the strain path of the critical point (Fig. 9), the near 90° turn in the path is what is expected to cause trouble. The critical strain path starts out in a plane strain condition up until the turn. After the turn, the path could be interpreted so that a plane strain condition is present, but in a different direction than of the first part. According to Mattiasson et al. [6] the only parameters that matter is the plastic strain and the plastic flow direction. With the assumption of associated flow rule, the plastic flow direction is equivalent to the normal to the yield locus. Figure 11 outlines the value of α at different locations on the yield locus.

As presented in Figure 11, at the equi-biaxial point, α will take the value of 1. From here, the α value will increase until the horizontal tangent of the yield locus where α is infinitive. Continuing towards uniaxial stress, a negative normal is present and therefore α will be less than zero. The green arrow on Figure 11 indicates the jump the critical strain path takes when performing the turn. The script used for the post-processing in this study does not account for the fact that the point passes over the theoretical maximum value of α. Some sort of correction for this behavior should be implemented. One approach could be to assume the yield locus to be double symmetric and bounding the α-value between -1 and 1. How this should be handled when α practically passes 1 needs to be investigated further.

Furthermore, when assessing the formability of a component with a strain path as the one presented in this study, the influence of the material anisotropy should not be neglected. The limit curve presented in Figure 4 has been determined with test specimens cut along the transverse direction. With a change in the loading direction the limit used to assess the remaining formability should also be altered as presented by Volk et al. [13].

Lastly, another concern that needs to be addressed is the fact the approach relies on the strain increments for the calculation of α. This could potentially mean that the approach is highly sensitive to the step size in the model. However, no investigation of this has been carried out in this study, why it is a topic for further discussion.

Conclusion

A path-independent approach to predict failure due to non-linear strain paths proposed by Zeng et al. [1] was investigated. As the proposed method relies on a transformation of the evaluation space from the principal strain space into an evaluation space defined by the equivalent plastic strain and the material flow direction, it was initially investigated if the yield criterion used for the transformation of the Forming Limit Curve could be decoupled from the material model used for the simulation. Three different yield criteria were tested for the transformation of the limit curve: von Mises, Hill'48, and BBC 2005. It was concluded that even though the curves generated with the Hill'48 and BBC 2005 yield criteria were highly similar, the study should move forward with the one generated by using the BBC 2005 criteria to match what was used in the simulation. This conclusion was reached after consulting a comparison of the yield loci of the two criteria for the material, as well as major and minor strain predictions compared to experimental data of a Limiting Dome Height (LDH) test. Therefore, it was concluded that the yield criteria for the transformation of the limit curve could not be decoupled from the material model used for the simulation.

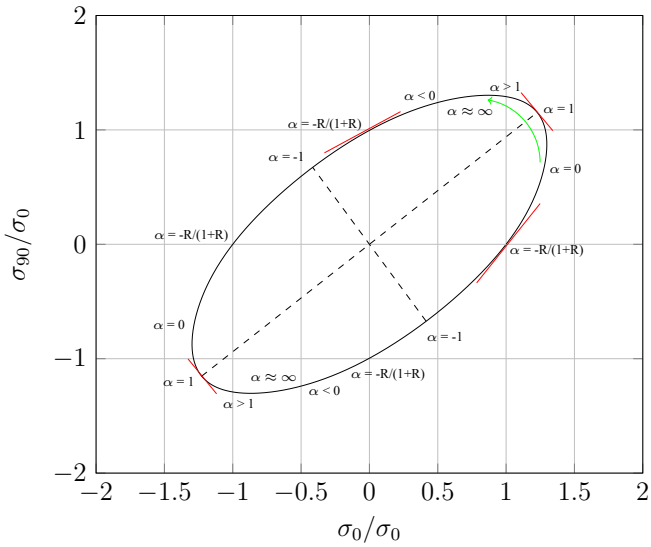

Fig. 11: Illustration of different α-values on different locations of the yield surface. When the 90° occurs in the critical strain path, the element jumps on the yield locus following the green arrow.

Furthermore, the approach using the transformed path-independent limit curve was tested on an industrial case from Volvo Cars that had produced a through thickness crack partially due to nonlinear strain paths. Four arbitrary elements, chosen to check for false positives, and the critical element of the simulation were all tested against the transformed limit curve. None of the elements indicated failure, why initially the approach has failed. However, due to the strange nature of the strain path of the critical element, it was argued that the approach should not be discarded before further investigation into the phenomena of radical turns in the strain path has been investigated.

Acknowledgements

Open Access funding was provided by Blekinge Institute of Technology. This study was also funded by VINNOVA in the Sustainable Production sub-program within Vehicle Strategic Research and Innovation (FFI) program (grant number 2020-02986).

References

[1] D. Zeng, L. Chappuis, Z. C. Xia and X. Zhu, A Path Independent Forming Limit Criterion for Sheet Metal Forming Simulations, SAE Int. J. Mater. Manu, Vol. 1, No. 1 (2009), pp. 809-817.

[2] T. Stoughton, A general forming limit criterion for sheet metal forming, Int. J. Mech. Sci. 42 (2000), pp. 1-27.

[3] W. Volk and J. Suh, Prediction of formability for non-linear deformation history using generalized forming limit concept (GFLC), AIP Conference Proceedings 1567 (2013), pp. 556-561.

[4] International Standard Organization, Metallic Materials – Determination of Forming-Limit Curves for Sheet and Strip – Part 2: Determination of Forming-Limit Curve in the Laboratory (ISO 12004-2) (2008).

[5] M. Sigvant, K. Mattiasson and M. Larsson, The Definition of Incipient Necking and its Impact on Experimentally or Theoretically Determined Forming Limit Curves, 2008 IDDRG Conference Proceedings, 16-18 June, Olofström, Sweden (2008).

[6] K. Mattiasson, J. Jergéus, and P. DuBois, On the prediction of failure in metal sheets with special reference to strain path dependence, Int. J. Mech. Sci. 88 (2014), pp. 175-191.

[7] R. B. Colby, Equivalent Plastic Strain for the Hill's Yield Criterion under General Three- Dimensional Loading, Bachelor Thesis, Massachusetts Institute of Technology (2013).

[8] D. Banabic, Sheet Metal Forming Processes: Constitutive Modelling and Numerical Simulation, Springer Berlin Heidelberg (2010).

[9] M. G. Bandpay, Instability and Fracture Models to Optimize the Metal Forming and Bending Crack Behavior of Al-Alloy Composites, PhD Thesis, ETH Zurich (2015).

[10] M. Sigvant and J. Pilthammar, Sheet Metal Forming Simulations at Volvo Cars: The past, the present and the future, Keynote presentation, Forming Technology Forum (2019), Munich, Germany.

[11] N. Manopulo and B. Carleer, On the way towards a comprehensive failure modelling for industrial sheet metal stamping processes, IOP Conf. Ser.: Mater. Sci. Eng. 651 (2019), pp. 012004.

[12] T. Stoughton and X. Zhu, Review of theoretical models of the strain-based FLD and their relevance to the stress-based FLD, Int. J. Plast. 20 (2004), pp 1463-1486.

[13] W. Volk, M. Gruber and R. Norz, Prediction of limit strains during non-proportional load paths with a change in loading direction, IOP Conf. Series: Mater. Sci. Eng. 967 (2020), pp. 012069.

PAPER D

A Barlo, M Sigvant, L Pérez, M S Islam, and J Pilthammar (2022). ”A Study of the Boundary Conditions in the ISO-16630 Hole Expansion Test”. In: *IOP Conference Series: Materials Science and Engineering* 1238.1, p. 012031. DOI: 10.1088/1757-899X/1238/1/012031

A Study of the Boundary Conditions in the ISO-16630 Hole Expansion Test

A Barlo[1], M Sigvant[1,2], L Pérez[3], M S Islam[1], and J Pilthammar[1,2]

[1]Department of Mechanical Engineering, Blekinge Institute of Technology, Karlskrona, Sweden
[2]Volvo Cars, Dept. 81110 Strategy & Concept, Olofström, Sweden
[3]RISE IVF AB, Component Manufacturing Unit, Olofström, Sweden

E-mail: Alexander.Barlo@bth.se

Abstract. As new and more advanced sheet metal materials are introduced to the market, more accurate techniques for determination of failure limits are needed. One area that needs attention is edge formability, where the ISO-16630 standardized Hole Expansion Test currently is used to express this through the Hole Expansion Ratio. Over the years, this standard has been criticized for producing a large scatter in repeated tests. This paper investigates a new setup for the Hole Expansion Test which introduces draw beads into the setup to ensure sufficient restraining of the specimen during the test in an effort to reduced the scatter. In total 62 tests of a DP800 steel alloy were executed, but a large scatter in the results were still seen. It was therefore concluded that a lack of restraining force in the Hole Expansion Test was not the primary cause of the reported scatter seen in other tests.

1. Introduction

With the increased focus on combating the rising environmental issues in the world today, a key goal for most automotive manufacturers is to reduce the carbon-footprint of a vehicle throughout its lifetime. One way to do so is by introducing lightweight and eco-friendly materials into their products. These new materials are however much more advanced than their predecessors and therefore much more difficult to validate in the design and manufacturing feasibility analysis stages. One of the large challenges these new materials bring, is how to accurately predict edge fractures caused by straining of punched holes during the forming process.

In the past decade and more, the Hole Expansion Ratio (HER) has been used as a measure for the edge formability of materials. The HER value is determined through the ISO standardized Hole Expansion Test [1] where a conical punch is driven through a hole in the test specimen, with a diameter of 10 mm, until a through-thickness crack appears. The HER value is then determined as presented in Eq. 1, where D_h is the average hole diameter after rupture, and D_o is the original hole diameter.

$$\lambda = \frac{D_h - D_o}{D_o} \times 100 \tag{1}$$

Over the years, the Hole Expansion Test has however been criticized by several authors, including Schneider et al. [2] and Larour et al. [3], for producing a high scatter when repeating the test on identical material from the same batch. Some authors, including Schneider et al. [2] and Chiriac & Chen [4], have attributed this to the operator reliant post-processing of the test,

however, this paper work with a different hypothesis: That the scatter is caused by insufficient restraining of the material during the test.

2. Experimental Setup and Specimen Preparation

In order to test if the restraining of the material during the Hole Expansion Test has an impact on the reported scatter, a new experimental setup was designed. In order to restrain the material, draw beads were introduced to the setup, where a die set from the Nakajima test setup, normally used to determine Forming Limit Curves, was used. With the application of an already existing die set for the Nakajima test setup, another benefit is also that the 3D Digital Image Correlation (DIC) system ARAMIS from GOM GmbH is embedded in the setup. According to Larour et al. [3] it should however be noted, that 3D DIC cannot be applied to materials where $\lambda > 70\%$ since the cameras in the ARAMIS 3D DIC setup fails to focus once a punch displacement of 50 mm has been passed.

The main criteria to the punch according to the ISO standard is that the cone of the punch should have a tip angle of $60.00 \pm 1°$. This criteria was taken into the design of the new punch, where the punch was scaled up to have a diameter of Ø100 mm to fit in the Nakajima die. Another change that was implemented in the new punch is that the tip of the punch is cut away, so that the top of the punch is circular with a diameter of Ø8 mm. This was done in order to provide the cameras for the 3D DIC with the most optimal conditions, and since the initial hole diameter of the test specimen is Ø10 mm, this should have no influence on the test results. The new experimental design can be seen in Figure 1.

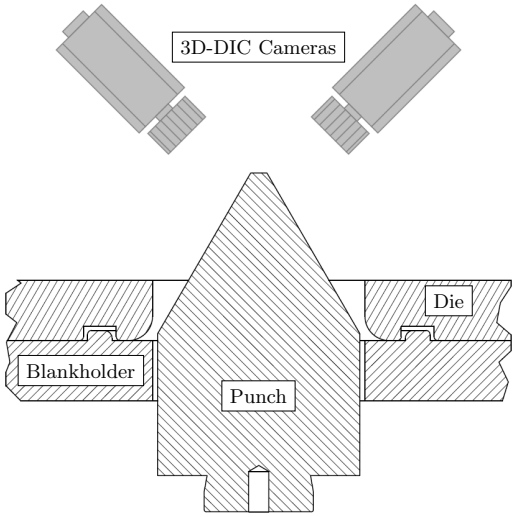

Figure 1. Cross-section view of the new experimental setup introducing draw beads and DIC system to the Hole Expansion Test.

Another change that was made from the ISO standard Hole Expansion Test is the shape of the blank. In the standard, the specimen is exemplified with a square blank, but in order to fit into the new setup with the die and blankholder from the Nakajima setup, the shape of the blank is changed to be circular. A requirement for the blank geometry is that "*The test piece shall be flat and of such dimensions that the centre of any hole is not less than 45 mm from any edge of the test piece...*" [1]. For this reason, the full-blank Nakajima geometry (Ø200 mm) was

chosen, which ensures that the centre of the hole is 100 mm from the edge of the specimen. The geometry of the modified blank geometry can be seen in Figure 2.

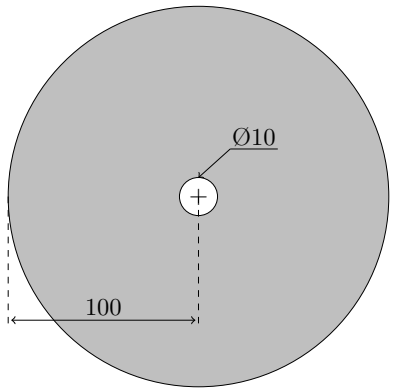

Figure 2. Modified blank geometry. All measurements in millimetres.

The cutting of the centre hole was performed using the punching operation, as specified in the ISO standard. This study focuses on a DP800 steel alloy with a sheet thickness of 1.2 mm, why a cutting clearance of 12 ± 1 % was used as in agreement with the standard. This resulted in an inside diameter of the die of $d_d = 10.288$ mm. Once the hole has been punched, a stochastic pattern is applied to the specimen to prepare it for DIC measurements. The pattern is applied so that the exit surface of the punched hole faces the die, thereby ensuring that the burrs created by the punching process faces away from the punch.

In order to ensure that the centre of the hole was aligned with the centre of the punch, a guide pin, mounted in a drilled hole on top of the punch, was used. The guide pin system can be seen in Figure 3 and a blank with formed draw bead can be seen in Figure 4.

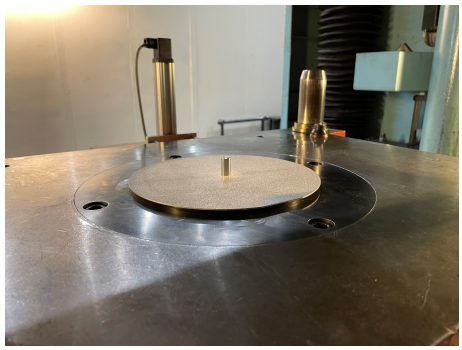

Figure 3. Guide pin used for ensuring the centering of the hole.

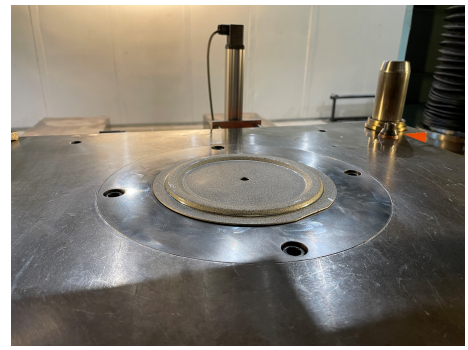

Figure 4. Pre-formed blank after removal of guide pin and with draw beads formed.

In order to form the draw bead, the rule of volume consistency dictates that the material used for this must be taken from somewhere else. Therefore, in order to ensure that the dimension of the centre hole was not changed radically during this "pre-forming" a test was conducted without the punch, so that only the draw bead was formed. A manual measurement of the

blank before the forming showed that the initial hole diameter was $D_o = 10.013$ mm and the hole diameter after forming of the draw bead was $D_h = 10.047$ mm. This results in an increase of the diameter of $\lambda_{pre} = 0.34$ %, which is deemed negligible compared to the spread of the HER-values and to not influence the results of the Hole Expansion Test.

3. Experimental and Post-Processing Procedure

By moving the setup into a single-action Wemhöner hydraulic press with a press capacity of 1300 tons, another deviation from the ISO standard needs to be done. In the standard, a testing speed of 1 mm/s is specified, however, the minimum speed of the utilized press is 5 mm/s. Another challenge when moving to a hydraulic press is how to determine when a through-thickness crack has appeared. In the Nakajima test setup, the operator does not visually observe the crack, but detects it by listening, and once the crack is heard, the test is terminated. The edge cracks in the Hole Expansion Test are not possible to detect by listening for the particular material tested, why a certain point in time where the test should be terminated is difficult to determine. This causes a risk that too deep of a draw could damage the tooling. Therefore, a mechanical stop was implemented in the press ensuring a fixed depth of the drawing. Based on initial experiments, a maximum drawing depth of 28 mm was chosen.

Another factor, and an important one in this study, is the restraining force applied to the specimen. In the standard, the following is specified about the clamping force: " *Apply sufficiently high clamping force to the test piece to prevent any material draw-in from the clamping area during the test"*[1]. The term 'a sufficiently high clamping force' is open to interpretation, but an example is given in the standard stating that a clamping force of 50 kN or higher should be sufficient for a test piece with the dimension 150×150 mm. As this investigation focuses on a DP800 steel grade, the blank holder force used in the press was increased significantly to a starting force of 330 kN, and the force increases as the tests proceeds to more than 380 kN. This scenario is exemplified in Figure 5. With the combination of the draw bead and this level of blank holder force, it is believed that no draw-in will occur during the testing.

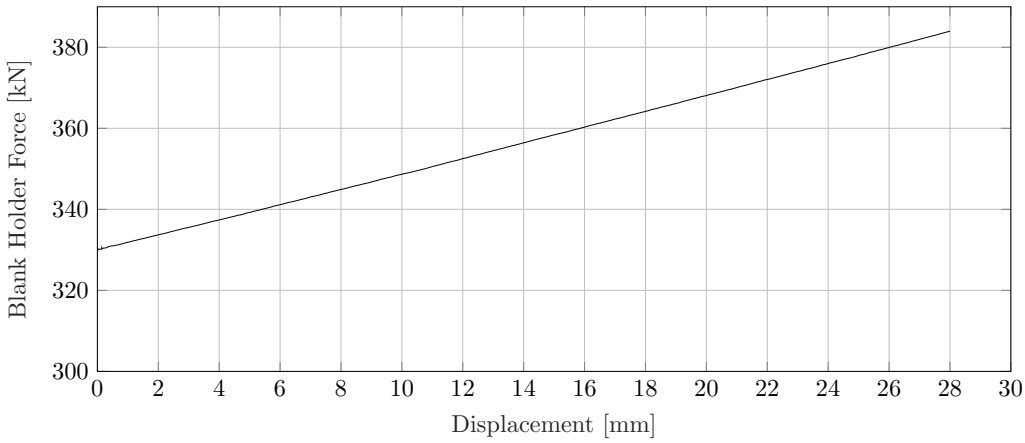

Figure 5. Blank holder force during one of the Hole Expansion Tests.

Fixing the draw depth is not without consequences. The obvious issue is that the final specimen will in the vast majority of the cases have passed a point where a through-thickness crack first appears. In the same way, cases where a through-thickness crack has yet not presented itself could occur. In the case of the latter, not much can be done in the setup, except changing

the mechanical stop, and try again. In the first case, the general methodology presented by Chiriac & Chen [4] can be utilized, where the Hole Expansion Test was recorded with a digital camera, and a digital measurement of the hole diameter occurs at the frame that shows the first through-thickness crack.

Therefore, by utilizing the images captured by the 3D DIC system (with a sampling frequency of 60 Hz), a measurement of the hole diameter of any given stage in the test is possible, and should result in a reduction of the uncertainties introduced by the operators reaction time. Figures 6 and 7 presents a close up of the collar on a Hole Expansion Test at two different stages with a draw depth difference of approximately 0.17 mm. In Figure 6 it can be seen that the crack has been initiated in the outer diameter, but has not yet propagated all the way through the thickness. Figure 7 presents the state of the collar two stages later, and here a full through thickness crack is present.

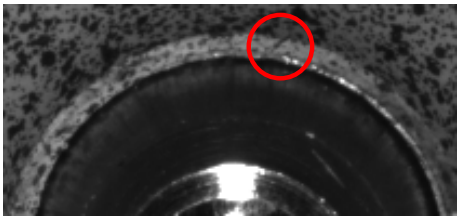

Figure 6. Close up of collar on test exhibiting crack initiation.

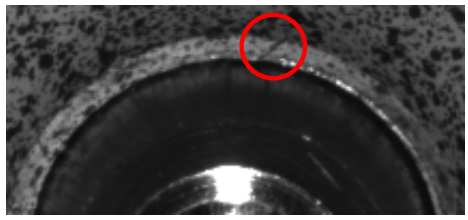

Figure 7. Close up of collar on test exhibiting through thickness crack.

Once the stage where the initial through thickness crack appears had been identified, the diameter of the hole is measured based on a method mapping a certain number of pixels in the image to a reference length. In total, four measurements of the diameter were taken, two from the image of the left camera (D_{h1} and D_{h2}) and two from the right camera (D_{h3} and D_{h4}). The known reference length in the image is the hole made for mounting the guide pin presented in Figure 3, where the length is known to be 6.004 mm. Figure 8 presents where the reference geometry was taken, and how the two measurements are placed in relation to each other. Once the four measurements were obtained, the average Hole Expansion Ratio $\overline{\lambda}$ was calculated using the average hole diameter $\overline{D}_h$ as presented in Eq. 2.

$$\overline{\lambda} = \left(\frac{\left(\frac{D_{h1}+D_{h2}+D_{h3}+D_{h4}}{4} \right) - D_o}{D_o} \right) \times 100 \tag{2}$$

4. Results

In total 62 test specimens were tested in the new experimental setup, where 59 of the executed tests were successful, and a through thickness crack was detected before the mechanical stop was reached. Three of the executed tests showed no evidence of fracture or only partial fracture (not through the thickness) at the point where the mechanical stop was reached. Figure 9 presents the $\overline{\lambda}$-values of the 62 tests, and the three unsuccessful tests have been marked separately. A mean value of the 59 successful tests was found to be 31.184 %, with a standard deviation of $\sigma = 4.2910$.

As it can be seen from the results presented in Figure 9, the test still produces a large scatter, indicating that the lack of restraining force in the test is not the primary cause of the reported scatter. An interesting trend that can be observed from the results, is the decrease of the $\overline{\lambda}$-values beginning with sample number 48. No apparent reason stands out when looking at the

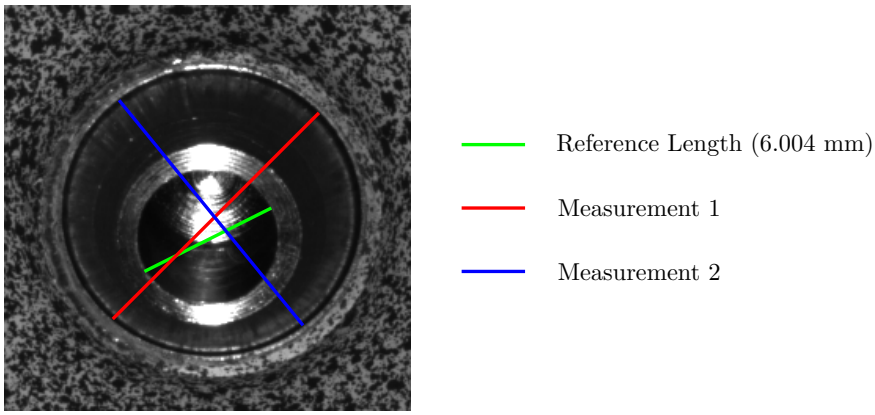

Figure 8. Illustration of the measurement of the hole diameter. Two measurements are taken on each of the images recorded by the DIC system.

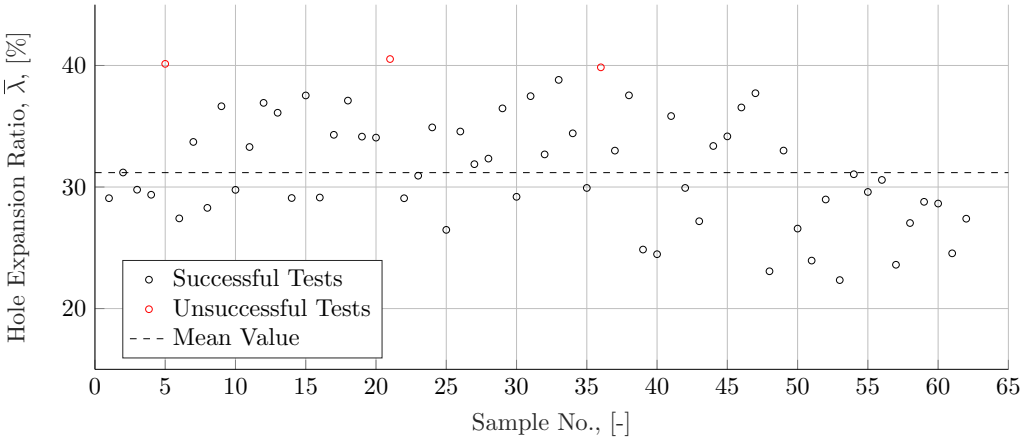

Figure 9. Hole Expansion Ratios of the 62 tests conducted. In total three tests were unsuccessful due to no presence of through-thickness cracks.

DIC stages at which the specimens failed, why a more in-depth discussion of the results must take place.

5. Discussion

As presented, the results of the 62 Hole Expansion Tests still produce a significant scatter, which indicates that the boundary conditions of the ISO-16630 test is not the primary cause for the scatter. Another factor that could highly influence the results of the test is the stochastic behaviour of fracture. Historically, the Hole Expansion Test has been evaluated once a through-thickness crack has appeared in the sample. With the previous setup this was the only way to proceed, but with the new setup presented in this paper, it is possible to evaluate the test in an arbitrary point in time due to the images recorded by the DIC system. Therefore, it could be

argued that the test should be evaluated at a stage before the first surface crack appears. The problem with edge cracks is that they are not induced by necking, but are subject to the direct fracture phenomena as described by Manopulo & Carleer [5]. Therefore, the current methods of determining the onset of localized necking as presented by e.g. Sigvant et al. [6] cannot be applied, and a different approach must be found.

Another interesting trend that was observed in the results is the downwards trend of the $\overline{\lambda}$-values on the last specimens tested (sample number 48-62). Several authors, including Yoon et al. [7] and Karelova et al. [8], have stressed the importance of the edge quality of the punched hole in the Hole Expansion Test. One possible explanation for the downwards trend in the results could be due to wear of the tool used for punching the holes in the test specimens. The tool used for punching in this series of experiments was new and never before used, why it is not unlikely what is seen is the tool experiencing some initial wear before settling into a stable condition. Another possible explanation for the trend could be an unintended wear of the conical punch. The scaled up punch used for the new setup was manufactured from a tool steel and subsequently vacuum hardened to have a hardness of 61±1 HRC. In order to get the punch to fit with the specifications, a grinding operation was performed after the hardening. If this grinding operation has removed most of the hardened material, it is possible that the conical punch has experienced some wear, which has resulted in a change in the friction conditions between the punch and the test specimen. Figure 10 presents a comparison of the Force-Displacement curves for test 15 and 49. This comparison shows that there are differences between the two curves, especially in the low displacement area, indicating that friction conditions might have changed between the punch and the sheet, as well as a difference in the total displacement accounting for the difference in the $\overline{\lambda}$-values of the two tests.

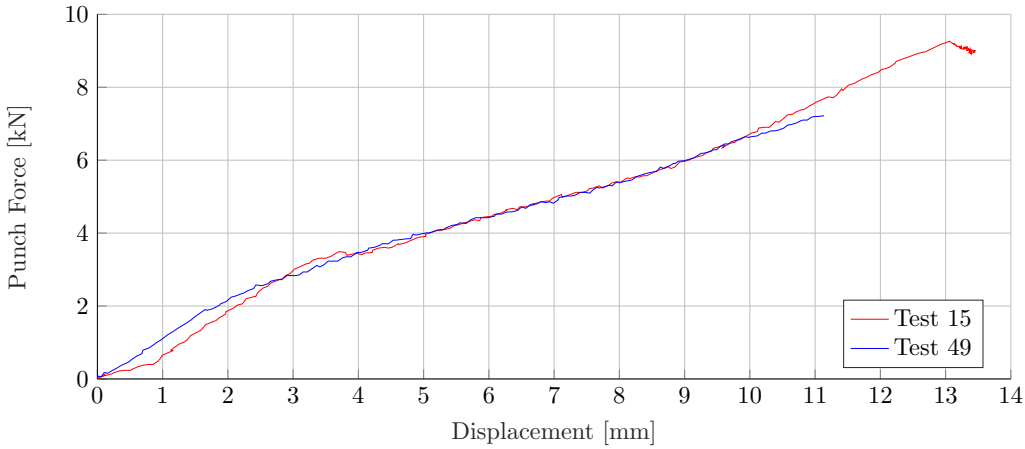

Figure 10. Comparison of the Force-Displacement response of two tests from each end of the test series.

6. Conclusion

A new experimental setup aiming to reduce scatter in the results of the ISO-16630 Hole Expansion Test was tested. The new setup was based on a hypothesis that the scatter reported by several authors was due to an insufficient restraining of the material during the test. Therefore, a conical punch was developed according to the specifications of the ISO-16630 standard and a

die set from a Nakajima test was used due to the presence of a draw bead. For the evaluation of the test, images from a 3D DIC system was analysed in a third party software where a mapping of pixels between a known distance and the hole diameter was used to determine the final hole diameter.

In total 62 tests of a DP800 steel alloy were performed, where 59 of these successfully presented a through-thickness crack, and the remaining three did not due to the test begin terminated by a mechanical stop in the hydraulic press used. The results of these 62 tests still presented a large scatter with a standard deviation of 4.291 % why it can be concluded that restraining force of the sample during the test is not the primary cause of the scatter in the Hole Expansion Test.

Acknowledgements
Open Access funding was provided by Blekinge Institute of Technology. This study was also funded by VINNOVA in the Sustainable Production sub-program within Vehicle Strategic Research and Innovation (FFI) program (grant number 2020-02986).

References

[1] International Standard Organization 2018 Metallic materials – sheet and strip - hole expanding test (ISO 16630)
[2] Schneider M *et al* 2015 Overview and comparison of various test methods to determine formability of a sheet metal cut-edge and approaches to the test results application in forming analysis *Mat.-wiss u. Werkstofftech* **46**(12) pp 1196-1217
[3] Larour P *et al* 2014 Evaluation of alternative stretch flangeability testing methdos to iso 16630 standard *IDDRG 2014 Conference Proceedings*
[4] Chiriac C and Chen G 2008 Local formability characterization of ahss - digital camera based hole expansion test development *IDDRG 2008 Conference Proceedings*
[5] Manopulo N and Carleer B 2020 A new workflow for the effective distinction between necking induced splits and direct fracture phenomena *IOP Conf. Series: Mater. Sci. Eng.* **967** 012066
[6] Sigvant M *et al* 2008 The definition of incipient necking and its impact on experimentally or theoretically determined forming limit curves *IDDRG 2008 Conference Proceedings*
[7] Yoon J I *et al* 2016 Factors governing hole expansion ratio of steel sheets with smooth sheared edge *Met. Mater. Int.* **22**(6) pp 1009-1014
[8] Karelova A *et al* 2009 Hole expansion of dual-phase and complex-phase ahs steels - effect of edge conditions *Steel Research International* **80**(1) pp 71-77

ABSTRACT

With the increased focus on reducing carbon emissions in today's society, several industries have to overcome new challenges, where especially the automotive industry is under a lot of scrutiny to deliver improved and more environmentally friendly products. To meet the demands from customers and optimize vehicles aerodynamically, new cars often contain complex body geometries, together with advanced materials that are introduced to reduce the total vehicle weight.

With the introduction of the complex body components and advanced materials, one area in the automotive industry that has to overcome these challenges is manufacturing engineering, and in particular the departments working with the sheet metal forming process. In this process complex body component geometries can lead to non-linear strain paths and stretch bending load cases, and newly introduced advanced materials can be prone to exhibit behaviour of edge cracks not observed in conventional sheet metals.

This thesis takes it onset in the challenges seen in industry today with predicting failure of the three complex load cases: Non-Linear Strain Paths, Stretch-Bending, and Edge Cracks. Through Finite Element simulation attempts are made to accurately predict failure caused by aforementioned load cases in industrial components or experimental setups in an effort to develop post-processing methods that are applicable to all cases.

BLEKINGE TEKNISKA HÖGSKOLA · BTH ·

ISSN 1650-2140

2023:03

ISBN 978-91-7295-451-9